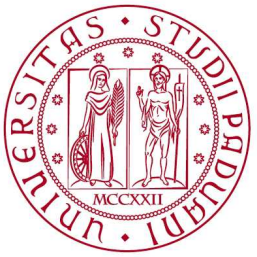

UNIVERSITÀ
DEGLI STUDI
DI PADOVA

Sede Amministrativa: Università degli Studi di Padova
Dipartimento di Fisica e Astronomia

SCUOLA DI DOTTORATO DI RICERCA IN ASTRONOMIA
CICLO XXIX

Mass transfer and hydrogen burning in white dwarf binaries

Direttore della Scuola: Ch.mo Prof. Giampaolo Piotto
Supervisore: Dott.ssa Marina Orio

Valutatori: Prof. Paula Szkody e Prof. Joe Patterson

Dottoranda: Polina Zemko

UNIVERSITÀ DEGLI STUDI DI PADOVA

Abstract

Dipartimento di Fisica e Astronomia

Doctor of Philosophy

Mass transfer and hydrogen burning in white dwarf binaries

by Polina Zemko

The thesis is devoted to a study of mass transfer, non-explosive hydrogen burning and the effects of the magnetic field in cataclysmic variables (CVs) in the context of their evolution and possible paths to Supernovae type Ia. I focused on the observational properties of CVs hosting massive white dwarfs (WDs) and/or accreting at high rate. My aims were to detect signatures of quiescent hydrogen burning, follow novae as they settle into quiescence and to assess whether the WD magnetic field alters secular evolution and the outcome of the nova explosions. The thesis consists of three chapters. The first one focuses on observations of VY Scl-type nova-like systems, or "anti-dwarf novae", exploring the idea that they can burn hydrogen during their optical low states. I analysed all the available archival X-ray and UV observations, in both, their high and their low states, and found that the proposed hydrogen burning at high atmospheric temperatures is ruled out. VY Scl-type stars cannot be Supernova type Ia progenitors since they either burn hydrogen but have too low-mass WDs or undergo rare nova explosions, expelling more material than was accreted. In the second chapter I investigate two post-novae with massive WDs, confirming the magnetic nature of one of them, and revealing that the second one is an intermediate polar candidate. I also show that a nova explosion in a magnetic system can leave an imprint on the surface of a WD, detectable in soft X-rays for several years after the explosion. It may be due to residual localized hydrogen burning, but a more likely explanation is a temperature gradient in the WD atmosphere. The last chapter represents monitoring of the old magnetic nova GK Per performed with *Swift*, *Chandra* and *NuSTAR* telescopes during its recent dwarf nova outburst. The main goal was to study the effects of increased mass transfer through the disk in a magnetic system. I measured the WD spin-up rate, localized the emission sites of different spectral components, revealed shrinking of the inner radius of accretion disk and redistribution of the accretion energy as the mass transfer grows.

UNIVERSITÀ DEGLI STUDI DI PADOVA

Abstract

Dipartimento di Fisica e Astronomia

Doctor of Philosophy

Mass transfer and hydrogen burning in white dwarf binaries

by Polina Zemko

Questa Tesi è dedicata allo studio del trasferimento di massa, del bruciamento non-esplosivo dell'idrogeno e degli effetti del campo magnetico nelle variabili cataclismiche (CVs), nel contesto della loro evoluzione e della possibile relazione con le Supernovae di tipo Ia (SN Ia). Mi sono concentrata sulle proprietá osservative di CV contenenti nane bianche (WD) massicce e/o che accrescono rapidamente materia. I miei obiettivi sono stati: rilevare diagnostiche di bruciamento quiescente dell'idrogeno, seguire novae che ritornano nella fase quiescente e valutare se il campo magnetico di una WD può alterare l'evoluzione secolare e il risultato delle esplosioni di nova. La tesi è composta da tre capitoli. Il primo capitolo riguarda le osservazioni di sistemi nova-like di tipo VY Scl, o "anti-novae-nane" (anti-dwarf novae), e vi esploro l'idea che questi sistemi brucino idrogeno durante i loro stati di bassa luminositá ottica. Ho analizzato tutte le osservazioni di archivio nelle bande X e UV, durante gli stati di luminositá ottica elevata e bassa, e ho scoperto che, se anche avviene il bruciamento dell'idrogeno, la temperatura atmosferica non è elevata. Le stelle di tipo VY Scl non possono essere le progenitrici delle SN Ia perchè o bruciano idrogeno ma WD sono di piccola massa, o avvengono rare esplosioni di nova, in cui espellono più massa di quella che hanno accresciuto. Nel secondo capitolo ho studiato due post-novae con nane bianche massicce, confermando la natura magnetica di una di esse, e rivelando che la seconda è una candidata "polare intermedia". Ho dimostrato anche che un'esplosione di nova in un sistema magnetico può lasciare un'impronta sulla superficie di una WD, osservabile ai raggi X per alcuni anni dopo l'esplosione. Questo effetto può essere dovuto a residuo bruciamento localizzato di idrogeno, ma la spiegazione più probabile è un gradiente di temperatura nell'atmosfera della WD. L'ultimo capitolo descrive come abbiamo seguito la vecchia nova magnetica GK Per con i telescopi spaziali *Swift*, *Chandra* e *NuSTAR* durante la recente esplosione di nova-nana. Il principale obiettivo è stato quello di studiare gli effetti di un aumento di trasferimento di massa attraverso il disco in un sistema magnetico. Ho misurato l'accelerazione delle rotazione della WD, ho localizzato i siti di emissione delle diverse componenti spettrali, e rivelato il restringimento del raggio interno del disco di accrescimento e la ridistribuzione dell'energia dovuta all'accrescimento di materia durante il periodo di aumento del trasferimento di massa.

Acknowledgements

I would like to thank my supervisor during the master program in the Moscow State University, Dr. S. Shugarov, who channeled my scientific interests to the field of the accreting white dwarfs and by doing this he determined my future life. In particular I would like to acknowledge Dr. T. Kato, who greatly improved my data analysis skills during my stay in the Kyoto University and showed me that I can write 2.5 papers in only three months. I have never managed to beat this record since that. Many thanks to Dr. Orio, my supervisor during the PhD program for her enormous help and support, especially for her efforts to bring me to the University of Padova.

I am also grateful to my collaborators: Dr. S. Ciroi, Dr. V. Cracco, for their help in the analysis of the optical spectra, to Dr. A. Bianchini, Dr. G. J. M. Luna and in particular to Dr. K. Mukai for their invaluable comments. I would also like to thank Prof. P. Szkody and Prof. J. Patterson for being the reviewers of this thesis.

I would like to acknowledge the optical observers from the Sternberg Astronomical Institute: Dr. E. Barsukova, Dr. V. Goransky, Dr. S. Shugarov, and Dr. A. Gabdeev who performed a part of the optical observations, analysed in this thesis. I acknowledge the observers who contributed to the AAVSO, ASAS and VSNET databases, which I used for the analysis. This work also made use of data supplied by the UK Swift Science Data Centre at the University of Leicester.

I am very grateful to my husband for supporting me and for helping me to overcome numerous difficulties throughout writing this thesis and my life in general.

Finally, this work would have not been possible without a pre-doctoral grant of the CARIPARO foundation at the University of Padova.

Contents

List of Figures

List of Tables

Abbreviations

WD	**W**hite **D**warf
CV	**C**ataclysmic **V**arriable
NL	**N**ova-**L**ike (star)
IP	**I**ntermediate **P**olar
VSNET	**V**ariable **S**tar **NET**work Collaboration[1] [1]
AAVSO	**A**merican **A**ssociation of **V**ariable **S**tar **O**bservers[2]
ASAS	**A**ll **S**ky **A**utomatic **S**urvay[3]

[1] http://www.kusastro.kyoto-u.ac.jp/vsnet/
[2] http://www.aavso.org
[3] http://www.astrouw.edu.pl/asas/

Physical Constants

Speed of Light	c	=	2.9979×10^{10} cm s^{-1}
Parsec	pc	=	3.0857×10^{18} cm
Solar mass	$\mathrm{M}_\odot$	=	1.9885×10^{33} g

Symbols

d	distance	pc
M	mass	$M_\odot$
L	luminosity	erg s^{-1}
F	flux	erg cm^{-2} s^{-1}
υ	velocity	km s^{-1}

Dedicated to my beloved husband.

Chapter 1

Introduction

Accreting white dwarfs in close binary systems are natural laboratories of all types of high energy phenomena. Because of their large numbers and proximity they offer the possibility to study mass transfer mechanisms, stellar winds, binary evolution and nucleosynthesis in detail, all important phenomena for many types of astrophysical objects. WD binaries are divided into three classes depending on the type of their secondary stars: cataclysmic variables (CVs), AM CVn-type stars and symbiotic systems. A schematic view of different classes of white dwarf binaries, together with their subtypes and the relations between them is presented in fig. 1.1. AM CVn-type stars consist of a WD with another WD or a helium star as the secondary. Symbiotic systems are WDs with a giant star. In the thesis I will focus on the third class of WD binaries — CVs.

Cataclysmic variables are close binary systems consisting of a WD primary and a lower-mass late type main sequence star transferring material via Roche-lobe overflow. The material from the secondary that passes beyond the L1 point, has high specific angular momentum and forms the accretion disk around the WD, if the WD magnetic field is not strong enough to prevent the disk formation. As their name implies, CVs are characterised by a pronounced variability on timescales from several seconds to centuries. Variability can be related to the orbital motion of binary components, WD rotation, fluctuations of mass transfer, thermal and/or tidal instabilities in accretion disks, and explosive or non-explosive hydrogen burning on the surface of a WD. Depending on their observational properties, outburst activity and the WD magnetic field strength CVs are divided into several types, however, the overall classification is quite complicated (as seen from fig. 1.1). The following section will be devoted to the properties of different types of CVs.

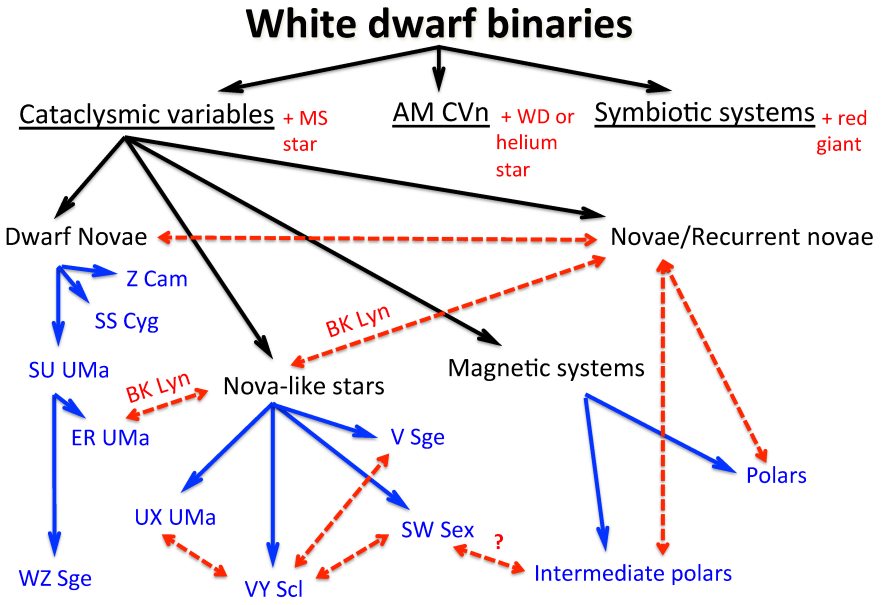

FIGURE 1.1: Classification of WD binaries. The black arrows show different classes of WD binaries and types of CVs. The blue lines show different subtypes of the latter. The red lines indicate the overlaps between different types and subtypes.

1.1 Phenomenological classification of CVs

1.1.1 Novae

If enough material is accumulated on the surface of a WD, the temperature and the pressure at the bottom of the accreted envelope can be high enough for nuclear burning ignition and a classical nova (CN) explosion (see e.g. [2, 3]). If more than one nova explosion was observed in a given system, it is called a recurrent nova. The recurrence time of nova explosions depends on the WD mass and the mass transfer rate [3] and is the shortest for massive WDs accreting at a high rate. The shortest known recurrence time has M31N 2008-12a, which undergoes nova explosions nearly once a year, or possibly even once in ∼6 months [4].

CNe are detected as bright sources in the optical band, but as the WD atmosphere contracts at rising temperature, the peak luminosity shifts towards shorter wavelengths: to UV, EUV and, in the majority of cases, to soft X-rays while the luminosity itself is constant and close to the Eddington limit. This phase of constant bolometric luminosity can last from several days to almost 10 years, until the WD atmosphere shrinks back to the pre-outburst radius. At this point the atmosphere, heated by the underlying hydrogen burning, usually has temperature above 200 000 K, high enough to emit soft X-rays in roughly blackbody-like form. If the ejected envelope is transparent to soft

X-rays, the system is observed as a super-soft X-ray source (e.g. [5–7]). Observations of novae in the super-soft X-ray source (SSS) phases allow a measurement of the chemical composition, temperature of the WD atmosphere and effective gravity, which gives the estimate of the WD mass. The SSS phase can last from days to years and ends when the WD atmosphere cools [7].

The amplitudes of nova explosions in the optical band are typically 8 – 12 mag, but can be as high as 15 mag (e.g. CP Pup [8]). Nova explosions are characterised by the, so-called, t_2 and t_3 times, which are the times to fade by 2 and 3 magnitudes from maximum. These times define the nova 'speed class' [8] and using the maximum-magnitude rate-of-decay (MMRD) relation [9] allows a rough estimate of the distance to the object. The speed class of a nova depends first of all on the WD mass, but also on the temperature at the bottom of the accreting envelope, metallicity, accretion rate and, possibly, the WD magnetic field strength (see section 1.1.4).

The binary components in a CV lose the angular momentum due to magnetic braking [10, 11] and gravitational radiation [12, 13] and evolve towards shorter orbital periods until the donor becomes degenerate, the system starts to evolve towards longer periods and becomes a "period bouncer". The top panel of fig. 1.2 shows the orbital period distribution of CVs of different types: non-magnetic DNe (light grey), novae (red hatched), novalikes (green) and the total number of these objects (white). The grey hatched region between 2 and 3 h shows the period gap, where the orbital angular momentum loss due to magnetic wind braking is expected to be less effective and the accretion stops (Gänsicke et al. [14] give a more precise value for the period gap: 2.4–2.7 h). The longer it takes for a given system to evolve through a range of orbital periods, the more systems will be observed in this range, which results in the period minimum spike in the period range of 80 — 86 min [14]. The percentage of novae in each bin with respect to the total number of CVs is nearly the same above the period gap, but is greatly reduced below the gap. Fig. 1.2 shows objects having orbital periods up to 10 h long, but nova explosions are observed also in longer period systems. There are 6 novae with orbital periods longer than 1 day: HV Cet (P_{orb} =1.772 d.), V1017 Sgr (P_{orb} =5.714 d., it is also a dwarf nova), V5589 Sgr (P_{orb} =1.5923 d.), X Ser (P_{orb} =1.48 d.), V2674 Oph (P_{orb} =1.302 d.) and GK Per (P_{orb} =1.99 d., it is also a dwarf nova and magnetic system) and two recurrent novae: U Sco and V394 CrA.

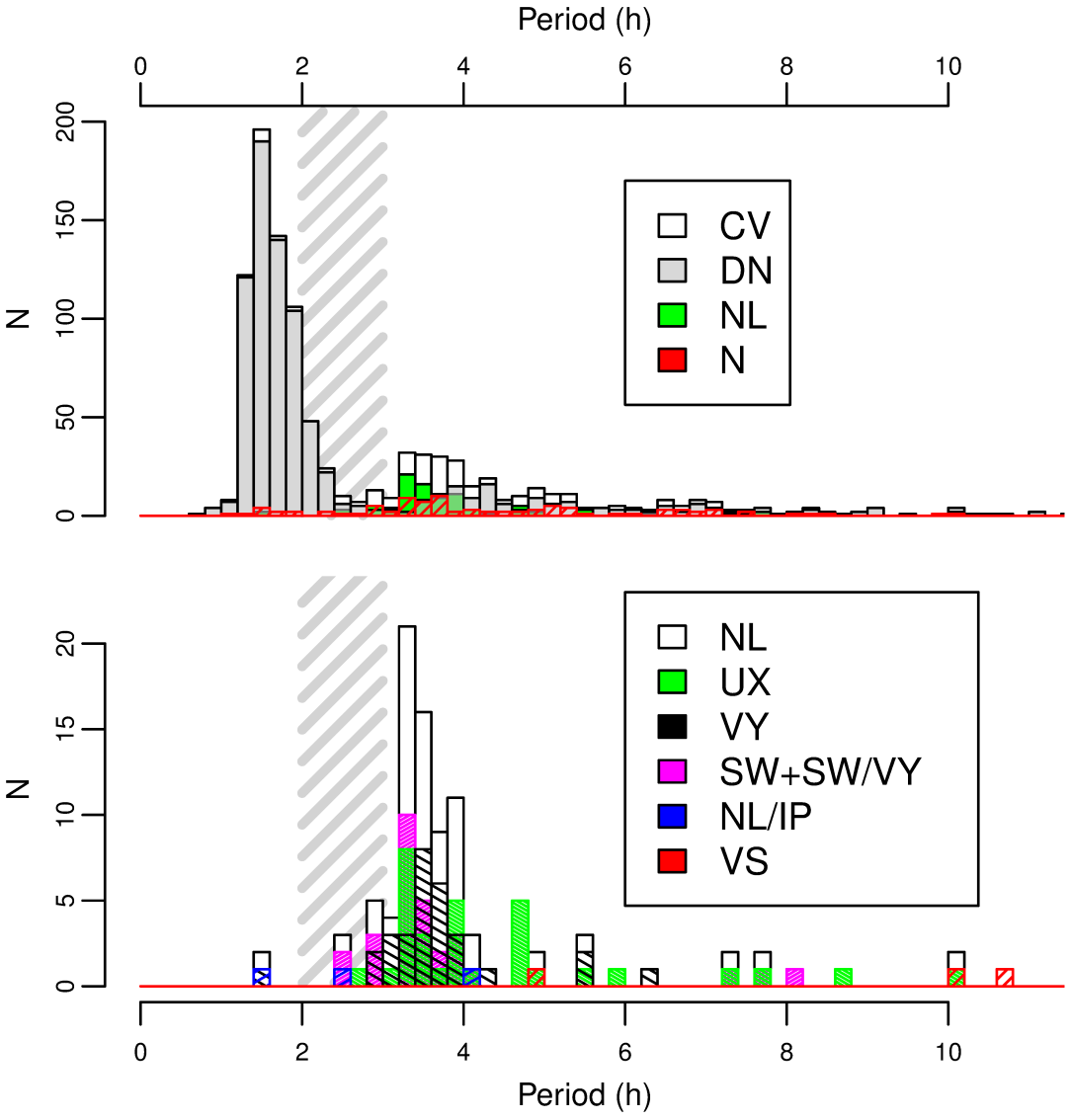

FIGURE 1.2: The orbital period distribution of CVs of different types. Top: non-magnetic DNe (light grey), novae (red hatched), NLs (green) and the total number of these objects (white). Bottom: the orbital period distribution of NLs of different types. The white columns represent the total number of NLs, the green are UX UMa-type NLs, the black hatched are VY Scl-type stars (excluding those that also belong to the SW Sex-type), the purple are SW Sex, including those with low states, the blue hatched are NLs with magnetic WDs (intermediate polars), and the red hatched are V Sge-type NLs. The list of the non-magnetic DNe, novae, VY Scl- and UX UMa-type NLs was taken from the Catalogue of cataclysmic binaries, low-mass X-ray binaries and related objects (7th Edition, Release 7.21, March 2014) [15]. In total, I plotted 806 DNe, 106 novae and 98 NLs (32 of the UX UMa type, 31 of the VY Scl type, 29 of the SW Sex type, including 12 with low states, 3 IPs and 4 of the V Sge type)

1.1.2 Dwarf novae

Accretion disks in CVs can be thermally unstable (see e.g. [16]). The instability occurs at temperatures where hydrogen is ionizing in the accretion disc, which causes the increase of opacity. At quiescence, accreted matter is accumulating in the accretion disk until the critical temperature is reached at some radius, triggering the instability. At this point dwarf nova (DN) outburst starts. The heating fronts then propagate into the cold regions of the disk, leaving behind ionized material in which the turbulence and angular momentum transport are enhanced. The thermal–viscous accretion-disc instability model or disk instability model (DIM), which utilizes the α-prescription [17] to parametrize the turbulent viscosity (α is assumed to be higher in outbursts than in quiescence) is able to reproduce the main properties of DNe [18, 19]. Depending on where the outburst starts, in the inner or in the outer region of an accretion disk, it will be called "outside-in" or "inside-out" outburst. These outbursts have different light curve profiles and start at different wavelengths: "outside-in" outbursts start first at longer wavelengths and "inside-out" — at shorter ones. Each DN usually shows only one type of outbursts, however, inclination of the accretion disk results in accumulation of material in its inner regions and the "outside-in" outbursts will be temporary suppressed [20–22]. For example, ER UMa has periods of "outside-in" and "inside-out" outbursts and the latter ones correlate with appearance of negative superhumps, which are a light curve modulation due to a nodal precession of the inclined accretion disk [20, 22].

Some DNe show not only outbursts, but also superoutbursts with higher amplitudes. These systems are called SU UMa-type stars and depending on the superoutburst's recurrence times (supercycle length) are divided into two subtypes: ER UMa subtype, having very short supercycle lengths and WZ Sge subtype, which have superoutbursts once in several decades with amplitudes about 7 mag (see also fig. 1.1). The supercycle length depends on the mass transfer rate and measuring how it changes with time, one can trace the variations of $\dot{m}$ [22–25]. ER UMa-type stars, with their extremely frequent outbursts and superoutbursts have the highest mass transfer rate among DNe.

SU UMa-type stars also show modulation of their light curves with periods a few percent longer than the orbital. If accretion disk is large enough and if the mass ratio of the binary components ($q = M_*/M_{\rm WD}$) is lower than 0.35, the disk edge can reach the 3:1 resonance radius and start to precess due to the tidal torque from the secondary [26]. Since the precession periods are of the order of days, the beat periods between them and the orbital ones are few percent longer. The resultant modulation of optical light curves with these beat periods is called positive superhumps (in contrast to negative superhumps, which have periods few percent shorter). This combination of the thermal and tidal effects is described by the thermal-tidal instability model (TTI) model [27].

The recent Kepler observations have shown that the TTI model successfully explains the behaviour of SU UMa-type DNe, including the change of the superhump period along the supercycle [28–30].

1.1.3 Nova-like stars

Nova-like (NL) stars are a group of CVs characterised by the absence of DN outbursts. The absence of DN outbursts indicates that the accretion disk in a NL star is in a stable, hot state, which prevents formation of the thermal-viscous instability. This requires a significantly high mass transfer rate of $\sim 10^{-8}$ $M_{\odot}yr^{-1}$, which was indeed confirmed observationally and is also supported by the temperature estimates of their WDs [31], [32]. On the other hand, accretion disks in NLs do not perfectly match the standard stable disk scenario (when the mass accretion rate is constant throughout the disc). Thus Rutten et al. [33] found that the radial temperature dependence in the inner regions of accretion disks in several NLs is flatter than the predicted $T\sim R^{-3/4}$ [33, 34]. This may indicate that the central regions of the disks release part of the accretion energy in a non-radiative form. A departure from the canonical steady-state profile was found also in the infrared (IR) and can be caused by bremsstrahlung emission or circumbinary dust [35].

According to the International Variable Star Index (VSX)[1], there are 136 NL systems, which can be subdivided into several groups according to their observational properties (see fig. 1.1). The existing classification of NLs is somewhat tricky since different types of NLs are defined according to different criteria, spectroscopic ones for the SW Sex-type NLs, photometric ones for the VY Scl type, and the X-ray properties for the V Sge type, and there are significant overlaps of characteristics. In addition, there are NLs that have never been observed to show specific properties of the aforementioned groups and are called UX UMa-type NLs.

From fig. 1.2 it can bee seen that NLs are clustered near the right edge of the period gap, and are the dominant population in the period range of 3 – 3.5 h. The bottom panel shows the orbital period distribution of NLs of different types. The white columns represent the total number of NLs, the green are UX UMa-type NLs, the black hatched are VY Scl-type stars (excluding those that also belong to the SW Sex-type), the purple are SW Sex, including those with low states, the blue hatched are NLs with magnetic WDs (intermediate polars), and the red hatched are V Sge-type NLs. For the SW Sex-type NLs I referred to the The Big List of SW Sextantis Stars (v5.1.1 – May 2015) [36][2]. The list of V Sge-type stars is presented in Oliveira et al. [37]. NL/IPs are LS Peg [38],

[1] https://www.aavso.org/vsx/

[2] See D. W. Hoard's Big List of SW Sextantis Stars at http://www.dwhoard.com/biglist.

V795 Her [39] and DW Cnc [40]. In total, I plotted 98 NLs (32 of the UX UMa type, 31 – VY Scl type, 29 – SW Sex type, including 12 with low states, 3 IPs and 4 of the V Sge type)

1.1.3.1 VY Scl-type stars and their low states

Some NLs show so-called low states, which are sudden drops of optical magnitude by more than 1.5 mag on a time-scale of less than 150 days [41]. So far, about 30 NLs with low sates are known (see the VSX catalog and also Ritter and Kolb [15]). These low states can be as deep as 7 mag and last for years (e.g. the low states in TT Ari). The drop of luminosity is associated with a sudden decrease of the mass transfer rate from the secondary. Two explanations of this phenomenon have been proposed: the appearance of star spots on the surface of the secondary drifting around the L1 point [42] and shielding of the WD radiation by the accretion disk, which can suppress the irradiation-driven mass transfer [43]. The secondary's stellar spots scenario is the most widely accepted. It can also explain the shape of light curves during the transition from the high to the low state. Honeycutt and Kafka [41] noticed that about 40% of the low states from their sample had dual slopes (transitions occurred in two steps, from a high to intermediate and then from the intermediate to a low state) while the rest had single slopes. This distribution is consistent with that of the diameters of umbra and penumbra regions in a typical sunspot and indicates that dual slopes arise from crossing of both star spot umbra and penumbra, whereas single slopes arise from crossing only the penumbra region. However, low states can last for years and it is not clear what can make a star spot so stable and hold it around one place for such a long time.

The low states in NLs are very intriguing for several reasons. Although a decrease of the mass transfer rate from the secondary should move the accretion disk from the stable and hot state to the zone of the DN instability, no DN outbursts were observed neither during low nor intermediate states [44]. Even if the mass transfer rate is switched off, there should be enough material left in the accretion disk for several dwarf nova eruptions. Leach et al. [45] proposed that a moderately hot WD (40 000 K) can irradiate the accretion disk, preventing the thermal-viscous instability, however this requires fine tuning [46]. Another explanation involves a magnetic WD, whose magnetosphere truncates the inner region of the accretion disk, preventing "inside-out" outbursts [46]. In fact, both these scenarios can work. Far ultraviolet (FUV) observations indeed show that the WDs in NLs have temperatures of 33 000 – 50 000 K [31, 32] and there are also several indications that these systems are weakly magnetic[3].

[3] The Magnetic Scenario for the SW Sextantis Stars http://www.dwhoard.com/biglist/magnetic.

Another question to answer is what happens with the accretion disks during low states. Some eclipsing NLs show shrinking of the accretion disks (see e.g. Stanishev et al. [47] for DW UMa), while other systems do not [48]. Zemko and Kato [49] attempted to measure the accretion disk radius change in TT Ari during its last transition to the low state following the period of negative superhumps, and showed that the accretion disk shrank by at least 15%.

The low states are also important for the CV evolution. The high state accretion disk is the dominant source of light in a NL system, outshining both binary components. Only during the low states can the WD be observed directly, allowing a measurement of its surface effective temperature and the long-term mass transfer rate.

1.1.3.2 SW Sex-type stars

The group of SW Sex-type stars is distinguished by their spectroscopic characteristics. Originally, SW Sex-type stars were defined as eclipsing binary systems, which show single-peak emission lines in their spectra in contrast to what is expected from a highly inclined accretion disk in Keplerian rotation [50]. These objects also show strong He II λ4686 emission, high velocity line wings and transient absorption features at orbital phase 0.5 [50]. Although single-peak emission lines are the most important characteristics of SW Sex stars, in the most current classification SW Sex are not only systems with high orbital inclination. The second classification criterium is an orbital phase offset of 0.1–0.2 cycles in the emission-line radial velocity curves with respect to the photometric ephemeris [51]. So far there are 30 confirmed SW Sex-type NLs and 40 more candidates[4]. 12 out of 30 confirmed SW Sex members also belong to the group of VY Scl-type stars since they undergo low states.

Although the high mass transfer rate in NLs should make them significantly bright in X-rays, many SW Sex-type stars are faint or not detected at all. This can be due to the intrinsic absorption, which is especially important for the soft X-rays (see Hoard et al. [52] and the *ROSAT* All Sky Survey). Since SW Sex stars are mostly high inclination systems, they can also be faint in X-rays due to absorption by the accretion disk, which is viewed almost edge-on.

1.1.3.3 V Sge

The less numerous and the most puzzling group of NLs are the V Sge-type stars. Steiner and Diaz [53] proposed that these stars have very high mass transfer rate ($\sim 10^{-7}$ $M_\odot$

[4] See D. W. Hoard's Big List of SW Sextantis Stars at http://www.dwhoard.com/biglist [36]

yr^{-1}), occurring on a thermal time-scale, which results in a hydrostatic nuclear burning on the surfaces of their WDs. Such hydrogen burning would result in luminous soft X-ray emission, which is not observed, but this may be because of the intrinsic (wind) and interstellar absorption (for more details see Steiner and Diaz [53] and Patterson et al. [54]). There are three known members of the V Sge group apart from the prototype itself: V617 Sgr, WX Cen and QU Car (the latter is a candidate) [37]. Their defining properties are high-ionization emission lines of O `VI` and N `V`, the equivalent widths ratio EW(He II 4686 A)/EW(Hβ)>2, the lack or weakness of He I lines and P Cyg profiles, which is a signature of a strong wind. Compared with the orbital periods of other NLs, those of V Sge-type stars are long: $\sim$ 5 – 12 h (see also fig. 1.2). The orbital light curves are either low-amplitude sinusoidal or high-amplitude asymmetric, with primary and secondary eclipses. They also show high/low states, with amplitudes smaller than those of VY Scl-type stars. The atmospheric absorption features from the secondary are not observed in these systems.

1.1.3.4 Ultraviolet observations and the evolution status of NLs

FUV observations allow an estimate of the WD temperature in a NL, which correlates with the time-averaged accretion rate. Many UV and FUV observations have shown that the WDs in NLs can be as hot as 50 000 K. Townsley and Gänsicke [55] plotted the T_{eff}-P_{orb} diagram and found that NLs do not fit the general trend of non-magnetic CVs in the same range of the orbital periods and have higher temperatures than what is expected from accretion driven by magnetic braking. The authors proposed that NLs represent an exceptional stage of CV evolution and were probably born with the 3 – 4 h orbital periods. However, Schmidtobreick [56] noticed that almost all eclipsing CVs in this period range are SW Sex stars and suggested that CVs crossing this 3 – 4 h stripe during their evolution from longer to shorter orbital periods can show properties of SW Sex stars. The fact that old novae with the same range of orbital periods have much lower mass transfer rate and spectroscopic characteristics similar to those of DNe rather than those of NLs may be the result of the response of the secondary to the nova explosion (a variation of the hibernation model) [57]. So far, there are only two old novae (BT Mon and V533 Her) among the confirmed SW Sex stars and V630 Sgr is a nova and VY Scl-type candidate [58]. Mass transfer rates in NLs are closer to those of recurrent novae, but NLs do not undergo recurrent nova explosions.

1.1.4 Magnetic CVs

Different studies indicate that 20-25% of CVs may host magnetic WDs (see Ferrario et al. [59] for a review). Depending on the magnetic field strength magnetic CVs (MCVs) are observed as "intermediate polars" (B$\sim 10^{0.5} - 1^{1.5}$MG) or "polars" (B$\sim 10^{0.7} - 1^{2.5}$MG). In polars the magnetic field is strong enough to lock the two components of a binary system and to prevent formation of the accretion disk. The accretion stream is channeled by the magnetic field lines onto the WD polar caps directly from the L1 point, or even from the surface of the secondary. In IPs, instead, the accretion disk forms, but it is truncated at the radius where the ram pressure of the matter in the disk is equal to the magnetic pressure of the WD's magnetic field (the Alfvén radius).

WDs in IPs are not synchronized and since the magnetic axes of WDs are in general inclined with respect to their rotation axes, the asynchronous primary is an *oblique rotator*. X-ray flux modulation with the WD spin period is one of the main observational properties of IPs. Because of the torque of the accretion flow, the WD spin periods in IPs are shorter than the orbital ones. In the P_{orb}–P_{spin} digram the majority of IPs lie below the $P_{orb}=10\times P_{spin}$ line, and have orbital periods between 3 and 10 h[5], while polars in average show orbital periods shorter than 4 h. By now, 110 polars and 49 intermediate polars were discovered and there are also 58 IP candidates.

Magnetic field lines channel accretion on to a small fraction of the WD surface near the magnetic poles, where a strong shock occurs, since in order to be accreted the infalling material must be first decelerated to subsonic velocities. The resulting configuration is called "accretion column". The hot, dense, subsonic, post-shock gas cools mostly via bremsstrahlung continuum and K and L shell line emission as it settles onto the WD. A part of this radiation is intercepted by the WD surface and then re-emitted with a continuum that can be roughly approximated with a blackbody. A blackbody component with temperature in the range 20–100 eV is observed in many IPs [60–62]. These objects constitute a group of so-called "soft IPs".

The maximum temperature of the post-shock plasma is an important parameter for an IP, since it allows us to determine the WD mass. Under the assumption of a small shock height and the pre-shock gas having the free-fall velocity ($\upsilon_{\rm ff}$) the shock temperature is:

$$kT_{\rm s} = \frac{3}{8}\frac{GM}{R}\mu m_{\rm H} \quad [\rm keV] \tag{1.1}$$

[63], where $m_{\rm H}$ is the mass of the hydrogen atom, and μ is the mean molecular weight.

[5] see http://asd.gsfc.nasa.gov/Koji.Mukai/iphome/catalog/alpha.html

Strictly speaking the velocity of the accreted mass is not $v_{\rm ff}$, since it does not fall from infinity but from the Alfvén radius ($R_{\rm A}$), which in turn depends on the mass accretion rate. This is particularly important for systems with small magnetospheres and with variable mass transfer, for example for magnetic DNe or magnetic systems with low states. This effect changes the derived WD mass by a factor of:

$$M_{\rm WD}(R_{\rm A}) = M_{\rm WD}(\infty)\left(1 - \frac{R_{\rm WD}}{R_{\rm A}}\right) \tag{1.2}$$

[64].

An interesting question to answer is how the WD magnetic field influences the frequency and the mechanism of nova explosion. Several possible effects of the magnetic field were proposed (for the discussion see Shore et al. [65]):

- Because of the disruption of the accretion disk, shear mixing can be inhibited [66]. Shear mixing can play an important role in the enrichment of the envelope by heavy elements, which influences the nova speed class. In this result, a nova explosion in a magnetic system is expected to be less strong and to have longer t_3.
- The magnetic field strength $\sim 10^8$ G can suppress convection during the TNR, affecting the optical light curve.
- Collimation and acceleration of the plasma in the emitting envelope by the magnetic field can result in a faster development of the nova explosion.
- The magnetic field can change the morphology of the nova ejecta.
- IP nova systems can enter the regime of centrifugal magnetic rotators, in which all the accreted envelope will be ejected, independently of the conditions of the thermonuclear burning [67].

Before this work, only three novae were detected in magnetic CVs (one in a polar, V1500 Cyg, and two in IPs, GK Per and DQ Her) and there are also several IP candidates among novae (V4743 Sgr, V2491 Cyg, V1425 Cyg, V533 Her, V842 Cen). All the confirmed magnetic novae were indeed fast or moderately fast, but DQ Her had high metallicity in the ejecta, in contrast to the predictions. In order to reveal the possible differences between the magnetic and non-magnetic novae better statistics are required.

1.2 Relation to the Supernovae type Ia

Type Ia Supernovae (SNe Ia) are thermonuclear explosions of a C+O WD [68]. The majority of the proposed scenarios for SN Ia involve a WD in a binary system, however

some of them require also a third body [69], while some show that the explosion can be produced in an isolated WD [70, 71].

The proposed mechanisms for the formation of SNe Ia in binary systems can be roughly divided into three classes: single degenerate (SD) scenario, where the progenitors are CVs or symbiotic systems [72, 73], double degenerate (DD) scenario, which involves merging of two WDs [74, 75] and core degenerate (CD) scenario in which a WD merges with an asymptotic giant branch (AGB) star [76].

In the SD scenario a WD accretes material from the non-degenerate companion until the Chandrasekhar mass is reached. The main difficulty of this scenario is that in order to grow in mass a WD needs to avoid nova explosions or at least reduce somehow the amount of the ejected material. During each nova explosion a WD can eject all the material that was accreted in quiescence or even some part of matter from the WD itself [3]. There are two main possibilities to overcome this obstacle. The first one is based on calculations that show that the shorter is the recurrence time of nova explosions the less material is ejected [3]. Short recurrence times have massive WDs, accreting at high rates. The second option involves stable hydrogen burning on the surface of a WD, which can occur in a certain ranges of WD mass and accretion rates. In this case all the material transfered from the secondary can be accreted by the WD without triggering a nova explosion. Such systems would be observed as persistent SSS and are of particular importance for the CV evolution.

1.3 Motivation

This PhD project is devoted to observational study of systems that may become Supernova type Ia progenitors. I focused on CVs, hosting massive and/or accreting at a high rate white dwarfs. The aims were to detect signatures of quiescent hydrogen burning, follow high WD-mass novae as they settle into quiescence and to assess whether the WD magnetic field alters secular evolution and the outcome of the nova explosions.

1.4 Methods

The majority of the analysed data are X-ray observations from different instruments. The *Swift*, *SUZAKU* and *ROSAT* X-ray data were processed and analysed using the standard `ftools` package in `HEASOFT` (v.6-13 in Chapter 1 and v.6-14 in Chapter 2 and 3). I read the event files with `xselect`. The detector and mirror responses were either downloaded from the calibration databases or generated using appropriate tools (`xrtmkarf`

for the *Swift* XRT, `xisarfgen` and `xisrmfgen` for *SUZAKU*). For the *SUZAKU* I combined the XIS 0 and XIS 3 data from the front-illuminated (FI) CCD chips taken in 3x3 and 5x5 modes using `addascaspec` tool. The FI CCD spectra and the back-illuminated (BI) CCD spectra (from the XIS 1 detector) were analysed separately. The *Chandra* ACIS-S+HETG grating spectra were extracted with `CIAO` version 4.3. Where it was necessary to combine different partial exposures of the *Chandra* HETG observations the `addascaspec` tool was used. The spectral analysis of the X-ray data was performed with `xspec`. Background subtraction and binning of the X-ray light curves were performed with the `xronos` sub-package of `ftools` after the barycentric corrections.

Optical spectroscopic observations were processes using the standard procedure (bias and dark correction, flat field subtraction, lines calibration etc.) in `IRAF`.

Optical photometric observations were processed with `IRAF/DAOPHOT`.

I used the R software[6] for the timing analysis and plotting purposes.

1.4.1 X-ray spectral models

For the analysis of the X-ray spectra I used several models:

- The `apec` model, representing emission from an optically thin plasma plasma in collisional-ionization equilibrium (CIE), calculated using the `atomdb` code v2.0.2. The normalization constant of the model gives the emission measure. Its variation, `vapec`, is the same model but with variable abundances of individual elements. Another modification, `bvapec`, also accounts for the emission line broadening. Since in both magnetic and non-magnetic accreting WDs the X-ray emission originates from a multi-temperature plasma in CIE, a two-temperature `apec` model is a good approximation for the majority of low-resolution X-ray spectra. The same model can be applied to post-shock plasma originating in colliding winds.

- `mkcflow`, a model that calculates a stationary cooling post-shock plasma in CIE with a range of temperatures. The emissivity function is the inverse of the bolometric luminosity. This model was originally created for clusters of galaxies [77] but Mukai et al. [78] have shown that it can also be used for CVs. The model's normalization constant gives the mass accretion rate, but it also depends on the distance. `vmcflow` model is a modification of the `mkcflow` with variable abundances of individual elements.

[6] The R Foundation for Statistical Computing <http://cran.r-project.org/>.

- Tabulated Tübingen Non Local Thermal Equilibrium Atmosphere Model (NLTE TMAP) for a WD atmosphere in spherical or plane-parallel geometry in hydrostatic and radiative equilibrium, described by Rauch and Deetjen [79], with chemical composition of elements from H to Ni #007. This grid of models describes emission from a hot WD atmosphere, heated, for example, by the underlying nuclear burning.

- A blackbody to represent emission from the WD atmosphere, heated by the accretion column.

1.4.2 Timing analysis

The timing analysis was performed with three methods:

- Fourier transform, using the `Period04` program. Fourier transform is important for "blind search" of periodicities in a broad range of periods.

- Lomb-Scargle method [80] using the `lomb` package in R. The Lomb-Scargle (LS) method is a modification of the Fourier transform based on a least squares fit of sinusoids to data samples. The advantage of the LS method with respect to the Fourier transform is that the height of a peak in a periodogram depends also on the data quality: the better the data are, the more prominent is the peak. The significance of a single peak is determined in comparison with the 0.3% false alarm probability level, which is based on an exponential distribution. Where it was necessary to additionally check the significance of the periodicity I also applied the bootstrap method, repeatedly scrambling the data 10000 times and calculating the probability that random peaks in Lomb-Scargle periodogram (LSP) exceed the hight of the main peak in the original LSP. The 1σ error for a period was estimated from the Gaussian fit of corresponding peak in the LSP.

- The Phase Dispersion Minimization (PDM) method [81]. The PDM utilizes a different from Fourier transform technique, which involves guessing a trial period, folding the light curve with this period and calculating the variance of the amplitude of the folded light curve. The 1σ errors were estimated by the method of Fernie [82] and Kato et al. [83]. PDM is particularly useful in case of non-sinusoidal variations.

Chapter 2

X-ray observations of VY Scl-type nova-like binaries in the high and low state

Some authors hypothesized that during the low states of VY Scl-type stars hydrogen burning is briefly ignited, but it is immediately quenched avoiding outflows in nova outbursts, and allowing the white dwarf to grow steadily in mass towards the Chandrasekhar value. I analysed all the available archival X-ray observations of VY Scl-type NLs in their low and high states in order to find observational confirmation of the hypothesized shell hydrogen burning. This work was published in Zemko et al. [84]. The co-authors are Dr. M. Orio, Dr. K. Mukai and Dr. S. Shugarov.

2.1 Introduction

Greiner et al. [85] found an anti-correlation in the optical and X-ray intensity in a VY Scl-type star — V751 Cyg — and proposed that this object can burn hydrogen quietly during low states. Greiner and Teeseling [86] and Greiner et al. [87] also suggested that thermonuclear burning occurs in the low states of V Sge and BZ Cam, implying that they may periodically become super soft X-ray sources. The hydrogen burning scenario was also supported by the observations in other wavelengths. Hachisu and Kato [88] explained the orbital curves and high/low state transitions of V Sge with an optically thick, massive wind, completely obscuring the soft X-rays. Honeycutt [89] noticed that during the high states many NLs show so-called "stunted" outbursts, which may be normal thermal instabilities in the accretion disk occurring at steady background luminosity, resulting from nuclear burning on the WD surface. Patterson et al. [54] found

TABLE 2.1: Binary parameters

	BZ Cam	MV Lyr	TT Ari	V794 Aql
Dist. (pc)	830±160[1]	505±50[3]	335±50[7]	690±100[10]
$P_{orb}(d)$	0.1536[2]	0.1329[4]	0.1375[8]	0.1533[11]
i^o	12–40[1]	10–13[4]	17–22[9]	60[10]
$M_{WD}(M_\odot)$		$0.7\pm0.1^{[3]}_{\texttt{FUV}}$	$0.57–1.2^{[9]}_{\texttt{Opt}}$	0.88±0.39[10]
$\dot{m}_{High}{}^a$		$2–3_{\texttt{FUV,Opt}}{}^{[5],[6]}$	$11_{\texttt{Opt}}{}^{[9]}$	$3.2–10_{\texttt{FUV}}{}^{[10]}$
$\dot{m}_{Low}{}^b$		$0.03_{\texttt{Opt}}{}^{[3]}$	$0.1–1_{\texttt{UV}}{}^{[7]}$	
$T_{WD\ High}$ (K)		$\geq 50000^{[5]}_{\texttt{FUV}}$		
$T_{WD\ Low}$ (K)		$47000^{[3]}_{\texttt{FUV}}$	$39000^{[7]}_{\texttt{UV}}$	$45000^{[10]}_{\texttt{FUV}}$
$T_{Disk\ Low}$ (K)		$< 2500^{[6]}_{\texttt{FUV}}$		
FUV $Flux_{High}$		1.4×10^{-10}[5]^c	7.8×10^{-10}[12]^c	
FUV $Flux_{Low}$		9.4×10^{-12}[3]^d		

Notes: FUV, UV, Opt — values obtained from Far *UV*, *UV* and optical observations, respectively.
$^a\times10^{-9}M_\odot$ yr^{-1}, $^b\times10^{-15}M_\odot$yr^{-1}, ^{c}erg cm^{-2} s^{-1} *FUV* flux was evaluated from the mean continuum level of a spectrum in a rage 910–1190Å. ^{d}erg cm^{-2} s^{-1} *FUV* flux was evaluated from the mean continuum level of a spectrum in a rage 920–1180Å.

[1]Ringwald and Naylor [90], [2]Patterson et al. [91], [3]Hoard et al. [31], [4]Skillman et al. [92], [5]Godon and Sion [93], [6]Linnell et al. [94], [7]Gänsicke et al. [32], [8]Thorstensen et al. [95], [9]Belyakov et al. [96], [10]Godon et al. [97], [11]Honeycutt and Robertson [98], [12]Hutchings and Cowley [99]

that V Sge is optically very luminous and there must be a strong ionizing source in the system. Moreover, a hot hydrogen burning WD can heat the accretion disk and prevent the thermal instability, explaining the absence of DN outbursts in VY Scl-type stars. If the WDs in NLs burn hydrogen quietly without triggering a thermonuclear runaway, these objects are of particular importance for the evolution since they can reach the Chandrasekhar mass and the conditions for type Ia supernovae outbursts.

However, the X-ray observations of both V751 Cyg and V Sge, performed with the *ROSAT* High Resolution Imager (HRI)[1], did not offer the spectral resolution that is necessary to draw conclusions on the hardness of the X-ray spectrum. In more recent years an X-ray observation of the VY Scl system V504 Cyg in the low state failed to reveal a luminous SSS [100].

Using archival X-ray observations I compare high and low state X-ray data, and some new *UV* data, for four VY Scl-type stars. I seek observational confirmation of the hypothesized surface hydrogen burning in these systems.

[1] *ROSAT* HRI has a high time resolution but negligible energy resolution.

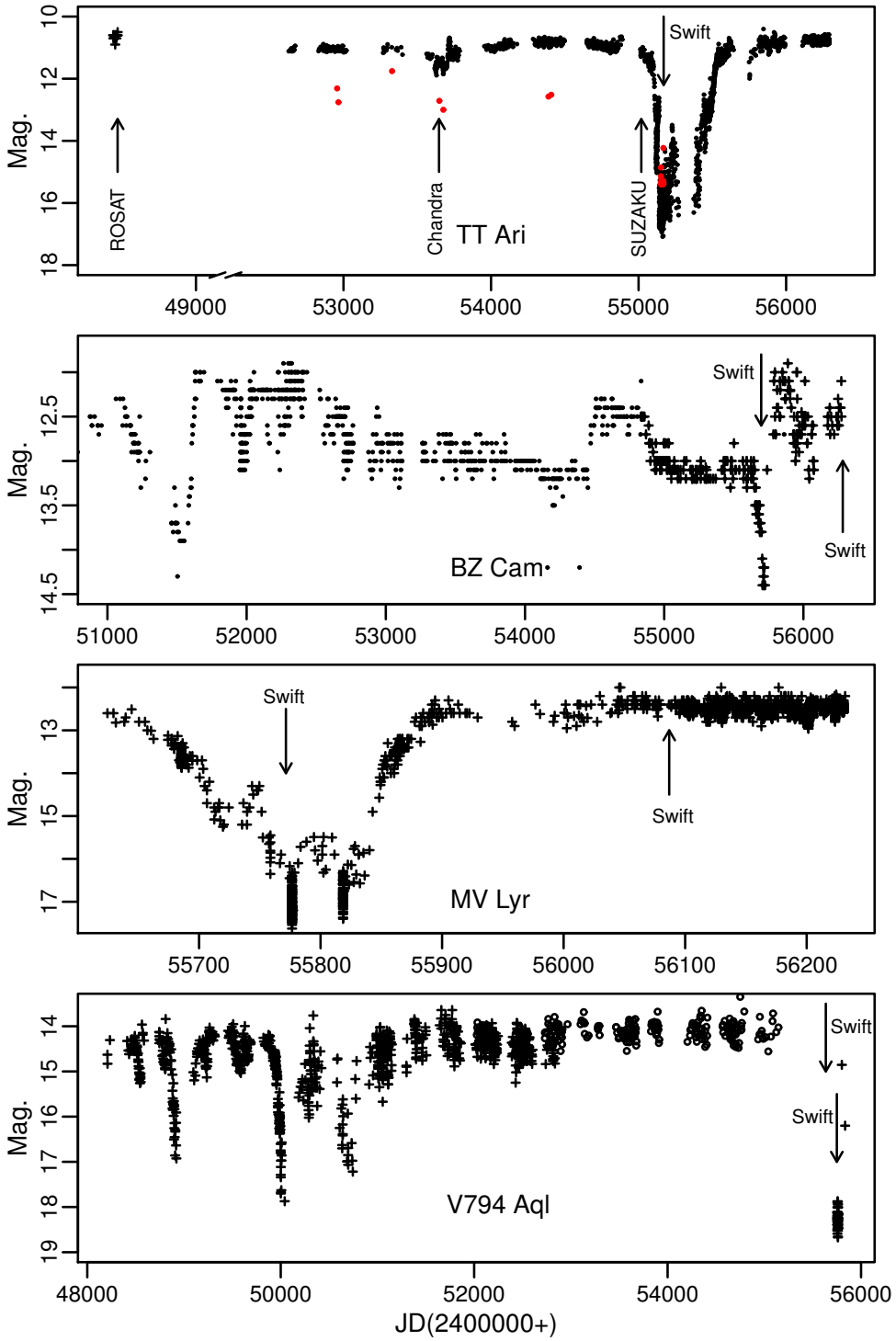

FIGURE 2.1: Light curves of TT Ari, BZ Cam, MV Lyr and V794 Aql (from top to bottom) obtained from the AAVSO (crosses), VSNET (filled circles) collaboration and ASAS (open circles) data. The times of the X-ray observations are marked with arrows. The red points represent the GALEX observations.

2.2 Previous optical and *UV* observations

In table 2.1 I report parameters from the published results of observations in the optical, near (*NUV*) and far (*FUV*) ultraviolet wavelength ranges. These objects have orbital periods just above the period gap, in a narrow range between 3.2 and 3.7 hours. For the three systems MV Lyr, TT Ari and V794 Aql the WD effective temperature T_{eff} was estimated in previous low states (not shown in fig. 2.1) from *UV* and *FUV* observations, to be in the range between 39 000 K and 47 000 K. These systems could not have been SSS at the time of those observations, because T_{eff} places the flux peak in the *FUV* range. On the other hand, we cannot rule out ignition of thermonuclear burning, neither the possibility that the WD may become hotter with time in subsequent low states. It should be emphasised that *FUV* observations most probably give only lower limits for the WD temperature and luminosity. An accurate determination of T_{eff} is important: even an upper limit inferred from the absence of an SSS in the X-rays is useful to constrain the evolutionary models.

2.3 Observations and data analysis

I examined the archival X-ray data of VY Scl-type stars obtained with *Swift*, *ROSAT*, *Suzaku* and *Chandra* and chose the objects that were observed both, in the high and low states: BZ Cam, MV Lyr, TT Ari and V794 Aql. The data are summarized in table 2.2. All the data were never published except for the *ROSAT* observations of TT Ari, which I examined again, but were also previously analysed by Baykal et al. [101] and van Teeseling et al. [102].

In order to assess when the low and high optical states occurred, I relied on the data of the VSNET Collaboration, AAVSO and ASAS databases. The optical light curves are presented in fig. 2.1. The epoch of the X-ray observation is marked with an arrow in each plot. I did not find optical data for V794 Aql around the epoch of the X-ray observations taken on 15 March 2011. However, from the photometric observations of the object before and after this date presented in Honeycutt et al. [103] it is reasonable to assume that V794 Aql was in the intermediate state during the X-ray observation.

2.4 Results

2.4.1 TT Ari

TT Arietis is one of the brightest CVs, usually between V magnitude 10 and 11. Sometimes it abruptly falls into an "intermediate state" at $V\simeq14$ or even into a "low state" decreasing to $V\simeq18$. According to Belyakov et al. [96] this binary system consists of a 0.57–1.2 $M_\odot$ white dwarf and a 0.18–0.38 $M_\odot$ secondary component of M 3.5±0.5 spectral type [32]. The only low state before the one discussed in this paper was observed in the years 1980–1985 [104, 105]. The first panel of fig. 2.1 shows the long term light-curve of TT Ari between 1990 and 2013. The optical brightness started to decline dramatically at the beginning of 2009 and the low state lasted for about 9 months, with a drop in optical luminosity of about 7 mag. However, in the low state the optical luminosity was not constant and showed variations between V=15 and V=18.

The high state X-ray spectrum of TT Ari was at first obtained by *EXOSAT* on 21/22 Aug 1985 [106]. The authors found that the X-ray flux in the range of 0.2 – 4.0 keV was about 1.9×10^{-11} erg cm^{-2} s^{-1}. They also proposed that there are two or more hot X-ray emitting regions and two or more cold absorbing or scattering regions in TT Ari. On 20/21 January 1994 TT Ari was also observed with *ASCA* with an effective exposure time of $\sim$ 14000 s. A detailed analysis of these data was performed by Baykal and Kiziloğlu [107]. One of the most interesting findings of the previous X-ray observations is the rapid variability of the X-ray flux, a quasi-periodic oscillations (QPO) with periods ranging between 15 and 26 minutes [101, 107]. I will show that QPO with periods in this range are observed in all the high state observations I examined. In 2005 the *Chandra* HETG spectra of TT Ari were obtained by C. Mauche (first shown in a presentation by Mauche, 2010[2]). Below I will discuss this set of observations in details.

2.4.1.1 The X-ray data: the high state

A set of four *Chandra* High Energy Transmission Gratings (HETG) exposures was obtained within 5 weeks in 2005 (for details see table 2.2). In the optical, the source was undergoing a 'shallow decline' from the average optical magnitude in the high state, from $V\simeq10.5$ to $V\leq11.5$. Since there was no significant flux or spectral variability between the different exposures, I shall describe the co-added MEG and HEG spectra, which are presented in fig. 2.2. The *Chandra* observations revealed a rich emission line spectrum, with strong lines of Mg, Si, Ne and S.

[2] http://cxc.harvard.edu/cdo/accr10/pres/Mauche_Chris.pdf

TABLE 2.2: Details of the *ROSAT*, *Swift*, *Suzaku* and *Chandra* observations of VY Scl-type nova-likes that were analysed.

Name	State	Date	Instrument	Exposure(s)	Count rate (cts s^{-1})
BZ Cam	High	21/12/2012	*Swift*-XRT	15001	0.0720 ± 0.0024
	Low	15/05/2011	*Swift*-XRT	2710	0.100 ± 0.006
MV Lyr	High	08/06/2012	*Swift*-XRT	7569	0.096 ± 0.003
	Low	29/07/2011	*Swift*-XRT	3282	0.039 ± 0.004
TT Ari	High	01/08/1991	*ROSAT*-PSPCB	24464	0.098 ± 0.007
	High	06/09/2005	*Chandra*-HEG	95362*	0.0266 ± 0.0003
	High	06/09/2005	*Chandra*-MEG	95362*	0.0588 ± 0.0005
	High	06/07/2009	*Suzaku*-XIS FI**	28617	0.671 ± 0.003
	High	06/07/2009	*Suzaku*-XIS BI**	28617	0.836 ± 0.005
	Intermediate	16/10/2009	*Swift*-XRT	4421	0.278 ± 0.008
	Low	22/11/2009	*Swift*-XRT	12030	0.0285 ± 0.0019
V794 Aql	Intermediate	15/03/2011	*Swift*-XRT	6148	0.176 ± 0.005
	Low	12/07/2011	*Swift*-XRT	4629	0.055 ± 0.003

*Four observations were taken with *Chandra* Medium Energy Grating (MEG) and High Energy Grating (HEG) on September 6 and October 4, 6 and 9 2005. **_Suzaku_- X-ray Imaging Spectrometer (XIS) FI – are XIS 0 and XIS 3 detectors with front-illuminated (FI) CCDs, while *Suzaku*-XIS BI is the XIS 1 that utilizes a back-illuminated (BI) CCD

The strongest lines of the *Chandra* Medium Energy Grating (MEG) spectrum are listed in table 2.3. For the H-like lines I evaluated the flux with a Gaussian fit to the line; I also estimated the flux in the He-like triplet lines using a three Gaussian fit, but this could only be done with larger uncertainty because the lines are blended (note that the intercombination lines are not resolved). Moreover, the triplets of He-like lines are observed in a region of the spectrum which is rich in other lines, like those due to transitions of Fe. Despite these difficulties, I performed the fit with three Gaussians for the triplets of Si XIII and Mg XI. I added a fourth line of Fe XVIII at 13.509 Å for Ne IX. I thus evaluated the R ratio f/i (intensity of the forbidden to the intercombination line) and the G ratio $\frac{(f+i)}{r}$ (where r is the intensity of the resonance line). I estimated an uncertainty of about 20% on both these ratios. I obtained R=0.63 and G=0.78 for Ne IX, R=0.36 and G=0.66 for Mg IX, R=0.33 and G=0.66 for Si XIII.

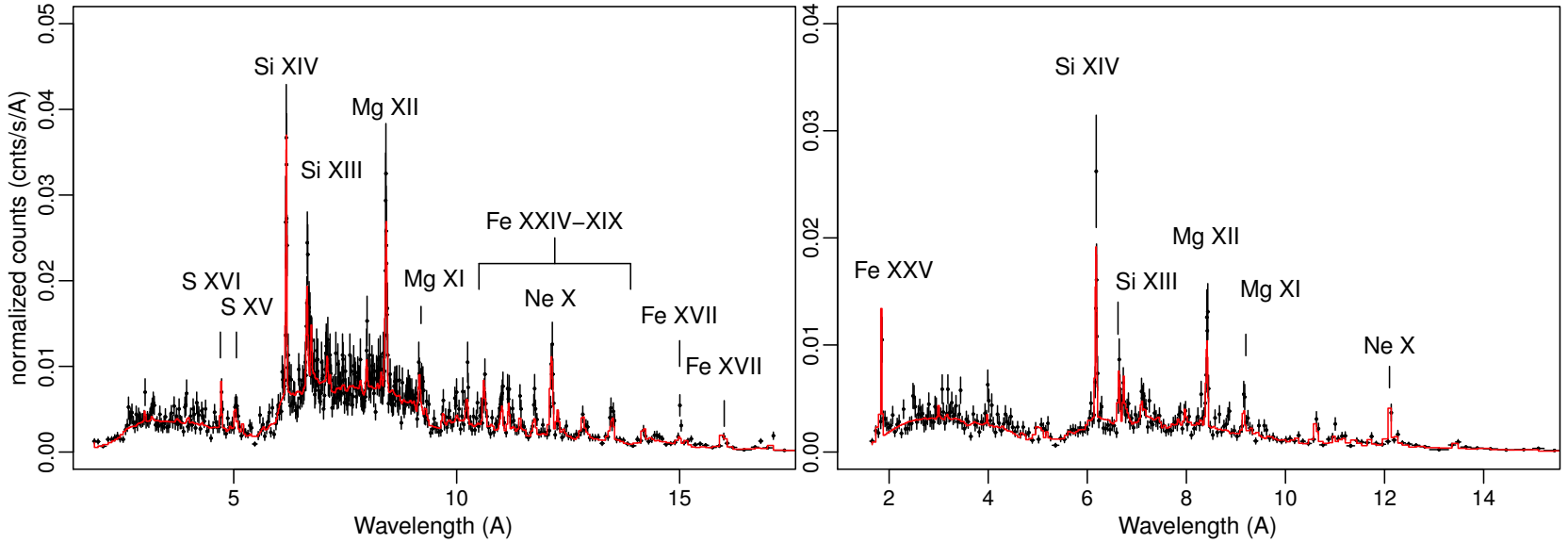

FIGURE 2.2: TT Ari spectra observed with the *Chandra* MEG (left) and HEG (right) grating. Four observations and +1 and -1 orders were summed. The red lines represent the fit with two `vapec` components. The emission lines are indicated.

TABLE 2.3: The wavelengths and fluxes in erg cm^{-2} s^{-1} $\times 10^{-14}$ of the emission lines identified in the summed *Chandra* MEG spectrum.

Element	E_{obs} (keV)	λ_{obs} (Å)	MEG flux$^{[1]}_{abs}$
S XV	2.4606^{r}	5.0387	2.8
	2.448^{i}	5.064	3.3
	2.4260^{f}	5.1106	3.4
Si XIV	$2.0061^{+0.0006}_{-0.0010}$	$6.1803^{+0.003}_{-0.0017}$	6.12
Si XIII	1.8650^{r}	6.6479	3.4
	1.854^{i}	6.687	1.7
	1.8396^{f}	6.6739	0.57
Mg XII	$1.4733^{+0.0003}_{-0.0011}$	$8.4154^{+0.006}_{-0.002}$	3.07
Mg XI	1.3522^{r}	9.1687	2.0
	1.3434^{i}	9.2291	1.6
	1.3312^{f}	9.3136	0.59
Ne X	$1.0211^{+0.0007}_{-0.0004}$	$12.142^{+0.005}_{-0.008}$	5.25
Ne IX	0.9220^{r}	13.44	3.3
	0.9149^{i}	13.55	1.8
	0.9051^{f}	13.69	0.59
Fe XVIII	0.8735	14.19	0.74
Fe XVII	$0.8256^{+0.0004}_{-0.0005}$	$15.017^{+0.008}_{-0.008}$	2.98
Fe XVII	$0.7388^{+0.0006}_{-0.0005}$	$16.781^{+0.014}_{-0.013}$	4.8

[1] For the calculation of the fluxes in the lines I assumed $N_{\rm H} = 0.06 \times 10^{22}$. r – resonance, i – intercombination and f – forbidden lines.

I consulted Porquet and Dubau [108], who explored the dependence of these ratios on electron density and plasma temperature. The authors assumed a photoionezed plasma, with or without additional collisional ionization. I see from their fig. 8 that the R ratios I obtained correspond to high density; I obtain a lower limit on the electron density $n_e = 10^{12}$ cm^{-3}, 10^{13} cm^{-3} and $\geq 10^{14}$ cm^{-3} for Ne, Mg and Si, respectively. However, it is known that the R ratios appears smaller, as if the density was higher than its actual value, when there is also photoexcitation by a strong *UV/EUV* source, exciting the f level electrons into the i level [108]. I do expect additional photoexcitation if the lines are produced very close to the hot and luminous WD of TT Ari, thus, the R ratio can be not a completely reliable indicator. The G ratio, on the other hand, is reliable and indicates plasma temperature $\geq 3 \times 10^6$ K, $\geq 4 \times 10^6$ K and $\geq 7 \times 10^6$ for Ne, Mg and Si, respectively.

The next step was to fit the observed spectra with a physical model. A fit with a single temperature plasma in collisional ionization equilibrium is not acceptable because of too high χ^2, but adding a second temperature I obtained a more reasonable fit, with χ^2=1.2. I adopted two `bvapec` models in `xspec` (see tab. 2.4 and fig. 2.2). By letting the abundances of single elements vary, I found the best fit with the following values for the abundances: [Ne/H]=6.3 ± 1.2, [Mg/H]=4.8 ± 0.8, [Si/H]=4.9 ± 0.9, [S/H]=11 ± 4,

[Fe/H]=1.46 ± 0.25, [O/H]=10 ± 4. The emission measure of the cooler component is 3.1×10^{53} cm^3 and the emission measure of the hotter component is 3.6 $\times10^{54}$ cm^3. I note that, if these two regions are related to accretion, for an electron density of order of 10^{14} cm^{-3} (the minimum electron density derived from the G ratio for Si), the linear dimension of the emission region is of order of 3.1 $\times10^8$ cm and 7.1 $\times10^8$ cm, respectively. This is, of course, an purely phenomelogical model; two large and distinct regions with different plasma temperature are difficult to explain in a physically realistic way.

With the `bvapec` model the emission lines are fitted with Gaussians and the width of the lines is parameterized differently for each of the two components (see table 2.4). This model gives the full width at half maximum of the emission lines about 1100 and 1500 km s^{-1}.

Mukai et al. [109] have shown that accretion in many CVs is best described by a stationary cooling flow model. I thus used the cooling flow `vmcflow` model in `xspec`. However, this fit yields a larger χ^2 value than the previous simplified model, and this is mainly because there is more flux in the He-like lines than predicted by the model. This may be due to additional photoionization, for instance in a wind from the system, implying that not all the X-ray flux is produced in the accretion flow. The main problem, however, is that the cooling flow model includes the mass accretion rate $\dot{m}$ as a parameter, but predicts a very low value for $\dot{m}$, only 3.48×10^{-11} M$_\odot$ yr^{-1}, while the UV and optical observations indicate 10^{-8} M$_\odot$ yr^{-1} for the high state $\dot{m}$ (see table 2.1). I thus conclude that either the observed X-ray flux does not originate in the accretion flow that produces the luminous accretion disk, or that accretion energy is mostly re-radiated in the *EUV* and not in the X-ray range.

The light curves of these *Chandra* exposures still show quasi periodic oscillations (QPOs), although the modulation has ≃21 min period. I will discuss below a similar light curve I extracted from an additional archival observation obtained with *Suzaku*, which has higher S/N.

Suzaku observations of TT Ari were obtained by K. Saitou in 2009 just before the low state (see the top panel of fig. 2.1). The average X-ray flux during this observation was higher by almost a factor of 2 than during the *Chandra* observation. In order to exclude the effect of a slightly different energy ranges of the detectors I compared the X-ray flux in the range 0.5–10.0 keV, common for both instruments. The difference between the X-ray flux measured with *Chandra* and *Suzaku* may be correlated with the optical one. The *Chandra* HETG observations were taken at the time when TT Ari was optically less luminous (≥ 1 mag).

TABLE 2.4: Fitting models and parameters for TT Ari. The errors represent 90% confidence region for a single parameter.

		high state				low state	
Satellite	*ROSAT*	*Chandra*		*Suzaku*		*Swift*	
Models	2 `apec`	2 `bvapec`	`vmcflow`	2 `vapec` +`gauss`*	`vmcflow` +`gauss`*	2 `apec`	`apec`
$N_{H1}{}^a$	$0.031^{+0.003}_{-0.003}$	$0.05^{+0.06}_{-0.05}$	$0.026^{+0.013}_{-0.015}$	$0.14^{+0.02}_{-0.02}$	$0.075^{+0.007}_{-0.010}$	$0.04^{+0.09}_{-0.04}$	$0.019^{+0.05}_{-0.019}$
$N_{H2}{}^a$		$0.12^{+0.03}_{-0.03}$					
T_1 (keV)	$0.89^{+0.09}_{-0.11}$	$0.93^{+0.03}_{-0.03}$		$0.80^{+0.13}_{-0.05}$		$0.7^{+0.3}_{-0.4}$	$3.4^{+1.4}_{-0.7}$
T_2 (keV)	25^{+25}_{-13}	$6.5^{+0.5}_{-0.4}$		$7.1^{+0.3}_{-0.3}$		$3.9^{+2.7}_{-1.0}$	
$\sigma_1{}^b$		650^{+80}_{-80}					
$\sigma_2{}^b$		460^{+120}_{-110}					
$EM_1{}^c$		$3.2^{+0.4}_{-0.3}$					
$EM_2{}^c$		$36.50^{+0.10}_{-0.10}$					
T_{min} (keV)			$0.20^{+0.03}_{-0.03}$		$0.120^{+0.016}_{-0.009}$		
T_{max} (keV)			$21.6^{+1.9}_{-1.4}$		$26.9^{+1.0}_{-1.5}$		
$\dot{m}^d$			$3.4^{+0.3}_{-0.2}$		$5.02^{+0.17}_{-0.11}$		
$Flux^e_{abs}$	$5.76^{+0.3}_{-0.13}$	$9.35^{+0.18}_{-0.27}$	$9.01^{+0.011}_{-0.3}$	$15.8^{+0.02}_{-0.02}$	$16.2^{+0.2}_{-0.3}$	$0.99^{+0.17}_{-0.18}$	$0.94^{+0.17}_{-0.18}$
$Flux^e_{unabs}$	$6.70^{+0.3}_{-0.13}$	$10.35^{+0.18}_{-0.27}$	$9.21^{+0.011}_{-0.3}$	$17.4^{+0.02}_{-0.02}$	$17.2^{+0.2}_{-0.3}$	$1.08^{+0.17}_{-0.18}$	$1.03^{+0.17}_{-0.18}$
χ^2	1.0	1.2	1.6	1.0	1.2	1.0	1.2

*I added a Gaussian at 6.41 keV in order to fit the Fe Kα iron reflection line in the *Suzaku* spectrum. $^a\times10^{22}$ cm^{-2}, ^{b}km s^{-1}, ^{c} emission measure $\times10^{53}$ cm^{-3}, $^d\times10^{-11}$ M$_\odot$ yr^{-1}, ^{e}the X-ray flux ($\times10^{-12}$erg cm^{-2} s^{-1}) was calculated in the following energy ranges: 0.2–2.5 keV for the *ROSAT* PSPC, 0.4–10.0 keV for the *Chandra* HETG, 0.5–12.0 keV for the *Suzaku* XIS FI and 0.3–10.0 keV for the *Swift* XRT

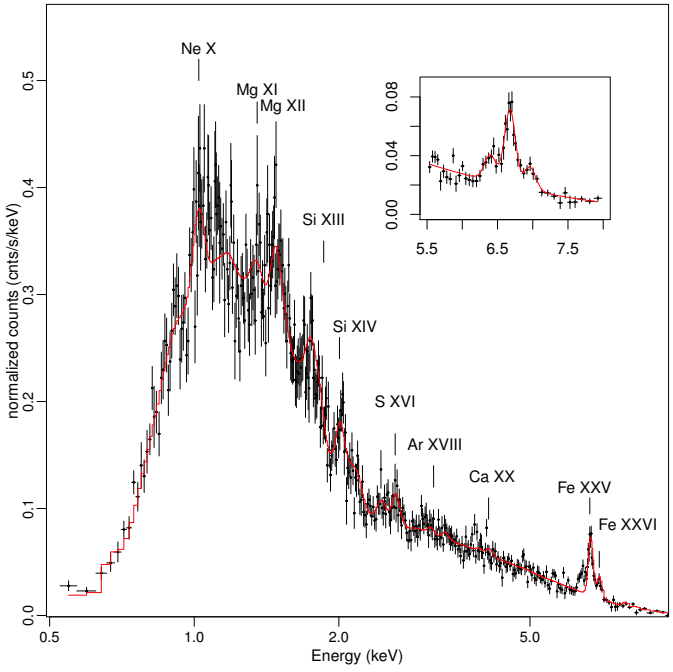

FIGURE 2.3: The spectrum observed with the *Suzaku* XIS FI detectors (the data from the XIS0 and XIS3 detectors taken in the 3x3 and 5x5 modes were summed). The red line shows the fit with two `vapec` components. The emission lines are indicated. The inset shows the Fe K emission lines at 6.41, 6.68 and 6.96 keV and their fit with three Gaussians.

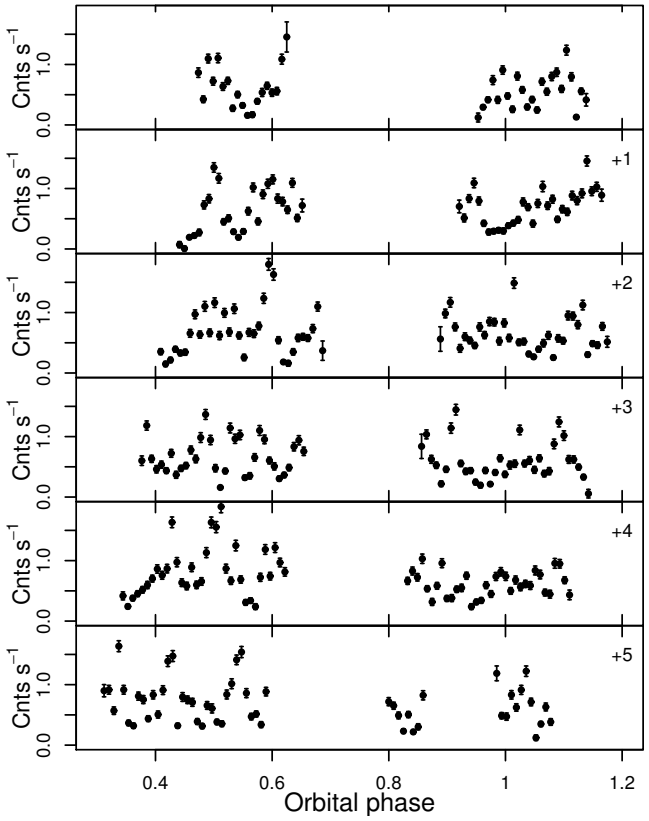

FIGURE 2.4: X-ray light curve of TT Ari, obtained by *Suzaku*, binned every 100 seconds. The horizontal axis is the orbital phase. The plots are in chronological order from top to bottom.

The broad band spectrum of TT Ari observed with *Suzaku* is presented in fig. 2.3. Emission lines of Ne, Mg and Si are clearly observed, like in the *Chandra* spectra, together with S, Fe XXV, and Fe XXVI lines. I fit this spectrum either with a two-component thermal plasma model with temperatures of 0.80 and 7.1 keV (for the details see table 2.4) and the abundances that were derived from the fit of the *Chandra* spectra. The residuals of the fit to the *Suzaku* spectrum indicate an extra line feature at 6.4 keV, which is the Fe Kα fluorescence line. In the inset in fig. 2.3 I show the fit of the 5.5–8.0 keV region with three Gaussians at 6.41, 6.68 and 6.96 keV. The equivalent width of the Fe K α line is 96^{+24}_{-24} eV. This line implies that the X-ray emission region is close to a 'cold' source, which may be the WD surface and/or an optically thick accretion disk.

The cooling flow model can be used also for the *Suzaku* spectrum because we do measure spectral lines to constrain the model. The fit is not optimal, and I run into the same problem of low $\dot{m}$.

The *Suzaku* light curve is shown in fig. 2.4 and is extremely similar to the light curve previously observed with *ROSAT* [101]. The data were integrated in bins of 100 s. The light curve shows QPOs, which have an amplitude of 50 %.

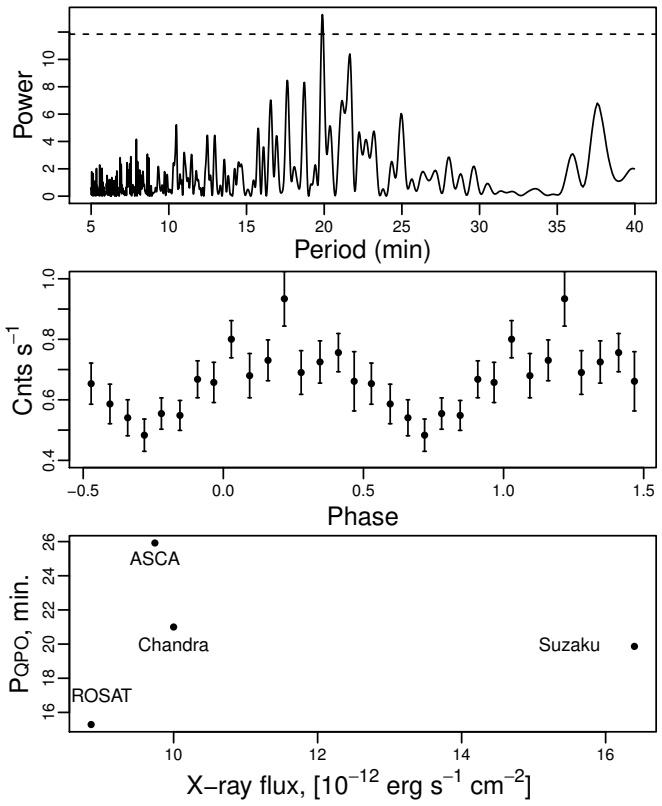

FIGURE 2.5: Top panel: the Lomb-Scargle periodogram of the *Suzaku* ligh curve of TT Ari. The horizontal dashed line shows the 0.3% false alarm probability level. The highest peak corresponds to the 19.9 min oscillations. Middle panel: phase folded *Suzaku* light curve with the 19.9 min period. Bottom panel: periods of the QPO and flux in the X-ray range 0.5–10.0 keV in the *ROSAT*, *ASCA*, *Chandra* and *Suzaku* observations. I assumed the values of Baykal and Kiziloğlu [107] for the *ASCA* observations and for the *ROSAT* X-ray flux. The period of the QPO observed with *ROSAT* was taken from Baykal et al. [101].

In fig. 2.5 I present the Lomb-Scargle periodogram [80] of the *Suzaku* light curve of TT Ari. The highest peak corresponds to the 19.9 min (0.84 mHz) period. According to Andronov et al. [110] at the time of the *Suzaku* observations TT Ari also showed QPOs at the optical range, with several peaks, at 2.5, 1.1 and 0.38 mHz. In Baykal et al. [101] the frequency of QPOs in X-ray was explained as the beat frequency between the Kepler frequency at the inner edge of the accretion disk and the WD's rotation period. Nevertheless, from the QPOs semi-periods measured by us in the *Chandra* and *Suzaku* observations and from those found by Baykal et al. [101] and Baykal and Kiziloğlu [107], no correlation emerges between the observed frequency of QPO and the X-ray flux of TT Ari (see the bottom panel of fig. 2.5).

In 1991 TT Ari was observed with *ROSAT* PSPC. The *ROSAT* X-ray spectrum is shown in fig. 2.6. Baykal et al. [101] found that the best-fitting model for this spectrum is an absorbed blackbody. I re-analysed the data and found that a blackbody fits only

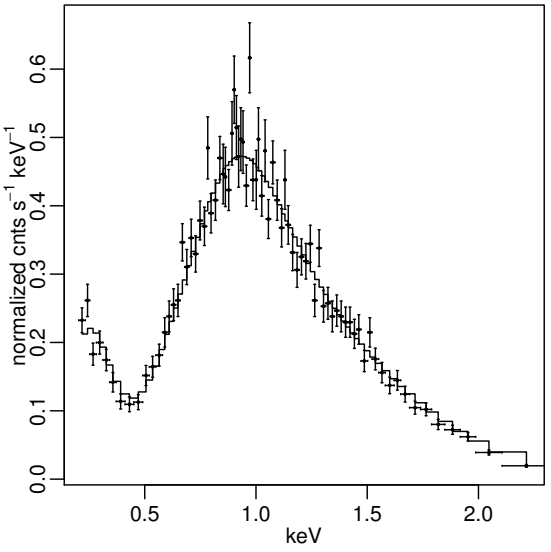

FIGURE 2.6: High state X-ray spectrum of TT Ari taken with *ROSAT* PSPC.

the soft part of the spectrum (the *ROSAT* energy range is 0.2–2.4 keV) and for more sophisticated fit I need a two-component thermal plasma model. The parameters of the best fitting model are presented in table 2.4.

2.4.1.2 The X-ray data: the low state

In the intermediate and low state TT Ari was observed with *Swift*. The observations in the intermediate state were presented by Mukai et al. [111]. The unabsorbed flux was about the same as during the *Suzaku* observation, 1.5×10^{-11} ergs cm^{-2} s^{-1}, the spectrum could only be fitted with a multi-temperature plasma, and a new quasiperiod of 0.4 days was also measured in optical.

The low state spectrum, presented in the top panel of fig. 2.9, is best fitted with two components of absorbed thermal plasma in collisional ionization equilibrium with a fixed metallicity (`apec` model) at 0.7 keV and 3.9 keV, respectively. I set the metallicity to the solar value because of the poorer data quality of this dataset. The low state X-ray flux appeared to be about ten times smaller than that in the high and intermediate state, and definitely no luminous supersoft X-ray phase was detected.

2.4.1.3 UV data

In the first panel of fig. 2.1, in addition to the optical light curve of TT Ari, the red points show the *GALEX* near *UV* (*NUV*) observations. In table 2.6 I give exposure times and the mean AB magnitudes in the *U*/*UV* filters during the low and high states.

The amplitude of the low to high state transition in *NUV* was much lower than in optical: 3 versus 7 magnitudes. Like in the optical range, TT Ari shows flaring activity in the *NUV*, with amplitudes up to 1 mag. However, the *UV* and optical flares occur at different times, and do not appear to correlated, neither anti-correlated.

2.4.2 BZ Cam

BZ Cam shows brightness variations around an average value $V = 12$–13, with rare occasional transitions to low states with $V = 14$–14.5. Besides the low state studied here, two additional low states were detected – in 1928 and at the beginning of 2000 ([112] and [87], respectively). BZ Cam is surrounded by a bright emission nebula with a bow-shock structure, first detected by Ellis et al. [113] and also studied by Krautter et al. [114], Hollis et al. [115], and Greiner et al. [87]. Hollis et al. [115] proposed that the bow shock structure is due to the interactions of the wind of BZ Cam with the interstellar medium. The wind in BZ Cam was also studied by Honeycutt et al. [116]. Greiner et al. [87] suggested that this nebula is photoionized by a bright central object that must be a super soft X-ray source, while the bow shock structure is due to the high proper motion of BZ Cam, moving while it emits the wind.

2.4.2.1 The X-ray data

The second plot of fig. 2.9 shows the X-ray spectra of BZ Cam observed with the *Swift* XRT. The luminosity is higher in the low state, however, in the very soft spectral region, at energy $\leq$0.5 keV, the X-ray flux is almost twice higher in the high state, which is exactly the opposite of the scenario predicted by Greiner et al. [85]. Interestingly, the spectral fits in both states indicate that we may be observing an unresolved, strong Ne X Lyman α line at 1.02 keV. In the high state spectrum the Fe XXV line at 6.7 keV is clearly detected. BZ Cam was also previously observed with *ROSAT* in the high state. van Teeseling and Verbunt [117] and Greiner [118] fitted the spectrum either with one component blackbody or with a highly absorbed bremsstrahlung (or `mewe`) model. Greiner [118] favoured the blackbody. However, with the larger energy range of *Swift* it can be seen that a fit is only possible with at least two components, and that the blackbody is not adequate. The black dots in the second panel of fig. 2.9 show the low state spectrum of BZ Cam, and a fit with a two-component `vapec` model. With only a broad band spectrum and no detected emission lines, I could not adequately fit the cooling flow model. The same is true for other low resolution X-ray spectra described below.

TABLE 2.5: Fitting models and parameters for BZ Cam and MV Lyr. The errors represent 90% confidence region for a single parameter.

	BZ Cam			MV Lyr		
	high state		low state	high state		low state
Satellite	*Swift*		*Swift*	*Swift*		*Swift*
Models	`vapec`	2 `vapec`	2 `apec`	`vapec+plow`	2 `apec`	2 `apec`
$N_H(10^{22})$	$0.14^{+0.03}_{-0.03}$	$0.26^{+0.12}_{-0.08}$	$0.7^{+0.4}_{-0.7}$	$0.2^{+0.5}_{-0.2}$	$0.69^{+0.16}_{-0.26}$	$0.7^{+0.7}_{-0.5}$
Photon Index				$1.0^{+0.5}_{-0.2}$		
T_1 (keV)	$9.3^{+2.8}_{-1.7}$	$0.51^{+0.3}_{-0.20}$	$0.3^{+0.0.4}_{-0.3}$	$0.2^{+0.4}_{-0.5}$	$0.11^{+0.03}_{-0.04}$	$0.12^{+0.07}_{-0.05}$
T_2 (keV)		$10.8^{+4}_{-2.3}$	$63.6^{+0.4}_{-54}$		58^{+6}_{-50}	$2.5^{+1.9}_{-1.6}$
$Flux_{abs}$*	$3.9^{+0.2}_{-0.3}$	$4.0^{+0.2}_{-0.3}$	6^{+5}_{-2}	$6.5^{+0.4}_{-1.6}$	6^{+4}_{-6}	$1.2^{+1.3}_{-0.4}$
$Flux_{unabs}$*	$4.2^{+0.2}_{-0.3}$	$5.0^{+0.2}_{-0.3}$	14^{+5}_{-2}	$9.7^{+0.4}_{-1.6}$	90^{+50}_{-90}	80^{+80}_{-30}
χ^2	1.6	1.1	1.0	1.0	1.2	

*The X-ray flux ($\times 10^{-12}$erg cm^{-2} s^{-1}) for the *Swift* XRT was calculated in the 0.3–10.0 keV range.

The high state of BZ Cam (red dots in the second panel of fig. 2.9) is best fitted with a two components `vapec` model. The fitting parameters are listed in table 2.5. I find the best fit with non solar abundances, [Fe/H]=(4.5 ± 2.4) and [Ne/H]=(~ 14). In the low state, the increased flux seems to be due to a higher maximum temperature, 64 keV instead of about 10 keV. The column density N_H appears to increase in the low state.

2.4.2.2 UV observations

BZ Cam was observed in *UV* with *Swift* during the low state with a 1172 s exposure and with a 121 s exposure during the high state. The UV magnitudes in the AB system in the high and low states, given in table 2.6 , indicate a smaller variation than observed in the other objects. This is explained by fig. 2.7 in which I show the UV image of the nebula obtained with the *Swift* Ultraviolet Optical Telescope (UVOT). Even with the poor spatial resolution of the UVOT, I detect an extended object; obviously the ionized nebula also emits copious UV flux. Comparing the UV image of BZ Cam in fig. 2.7 and the optical image in fig. 2.8 (which is the fig. 4 of Greiner et al. [87]), I see a trace of the bow shock oriented in the South – South-West direction.

2.4.3 MV Lyr

MV Lyr spends most of the time in the high state, having brightness in the range of $V = 12 - 13$, and during the occasional short low states it is in the $V = 16 - 18$ range of magnitudes. Historical light curves of MV Lyr can be found in [119–122]. With their *FUSE* (Far Ultraviolet Spectroscopic Explorer) observations Hoard et al. [31] estimated that during the low state $\dot{m} \leq 3 \times 10^{-13}$ $M_\odot$ yr^{-1}, a four orders of magnitude lower than the value of $\dot{m}$, estimated by Godon and Sion [93] in the high state.

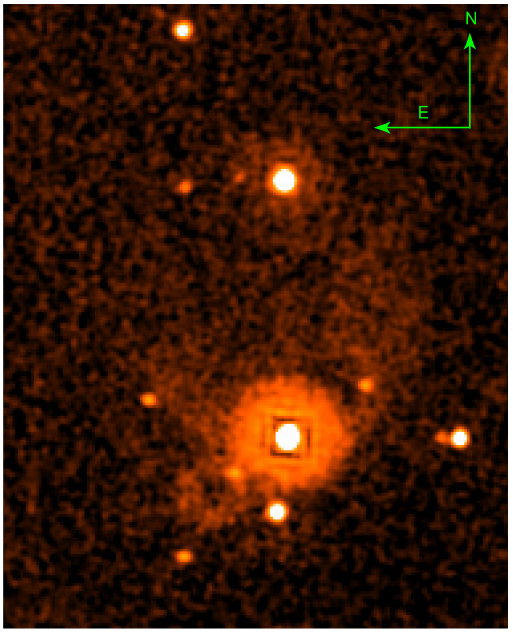

FIGURE 2.7: The *Swift* UVOT image of BZ Cam, notice the emission nebula. The ring in the bottom-left direction from the source is a *Swift* UVOT image artefact.

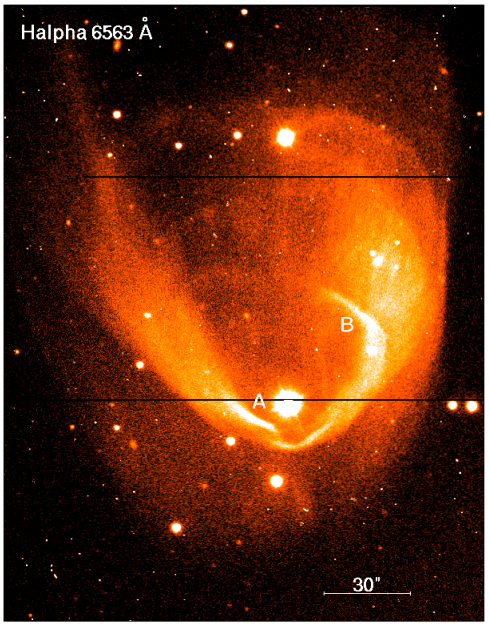

FIGURE 2.8: The Hα image of BZ Cam from Greiner et al. [87].

TABLE 2.6: UV observations

Object	State	Date	Instrument	Exp.(s)	Mag.$_{AB}$	Filter*
BZ Cam	High	21/12/2012	*Swift* UVOT	1200.74	13.0 ± 1.0	UVW2
	Low	15/05/2011	*Swift* UVOT	2737.32	13.198 ± 0.011	U
MV Lyr	Low	29/07/2011	*Swift* UVOT	2092.81	16.265 ± 0.019	U
TT Ari	High	01/11/2005	*GALEX*	1468.3	12.52 ± 0.001	FUV
	High	13/11/2003–03/11/2007	*GALEX*	80–1686	12.518 ± 0.003	NUV
	Low	15/11/2009–02/12/2009	*GALEX*	1466–1702	15.364 ± 0.003	NUV
	Low	22/11/2009	*Swift* UVOT	6311.28	15.091 ± 0.011	UVW2
V794 Aql	Intermediate	15/03/2011	*Swift* UVOT	6186.67	17.07 ± 0.03	UVW1
	low	12/07/2011	*Swift* UVOT	4732.45	19.26 ± 0.10	UVM2

Swift filters central wavelengths (Å): U – 3465, UVW1 – 2600, UVM2 – 2246, UVW2 – 1928. *GALEX* UV band (Å): NUV – 1750–2800, FUV – 1350–1750

2.4.3.1 The X-ray data

The third plot of fig. 2.9 shows the comparison between the high and low state X-ray spectra of MV Lyr obtained with *Swift* together with the spectral fits. Unlike in BZ Cam, the high state X-ray flux of MV Lyr is higher by an order of magnitude than in the low state. The spectrum is also harder, with an additional component prominent above 1.7 keV.

I fitted the high state spectrum of MV Lyr with two components of the thermal plasma

model, but a good fit is also obtained with a thermal plasma and a power law model. I fitted the low S/N, low state spectrum with two components of the thermal plasma model with abundances fixed to the solar value (see table 2.5).

A *ROSAT* observation of MV Lyr in November 1992 in the high state was studied by Greiner [118]. The authors fitted the spectrum with a blackbody, however, like in the case of BZ Cam, this model fails to fit the high energy part of the spectrum that I measured with *Swift*. Greiner [118] observed MV Lyr at the end of the 9 week-long optical low state in 1996 and obtained only an upper limit for the X-ray luminosity of $10^{29.7}$ erg s^{-1} assuming a distance of 320 pc (smaller than the most current estimate of 505±50 pc I give in table 2.1). Assuming a distance of 320 pc, the flux measured during the low state *Swift* observation (see Tab. 2.5) four months after the beginning of the decline to the low state and one month after minimum, would be 10^{31} erg s^{-1}, more than a factor of 10 higher than this upper limit. Thus, it seems that the X-ray flux of MV Lyr in the low state is not constant.

2.4.4 V794 Aql

In the high optical state V794 Aql varies between 14th and 15th magnitude, and in the low states it can plunge to 18–20 mag. (in the *B* filter, see [123]). Godon et al. [97] fitted spectra of the Hubble Space Telescope Space Telescope Imaging Spectrograph (*HST-STIS*) and of *FUSE*. They derived the following binary system parameters: $M_{WD} = 0.9$ $M_\odot$, high state $\dot{M} = 10^{-8.5} - 10^{-8.0}$ $M_\odot$ yr^{-1}, inclination $i = 60^o$, and distance to the system d = 690 pc.

2.4.4.1 The X-ray data

The spectra of V794 Aql in the intermediate ($V \simeq 15.5$) and in the low state are presented together with the model fitting in the bottom panel of fig. 2.9. The X-ray flux is three times higher in the intermediate than in the low state. I fitted the intermediate state spectrum of V794 Aql with two `vapec` components (see table 2.7). In both components I need high abundance of Mg ([Mg/H]$\sim$ 5).

2.5 Discussion

An important motivation for this research has been the claim by Greiner [118] and Greiner et al. [87] that some of the WD in VY Scl-type stars must be burning hydrogen quietly in the low state, without ever triggering thermonuclear flashes because of the

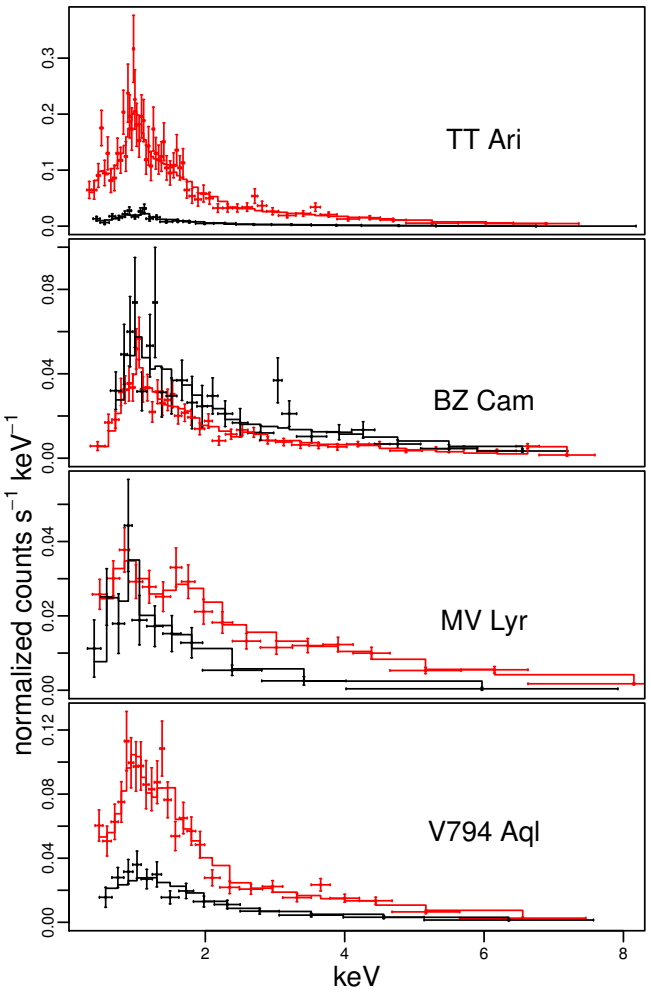

FIGURE 2.9: The low and high state X-ray spectra of BZ Cam and MV Lyr observed with *Swift*. TT Ari and V794 Aql were observed with *Swift* during the low and intermediate state. The high and intermediate state spectra are plotted in red and the low state spectra in black. The solid lines show the models, the dots with error bars indicate the data.

TABLE 2.7: Best-fitting models and parameters for V794 Aql. The errors represent 90% confidence region for a single parameter.

	high state	low state
Satellite	*Swift*	*Swift*
Models	2 `vapec`	`apec`
$N_{\rm H}(10^{22})$	$0.05^{+0.04}_{-0.03}$	$0.01^{+0.07}_{-0.05}$
T_1 (keV)	$0.9^{+0.3}_{-0.3}$	8^{+20}_{-3}
T_2 (keV)	16^{+39}_{-8}	
Flux$_{\rm abs}\times10^{-12}$erg cm^{-2} s^{-1}	$8.2^{+0.5}_{-1.3}$	$2.5^{+0.4}_{-0.6}$
Flux$_{\rm unabs}\times10^{-12}$erg cm^{-2} s^{-1}	$8.8^{+0.5}_{-1.3}$	$2.7^{+0.4}_{-0.6}$
χ^2	1.0	0.7

*The X-ray flux for the *Swift* XRT was calculated in the 0.3–10.0 keV range.

short duration of the burning. I found that the predicted supersoft X-ray source does not appear in both states, so the atmospheric temperature has to be below a certain upper limit, implying an upper limit to M_{WD} and lower limit to $\dot{m}$ if the burning occurs. I attempted to estimate the lower limits of the WD atmospheric temperatures, which would be detectable with the exposures, discussed here. I used the NLTE TMAP models for a WD atmosphere with $\log g = 8$, the estimates of the distances and the WD masses from tab. 2.1, the calibration files for the corresponding detectors, and the `fakeit` tool in `xspec`. The normalization of the atmospheric model is $norm = (R \times 10^{11}/d)^2$, where d is the distance and R is the radius of the emitting region. In case of surface hydrogen burning, R is the WD radius, which can be found from the $M_{WD} - R_{WD}$ relation [124]:

$$R = 7.8 \times 10^8 \left((1.44/M)^{2/3} - (M/1.44)^{2/3} \right)^{1/2} \text{ cm}, \tag{2.1}$$

where M is the WD mass in solar units. I found that the *Swift* exposures presented here rule out the hydrogen burning at atmospheric temperatures lower than 150 000 – 170 000 K (the limit depends on the exposure length). The temperature can be best constrained with *ROSAT* because of its sensitivity to soft X-rays: the upper limit for the high state hydrogen burning in TT Ari is 90 000 K.

Fig. 2.10 shows the stable burning models of accreting WDs for different WD masses and mass transfer rates from Wolf et al. [3]. The pink shaded region constrains the models with atmospheric temperatures higher than 170 000 K, which is the upper limit for the WD atmosphere temperature in VY Scl-type stars measurable with the short *Swift* exposures. Additionally, red and blue lines show the upper limits, found from the longer *Swift* exposures and from the *ROSAT* observation: 150 000 and 90 000 K, respectively. The 90 000 K limit rules out the hydrogen burning in TT Ari in the high state. However, it is still possible in the low state of TT Ari and in the other systems in both, high and low states, but only if the M_{WD} is below 0.6 $M_\odot$. This limitation on the M_{WD} indicates that the WD must accrete >0.7 $M_\odot$ in order to reach the Chandrasekhar limit, which is only possible if the secondary is more massive. However, for stable accretion in case of Roche-lobe overflow the mass ratio should be less than 1. From fig. 3 of Hillman et al. [125] we see that if there is no stable hydrogen burning in order to reach the Chandrasekhar limit the WD mass should be above 1.3 $M_\odot$, assuming the values of $\dot{m}$ from tab. 2.1. This WD mass is not consistent with the estimates in tab. 2.1 and would also imply short recurrence times of nova explosions, however, there are no confirmed VY Scl-type stars among novae. To summarize, VY Scl-type stars cannot be considered as SN type Ia progenitors because they either burn hydrogen quietly, but have too low-mass WDs to reach the Chandrasekhar limit or undergo rare nova explosions, expelling more material than was accreted.

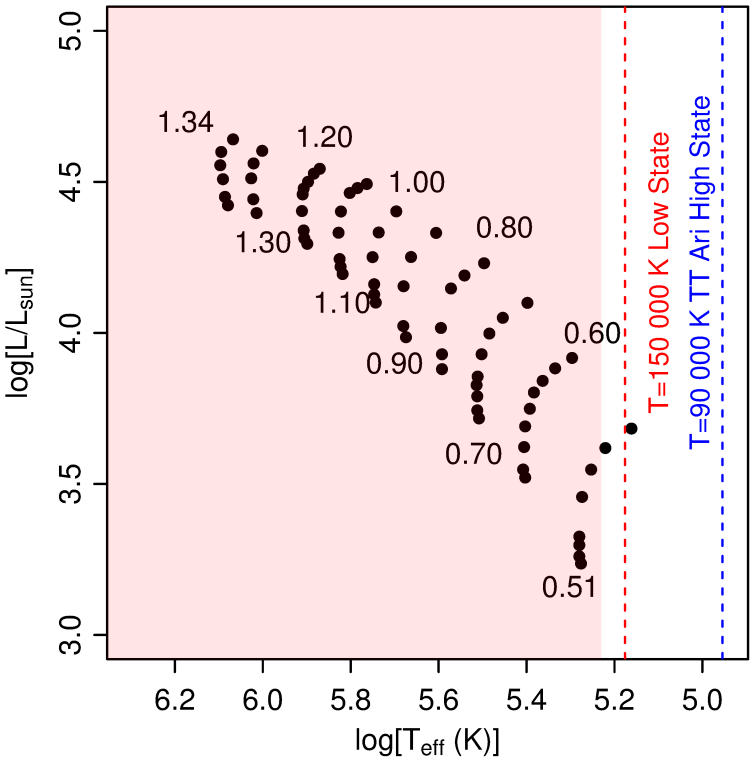

FIGURE 2.10: Stable burning models of accreting WDs for different WD masses and mass transfer rates from Wolf et al. [3]. The pink shaded region constrains the models with atmospheric temperatures higher than 170 000 K. The dashed lines show the limits for T_{eff}, obtained from the *Swift* exposures of better quality and from the *ROSAT* observations.

All the X-ray spectra of the VY Scl systems I examined appear complex, and the *Chandra* and *Suzaku* spectra of TT Ari clearly indicate more than one emission region or mechanism. The best-fitting model for all the 0.3–10.0 keV broad band spectra is a probably still simplistic two-component absorbed thermal plasma model. In the next sections I discuss the possible origins of the observed X-ray emission.

2.5.1 Accretion disk boundary layer

I found that in three of the systems the X-ray luminosity decreases during the optical and UV low states, although the X-ray flux variation is the smallest. The X-ray flux seemed to be anti-correlated with the optical and UV only in BZ Cam. Thus, if in the other three systems the main source of UV/FUV and optical luminosity is the accretion disk, it seems unlikely that the X-ray flux is due to the innermost portion of the disk. In fact, our fits with the cooling flow model, which generally yields good results assuming that all the X-ray flux is emitted in an accretion flow, for all four objects return unreasonably low values of $\dot{m}$, which cannot be reconciled with measurements at other wavelengths. This is not completely unexpected, since the accretion disks of systems accreting at high

$\dot{m}$, close to 10^{-8} $M_\odot$ yr^{-1}, seem to re-radiate mostly or completely in the *EUV* range [126], because the boundary layer is optically thick.

For TT Ari, the semi-regular variability (QPO) with periods of 17–26 minutes in the high state is best explained with the flickering of an accretion disk, however I also found that there is no correlation between the X-ray flux and the frequency of the QPO, which would be expected for accretion disk flickering [101, 127].

2.5.2 X-ray emission in a wind

If the origin of the X-ray emission is not in the boundary layer of the accretion disk, it may originate in a wind, either from the WD or from the accretion disk, depleting matter from the system. Such a wind may play an important role in the evolution, preventing the WD from reaching the Chandrasekhar mass. The fit of the TT Ari emission lines observed with *Chandra* indicates a FWHM in the range 1100–1500 km s^{-1}. However, the lines do not display any measurable blue or red shift to prove a wind scenario. There is significant broadening, but it may be due to collisional ionization in the accretion flow, or to matter in almost-Keplerian rotation. The WD effective temperature and the *FUV* flux reported in table 2.1 are consistent with a line driven wind, although if nuclear burning takes place, the radius of a WD at some stage may increase, and we cannot rule out that at some (still not observed) brief stage the WD reaches a luminosity where also the electron scattering opacity starts playing a role, causing a nova-like radiation pressure driven wind that depletes the accreted envelope. In either case, the most likely origin for the X-ray flux in the observations I examined is circumstellar material, shocked when it collides with a new outflow, possibly at a large distance from the WD. There may be circumstellar material left from the AGB phase of primary or old remnant of a previous nova, or a previous "thicker" wind caused by enhanced luminosity due to nuclear burning, that has slowed down. A strong stellar wind is very likely to play a role in the extended BZ Cam nebula, which was initially classified as a planetary nebula. Instead I would argue that for TT Ari this explanation cannot account for the largest portion of the X-ray flux, because this system shows the 6.4 keV reflection line, which indicates that a large fraction of X-rays (at least X-rays above 7 keV) must originate close to the white dwarf or to the disk.

There is a secure observation of X-rays far away from the accretion disk in UX UMa (see [128]), an eclipsing nova-like with a hard, absorbed, eclipsed X-ray component and a soft, unabsorbed, uneclipsed X-ray component. The soft X-rays in UX UMa may indeed originate in a wind from the system. A fast wind is also known to occur in CAL 87 [129, 130], another system that may be closely related to the VY Scl-type stars. The

X-rays and optical flux variations anticorrelate only in BZ Cam, so it is possible that in this system the wind increases in the low state, causing additional absorption and obscuring the accretion disk.

Disk winds are observed in many types of compact objects, while the mechanism that causes them is not completely clear. At optical and UV wavelengths a mass outflow from the disk has been inferred in some CV via the observation of P Cygni profiles, most notably of the C IV λ1549 Å line [131–133]. P Cygni line profiles or/and absorption features have also been detected in X-rays in low mass X-ray binaries [134, 135] and are assumed to originate in a high-velocity outflow from a flared and X-ray-heated accretion disk. Disk winds also cause additional circumstellar, sometimes time-dependent, absorption components in the soft X-rays in non-magnetic CVs [136, 137].

2.5.3 Polar caps

A tempting hypothesis is that, while one component of the X-ray flux is due to a mass outflow from the system, another component originates in a different, and coexistent mode of accretion other than the disk, i.e. a stream to the polar caps. In short, the VY Scl would be intermediate polars (IPs). This scenario explains the lack of a clear correlation of *UV*/optical versus X-ray flux variations. As in the model proposed by Hameury and Lasota [138] the stream to the polar caps still continues, at decreased rate, when the accretion disk is periodically disrupted in the optically low state. In an IP, the disk would emit in optical and *UV*, but it would be truncated instead of having an X-ray emitting boundary layer, no matter what the value of $\dot{m}$ is.

Mauche (2010)[3] compared spectra of magnetic and non-magnetic CV's and showed that division into the two classes is not clear-cut on the basis of the X-ray spectrum alone, because of the large variety of observed X-ray spectra of magnetic CVs. There is no "typical" spectrum among polars and IPs. There is evidence for and against the magnetic scenario for TT Ari, but the X-ray spectrum alone does not prove or disprove it.

An X-ray flux modulation due to the WD rotation period, which is very typical and is considerd the smoking gun to classify IPs, has not been detected in these systems so far. For three of them the reason may be low inclination, but not so for V794 Aql. However, if the major component of the X-ray flux in the high state is not the accretion stream to the poles, but is instead associated with a wind, isolating the accretion component for the timing analysis is a serious hurdle in detecting a periodicity due to the WD rotation.

[3] http://cxc.harvard.edu/cdo/accr10/pres/MaucheChris.pdf

Many SW Sex-type stars show emission line flaring, that is a modulation of the fluxes and equivalent widths of emission lines. This phenomenon is very often observed in IPs, because of the dynamics of the line-emitting source (see [139] and references therein) and occurs on a timescale of tens of minutes. QPOs observed in the X-rays in SW Sex- and VY Scl-type stars have the same characteristic periods of $\sim$ 1000 – 2000 s. Patterson et al. [140] noticed that this timescale is exactly the expected WD rotation period in a magnetic system in spin equilibrium with the orbital period of 3–4 h. and proposed that SW Sex-type stars can be a borderline polars and that the very high mass transfer rate may "drown" their magnetic properties.

Interestingly, Rodríguez-Gil et al. [141] found significant variability of the optical spectra of BB Dor, which is a SW Sex- and VY Scl-type star, during its low state and interpreted it as a result of accretion events on a timescale of tens of minutes. The source of this extra emission was located somewhere between two stars and was either related to the material transferred from the secondary to the magnetosphere of the WD in the absence of an accretion disc, or to the hot spot region in the outer rim of a cold, remnant accretion disc. The first possibility assumes that BB Dor hosts magnetic WDs and behaves like an IP during high states and like disk-less polars during low states. A similar variability of the optical spectra was observed in TT Ari during its last low state (Zemko et al. in prep.). In addition, TT Ari showed outburst-like events in the optical band with amplitudes up to 2.5 mag. on a timescale of 2 – 3 h, possibly related to sporadic accretion events. Although the magnetic scenario has some observational and theoretical support, there are only three confirmed IPs among NLs. Two of them are SW Sex-type stars, in which circular polarization was detected (LS Peg [38] and V795 Her [39]), and the third one, DW Cnc, shows an X-ray modulation associated with the WD spin period [40].

2.6 Conclusions

I analyzed a number of X-rays and UV observations of four VY Scl systems comparing phenomena occurring during the optically "high" and "low" state. We did not detect supersoft X-ray emission in either state. We cannot exclude H burning at a lower temperature, outside of the SSS window, however, it would imply very low WD masses: below 0.6 M_{WD}. We conclude that VY Scl-type stars cannot be considered as SN type Ia progenitors. The data collected and examined in this paper suggest that the X-ray emission has more than one component in all the four systems. One component most likely originates in the circumstellar material, shocked by the wind, possibly at a large distance from the WD while the second component can be due to accretion, for example,

emission from the polar caps. However, we are not able to prove neither clearly disprove the IP scenario for these systems.

It can be argued that these X-ray observations have posed more new puzzles than have resolved problems. I suggest that monitoring these systems over the years in optical, *UV* and X-rays as frequently and simultaneously as possible is a key to understand how accretion occurs and how it interplays with the thermal state of the secondary. More intensive monitoring, that may be done with *Swift*, would be very rewarding, allowing us to understand whether an evolutionary path at high mass transfer rate without mass loss in nova outbursts can be sustained for a long time, and whether it leads to "quieter" outflows preventing the WD growth in mass, or to evolution towards a type Ia supernova.

Chapter 3

Return to quiescence of novae with massive WDs

The focus of this observational project are novae with massive WDs, previously detected as super-soft X-ray sources, as they settle into quiescence. We selected two objects, V2491 Cyg (Nova 2008b) and V4743 Sgr (Nova 2002c). Indications of large WD mass and high $\dot{m}$, found in previous studies, suggest that these novae are a rather "extreme" accreting WDs, with characteristics expected in type Ia SN progenitors and possibly with strong magnetic fields. The novae were observed in the X-ray and optical bands, both photometrically and spectroscopically. A part of the analysis of the V2491 Cyg observations presented here was published in Zemko et al. [142]. The co-authors are Dr. K. Mukai and Dr. M. Orio. The result of the study of V4743 Sgr is partially published in Zemko et al. [143]. The co-authors are Dr. K. Mukai, Dr. M. Orio. Dr. A. Bianchini, Dr. S. Ciroi and Dr. V. Cracco.

3.1 V2491 Cyg

3.1.1 Introduction

V2491 Cyg was detected by Hiroshi Kaneda on 2008 April 10.728 at V=7.7 [144]. The nova was very fast: t_2 in the V band was 4.6 days and the ejecta velocity reached 4860 km s^{-1} [145, 146]. The nova had a short unusual "re-brightening" at the end of April, then reached the minimum brightness – $V\sim$16 after about 150 days. The interstellar reddening was E(B-V) = 0.43 [147] corresponding to a hydrogen column $N_{\rm H}$=2.5$\times$10^{21} cm^{-2} [148].

Jurdana-Sepic and Munari [149] discovered a persistent optical counterpart at V≃17.1, which had a short dimming before the nova outburst. No previous outburst was known, but several authors suggested that an early transition of the optical spectrum to the He/N type [145], the velocity of the ejecta, and the rapid visual decay were all typical of the recurrent novae (RNe). However, this hypothesis has not been proven.

V2491 Cyg is one of three novae detected in X-rays before the outbursts (see [150] for V2487 Oph and [151] for Nova 2008 Car). Pre-nova X-ray observations of V2491 Cyg obtained with *ROSAT*, *XMM-Newton*, and *Swift* were discussed in Ibarra et al. [152]. These authors found that the quiescence X-ray spectrum was variable on a time scale as short as 4 days and that one of the analysed *Swift* spectra was noticeably softer than at other epochs. The unabsorbed X-ray flux varied in the range from 1 to 30×10^{-12} ergs cm^{-2} s^{-1} [152], corresponding to $L_{\rm X} = 1.2 - 4 \times 10^{35}$ erg s^{-1}, assuming a distance of 10.5 kpc [153]. These values of the X-ray luminosity before the outbursts imply that the mass accretion rate can be as high as $\sim10^{-8}$ M$_\odot$ yr^{-1} for a 1.3 M$_\odot$ WD [154], close indeed to the expected RN range, with recurrence times ∼100 years [3].

During the outburst V2491 Cyg was observed with *XMM-Newton* [155, 156], *Suzaku* [156] and extensively monitored with *Swift* [157–159]. Page et al. [159] followed V2491 Cyg with *Swift*, from the day after the nova discovery until the pre-outburst flux level. The spectrum was quite hard before day 25 after the explosion and shortly thereafter the object evolved into a SSS. The peak soft X-ray luminosity remained constant for only two days and then faded slowly for 18 days, an unusual trend for post-nova SSS, most of which show an almost flat light curve after the peak and later fade rapidly. The WD in V2491 Cyg was among the hottest ever observed [155], therefore it must be very massive [2, 3]. Quite surprisingly, the WD did not seem to cool before the SSS final decay, while the luminosity significantly decreased, as if the nuclear burning region was shrinking on the surface of the WD itself.

Baklanov et al. [160] reported a variation with a period of 0.09580(5) days in the B and V bands between 10 and 20 days after the outburst. This variation may have been the orbital modulation of the binary system. However, Shugarov et al. [161] did not detect the above period, although they monitored V2491 Cyg in optical for more than one year. Also Darnley et al. [162] ruled out eclipsing orbital periods shorter than 0.15 days. Page et al. [159] observed V2491 Cyg during the decline to quiescence, but did not detect any modulation with a period ∼ 0.1 days in X-rays and UV. While the 0.09580(5) days period has not been confirmed, another variability on a shorter timescale has been reported by several authors. Shugarov et al. [161] detected a possible 0.02885 days (41 min) period. Darnley et al. [162] found evidence of a ∼0.025 days (36 min) modulation in the B band, but, unfortunately, their data were too sparse for period analysis. Ness

TABLE 3.1: Details of the X-ray observations of V2491 Cyg.

Date and time	Years AO*	Instrument	Exposure (s)	Count rate (cnts s^{-1})
2010 11 03 10:32:11	2.6	*Suzaku* XIS 0	74400	0.0494 ± 0.0010
2010 11 03 10:32:11	2.6	*Suzaku* XIS 1	74400	0.0681 ± 0.0012
2010 11 03 10:32:11	2.6	*Suzaku* XIS 3	74400	0.0550 ± 0.0010

* after the outburst, *Suzaku* XIS FI are XIS 0 and XIS 3 detectors with front-illuminated (FI) CCDs, while *Suzaku* XIS BI is the XIS 1 that utilizes a back-illuminated (BI) CCD

et al. [155] reported oscillations of the X-ray flux with a period of 37.2 min on day 39 after the outburst, however this variability was not observed in simultaneous UV observations and in the X-ray light curve obtained later, on day 49 after the nova explosion.

Several authors discussed the possibility of a magnetic scenario for V2491 Cyg [see 152, 154, 156]. Hachisu and Kato [154] proposed that magnetic activity explains the re-brightening seen in the optical light curve, and that V2491 Cyg is a polar. However, Page et al. [159] argued against this possibility. Using the synchronization condition they showed that if V2491 Cyg is a polar it should host one of most magnetic WDs known in binaries, assuming the WD mass about $1.3 M_{\odot}$ and 0.0958 days orbital period. Although V2491 Cyg has a number of properties that are quite typical of magnetic WDs, such as strong Fe emission features at 6.4, 6.7, and 7.0 keV, high X-ray luminosity in the range 2.0—10 keV [156], the existing data do not allow us to finally prove or disprove the magnetic scenario.

3.1.2 X-ray observations and data analysis

V2491 Cyg was observed with the *Suzaku* X-ray Imaging Spectrometer (XIS) on 2010 November 3 with an exposure time of 74.4 ks (for details see table 3.1).

3.1.2.1 Spectral analysis

The background subtracted 0.3–10.0 keV spectra of V2491 Cyg are presented in fig. 3.1. The combined XIS 0 and the XIS 3 data are plotted in black, while the XIS 1 data are plotted in red. The solid lines show the best fit. The dashed lines represent the components of this model. The spectra seem to have a very soft component and a harder one with emission lines of highly ionized Fe, in particular the Fe XXV line at 6.7 keV that indicates a thermal plasma. In order to fit the harder portion of the spectra I started with one thermal plasma component. However using one or two components of collisionally-ionized diffuse gas (`apec`) did not provide a statistically significant fit of the

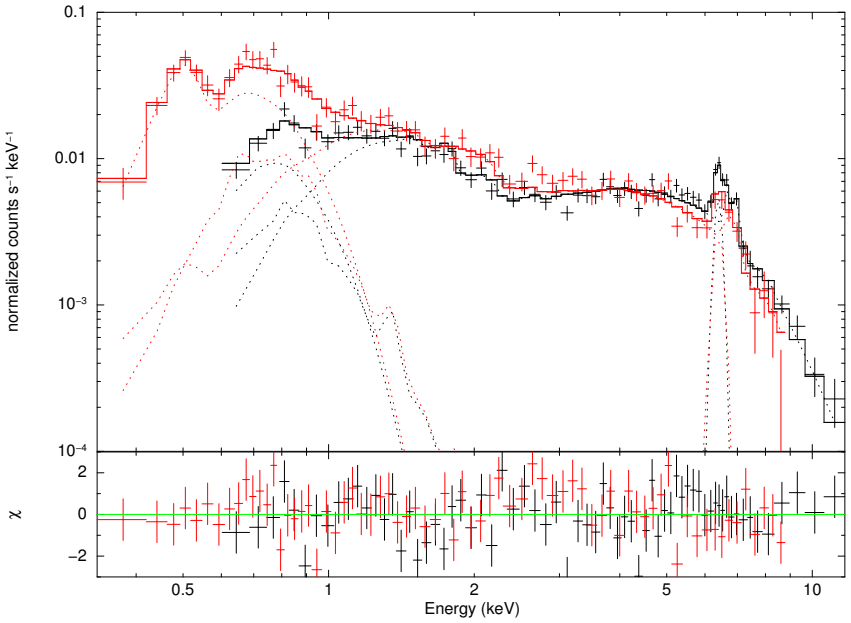

FIGURE 3.1: *Suzaku* XIS spectra of V2491 Cyg. The BI CCD data have been plotted in red and the FI data have been plotted in black. The solid lines represent the fit with `wabs`×(`bb`+`pcfabs`×(`apec`+`apec`+`gauss`)) model. The components of the model have been plotted with the dashed lines.

spectra with any temperature. The multi-temperature plasma emission model based on the `mekal` code (`cemekl`) also does not provide a good fit. I tried to add a reflection component, taking into account the presence of the very strong Fe Kα reflection line, but it resulted in unphysical values of the fitting parameters. The reflection scaling factor (R= $\Omega/2\pi$), which is the covering fraction of the reflector viewed from the plasma, was close to 10. Such a value of R would imply that the source of the X-ray emission is hidden by a Compton-thick material and that we only see the reflected component, which is a rather unlikely possibility. Moreover, R = 10 implies that the EW of the Fe Kα reflection line should be ≈1.5 keV [163], which is much larger than the EW inferred from the Gaussian fit of the line that I will show below.

The very flat slope in the 3.0–5.0 keV range points toward a complex absorption. The fit with the two-component thermal plasma model was much improved after multiplication by a partially covering absorber (`pcfabs` in `xspec`). I derived the following values of the column density and covering fraction of the partially covering absorber: $N_{\rm H}$ = 10–17 × 10^{22} cm^{-2} and CvrFract = 0.66. Page et al. [159] also used a partially covering absorber with almost the same value of $N_{\rm H}$ in their model to fit the spectra of V2491 Cyg obtained after day 80 after the outburst.

In order to fit the soft excess, measured in the XIS 1 data at 0.5 keV, I added a blackbody component that was absorbed only by the interstellar absorption. I will further discuss why the blackbody component is not effected by the partially covering absorber. By

TABLE 3.2: The parameters of the best fitting models – `wabs`×(`bb`/"*atm*"+`pcfabs`×(`apec`+`apec`+`gauss`)) for the V2491 Cyg X-ray spectra, where "*atm*" is the WD atmosphere model. The errors represent the 90% confidence region for a single parameter.

Parameter	+Blackbody	+Atmosphere
$N_{\rm H}(\times10^{22}$ cm$^{-2})$	$0.25^{+0.08}_{-0.06}$	$0.19^{+0.09}_{-0.07}$
$N^{a}_{\rm H}({\rm pc}\times10^{22}$ cm$^{-2})$	13^{+3}_{-2}	11^{+3}_{-2}
CvrFract^{b}	$0.66^{+0.03}_{-0.03}$	$0.63^{+0.03}_{-0.03}$
$T_{bb/atm}$ (eV)	77^{+7}_{-9}	$85.9^{+2.2}_{-1.5}$
T_1 (keV)	$0.2^{+0.2}_{-0.2}$	$0.29^{+0.05}_{-0.03}$
T_2 (keV)	$11.3^{+1.8}_{-1.5}$	15^{+4}_{-2}
Flux$_{\rm abs}{}^{c}(\times10^{-12}$ erg cm^{-2} s$^{-1})$	$1.92^{+0.03}_{-0.23}$	$1.93^{+0.11}_{-0.6}$
Flux$_{\rm unabs}{}^{c}(\times10^{-12}$ erg cm^{-2} s$^{-1})$	6.66	3.95
Flux$^{\rm bb/atm}_{\rm abs}{}^{d}(\times10^{-12}$erg cm^{-2} s$^{-1})$	0.346	0.284
Flux$^{\rm bb/atm}_{\rm unabs}{}^{d}(\times10^{-12}$erg cm^{-2} s$^{-1})$	7.80	2.66
χ^2	1.1	1.1
$L_{2.0-10.0{\rm keV}}(\times10^{34}$ erg s^{-1} $D^2_{10.5kpc})$	1.82	1.82
$L_{{\rm bb}/atm}{}^{e}(\times10^{35}$ erg s^{-1} $D^2_{10.5kpc})$	$1.4^{+2.4}_{-0.7}$	$1.72^{+2.9}_{-0.9}$
$R_{\rm WD}{}^{f}(\times10^{7}$ cm $D_{10.5kpc})$	$1.2^{+1.0}_{-0.4}$	$1.4^{+0.9}_{-0.5}$

[a] $N_{\rm H}$ of the partial covering absorber.
[b] Covering fraction of the partial covering absorber.
[c] The X-ray flux measured in the range 0.3–10.0 keV. Flux$_{\rm unabs}$ represents the value of the X-ray flux, corrected for the interstellar absorption only.
[d] The X-ray flux of the blackbody and WD atmosphere components measured in the range 0.2–10.0 keV.
[e] The bolometric X-ray luminosity of the blackbody and atmospheric components. $L_{{\rm bb}/atm}$ were calculated based on the normalization constants of the models. The atmospheric model gives the value of the radius $R_{\rm WD} = 10^{-11} \times \sqrt{\rm norm}\times D$, which can be translated to the L_{atm} using the Stefan-Boltzmann law.
[f] The radius of the emitting region.

adding to this four components a Gaussian to represent the Fe Kα line at 6.4 keV, I finally obtained a statistically acceptable result with a value of χ^2 equal to 1.1. The abundance of the thermal plasma components is $0.6^{+0.3}_{-0.2}$ with respect to solar. The value of $N_{\rm H}$ derived from our fit is in agreement with the pre-outburst values reported by Ibarra et al. [152] and with the estimates based on the interstellar reddening. The components and parameters of the fit are presented in table 3.2.

The origin of the blackbody-like component in the spectra of V2491 Cyg is not quite clear. Page et al. [159] speculated about the possibility of long-lasting hydrogen burning on the surface of the WD in this system. Aiming at distinguishing the possible sources of the soft X-ray emission in V2491 Cyg I compared the blackbody model with a WD atmosphere model, since the latter better describes the hydrogen burning on a WD. I used in `xspec` the publicly available NLTE TMAP model with chemical composition of

TABLE 3.3: The best-fit parameter values for the Fe K lines fitting. All the parameters were derived at 90% confidence level.

Parameter	Fe I	Fe XXV	Fe XXVI
Energy center (keV)	6.40 (frozen)	$6.65^{+0.03}_{-0.03}$	6.97 (frozen)
EW (eV)*	250^{+50}_{-50}	130^{+50}_{-30}	130^{+60}_{-50}
$\text{Flux}_{\text{unabs}}$**	7.20	4.95	3.49

χ^2 is 0.98. * Equivalents width. ** The X-ray flux ($\times 10^{-14}$ erg cm^{-2} s^{-1}).

elements from H to Ni #007 and $\log g = 9$ [79]. The blackbody and the NLTE TMAP are statistically equal, – both give a value of $\chi^2 = 1.1$. The values of the temperature and luminosity, and hence the emitting area, derived from the blackbody and WD atmosphere model are comparable (see tab. 3.2).

Finally I isolated the 5.0–9.0 keV region and for simplicity fitted it with a power-law continuum with $\Gamma = 2.0$ and three Gaussians representing the Kα fluorescent line of Fe I (corresponding to 2p $\rightarrow$ 1s electron transition), a Fe XXV resonance line and a Lyα line of Fe XXVI (see fig. 3.2). The N_{H} and parameters of the partially covering absorber were fixed to the values of the best-fitting model in table 3.2. First, I fixed the centroids of the lines to the rest values and the Gaussian widths to zero, since the natural widths of the lines and the broadening due to thermal motions of the emitting atoms are negligible compared with the instrumental resolution of the *Suzaku* XIS detectors, which is ~130 eV at 6 keV. This fit does not provide a good result, leaving a residual excess between the 6.4 and 6.7 keV lines. This may be due to the complex structure of the Fe XXV feature: it consists of the resonance line, the forbidden line, and two intercombination lines. Moreover, there are dielectric satellite lines in the range of 6.61–6.68 keV [164]. Therefore, I varied the centroid position of Fe XXV feature and significantly improved the fit. The best fitting parameters for the Fe K complex and the EWs of the lines are presented in table 3.3. The EW of the Fe Kα line in the *Suzaku* spectra is ~246 eV, which is comparable with the value measured on day 60 and 150 after the outburst [156].

The flux ratio of the Fe XXVI and Fe XXV lines gives an estimate of the highest temperature in the post-shock region [165]. From the fit of the Fe Kα complex of V2491 Cyg I found that this ratio is ~0.7 (see table 3.3), which corresponds to an ionization temperature of about 10 keV [165]. This value is close to that, derived from the global fit (see table 3.8).

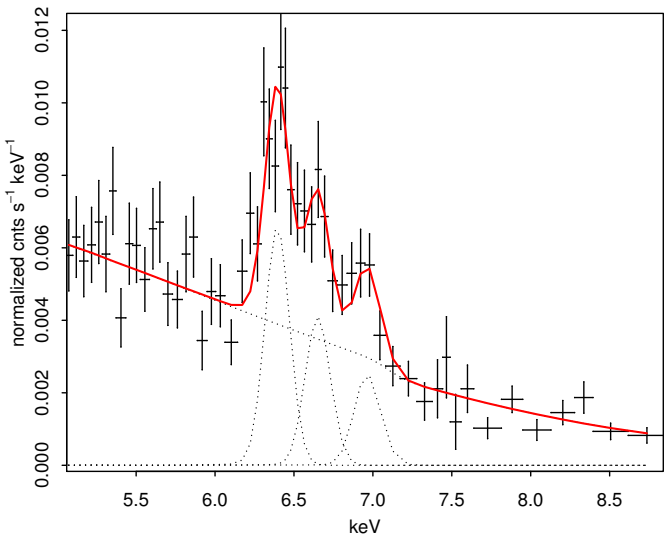

FIGURE 3.2: The *Suzaku* XIS spectra of V2491 Cyg in the 5.0–9.0 keV range showing the Fe K complex. The three Gaussians represent the Fe I, Fe XXV and Fe XXVI lines.

3.1.2.2 Timing analysis

For the timing analysis of V2491 Cyg I initially combined the FI and BI data in the 0.3–10 keV range and de-trended the light curves with a third-order polynomial. I searched periodic variations using both the phase dispersion minimisation (PDM) method, introduced by Stellingwerf [81] and the Lomb-Scargle (LS) method [80]. I found a peak at 0.02666(10) days with the PDM and at 0.02665(14) days with the LS method (see fig. 3.3). I did not detect any reliable periodic signal close to the suggested orbital period of 0.09580(5) days [160]. A false alarm probability level of 0.3% is marked with the horizontal line in the LS periodogram. The peak that corresponds to the 0.0266 days period lies above this line and can be considered statistically significant at the 3σ (99.7%) level. In order to further investigate the significance of the highest peak, I applied the bootstrap method. I repeatedly scrambled the data sequence and calculated the probability that random peaks in the 0.005–0.1 days range reach or exceed the peak of the unscrambled periodogram. I performed 10000 simulations and found that the probability that the peak is real is 99.7%.

The next step was to study the energy dependence of the pulses. I extracted the light curves from the FI and BI data independently in the following energy ranges: 0.3–0.8 keV, 0.8–3.0 keV, 3.0–5.0 keV and 5.0–10.0 keV. The comparison of the light-curves in different ranges is presented in fig. 3.4. I noticed that the amplitude of the variations in the BI light curve is larger than in the FI data. In the 0.3–0.8 keV BI light curve a flare-like event can be seen, that is almost absent in the FI data in the same energy range because of the low sensitivity of the FI CCD in the soft X-rays. I verified that this flare was not a background event. I convolved the BI light curves in different energy

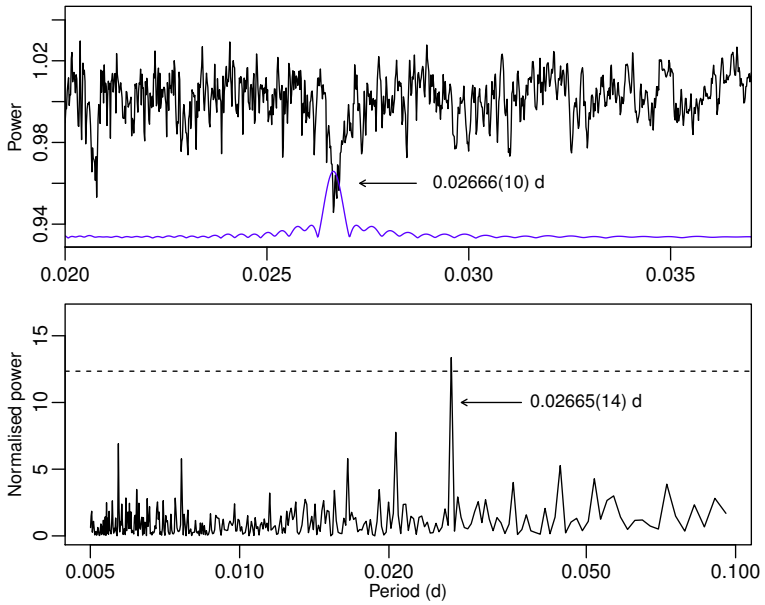

FIGURE 3.3: Periodograms of the *Suzaku* BI light curve of V2491 Cyg in the 0.8–3 keV energy range binned every 80 seconds. The upper panel shows the periodogram obtained with the PDM method and the bottom — with the LS method. The strongest peaks are marked with the arrows together with the corresponding values of the periods. The false alarm probability of 0.3% level is marked with the dashed line in the bottom plot.

ranges with the same period 0.0266 days (38.3 min) and found that the amplitude of the modulation decreases with energy. The modulation is present only in the range below 3 keV.

I also calculated the hardness ratios $HR^i = N^i{}_m/N^i{}_n$, where i is a phase interval and $N^i{}_m$, $N^i{}_n$ are the number of photons in the energy ranges m and n, respectively. It can be seen from fig. 3.5 that $HR^i = N^i{}_{0.8-3}/N^i{}_{0.3-0.8}$ showed hardening at pulse minimum while $HR^i = N^i{}_{3-5}/N^i{}_{0.8-3}$ and $HR^i = N^i{}_{5-10}/N^i{}_{3-5}$ were constant within the errors.

In order to localize the pulsating component I subdivided the 0.3–3.0 keV energy range in three spectral intervals: 0.3–0.6 keV, 0.6–1.0 keV, 1.0–2.0 keV and 2.0–3.0 keV. The energy intervals were chosen based on the spectral fit. I expected the 0.3–0.6 keV range to be dominated by the blackbody component, the 1.0–2.0 and 2.0–3.0 keV intervals to represent mostly the high temperature thermal plasma emission, and the 0.6–1.0 keV range to include emission from the blackbody and two thermal plasma components at the same time. The result is shown in fig. 3.6. The periodic variation is observed between the 0.6–2.0 keV, but it is almost negligible in the harder ranges. The pulse profiles are roughly phase aligned. There is a slight shift between the maxima of the profiles that is within the errors. In the 0.3–0.6 keV energy range the variations have the same amplitude, but are irregular.

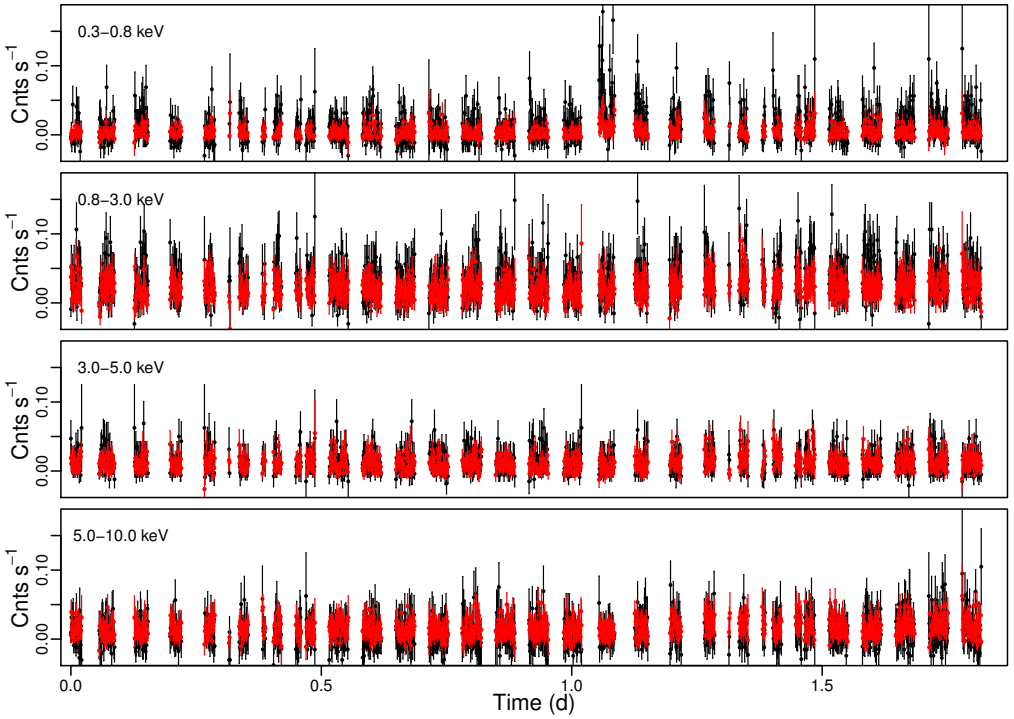

FIGURE 3.4: The X-ray light curve of V2491 Cyg binned every 80 seconds. The BI data are plotted in black and the FI data - in red.

In order to asses the stability of this period I split the *Suzaku* light curve in two intervals and searched the period in each of them. In fig. 3.7 the periodogram (left panels) and the phase folded light curves (right panels) of the first and the second parts of the dataset are plotted together. The light curves were folded with the same period of 0.0266 days in order to compare the pulse profiles. I found that the ∼38 min period does not seem to be stable: the best-fit periods measured in the first and the second halves of the observation are different by 1.4%.

The energy dependence of the amplitude and the hardening at minimum suggest that absorption causes the observed 38.3 min modulation in the X-ray flux. The absence of clear modulation in the 0.3–0.6 keV range (where the blackbody emission dominates) indicates that the blackbody-like component is not affected by the partially covering absorber. This is the reason why I only applied the interstellar absorption to the blackbody component. Evans and Hellier [60] discussed how the geometry allowed observations of a blackbody-like component in a soft IP even when the accretion curtain crossed the line of sight.

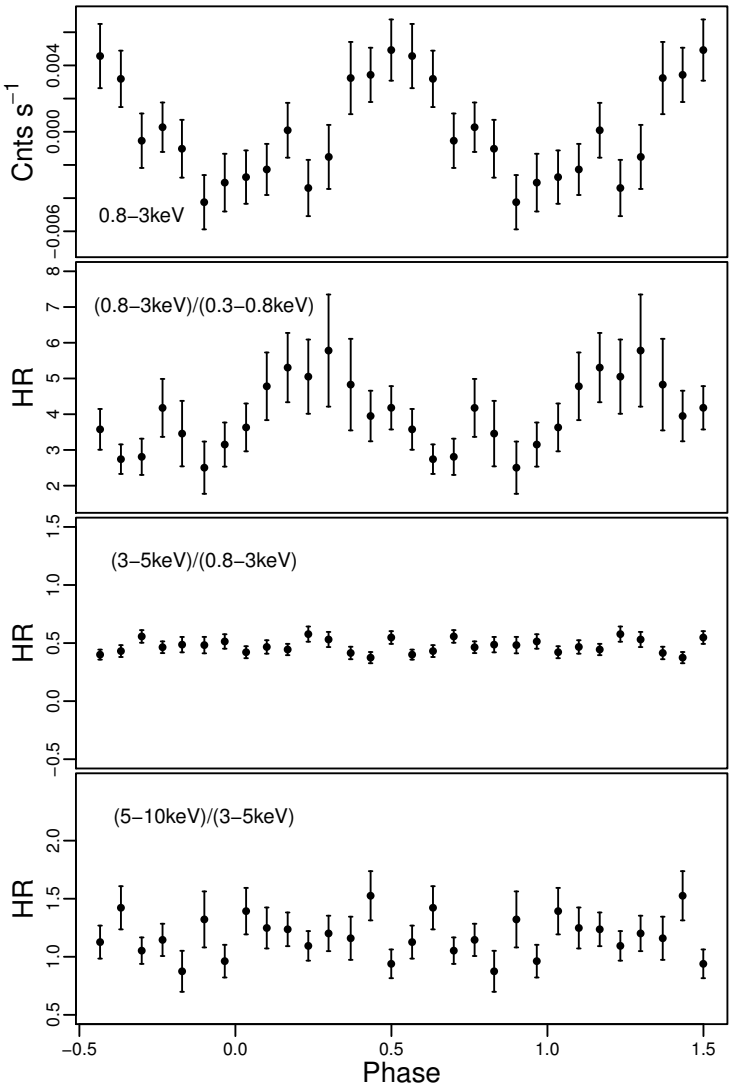

FIGURE 3.5: Top panel: the *Suzaku* FI+BI light curve in the range 0.8–3 keV binned every 80 s and folded with the period of 0.0266 days. Lower panels: variations of the hardness ratios ($HR^i = N^i{}_m/N^i{}_n$) in different energy ranges (m and n) during the 0.0266 days period.

3.1.3 The origin of the blackbody-like X-ray component

Using the `fakeit` tool in XSPEC, I found that the count rate obtained with *Suzaku* corresponds to a 0.039 cnts s^{-1} *Swift* count rate, which is comparable with the last *Swift* observations presented in [159], almost 250 days after the outbursts. Page et al. [159] obtained the best fit of the X-ray spectra of V2491 Cyg with an optically thin hard X-ray plasma and added a blackbody for the SSS phase. These authors also showed that the temperature of the blackbody initially increased and then stabilised around day 57 at the value ~ 70 eV. Further decrease of the X-ray flux in the soft X-ray range seemed to result from a shrinking of the emitting region. The emitting region continued to

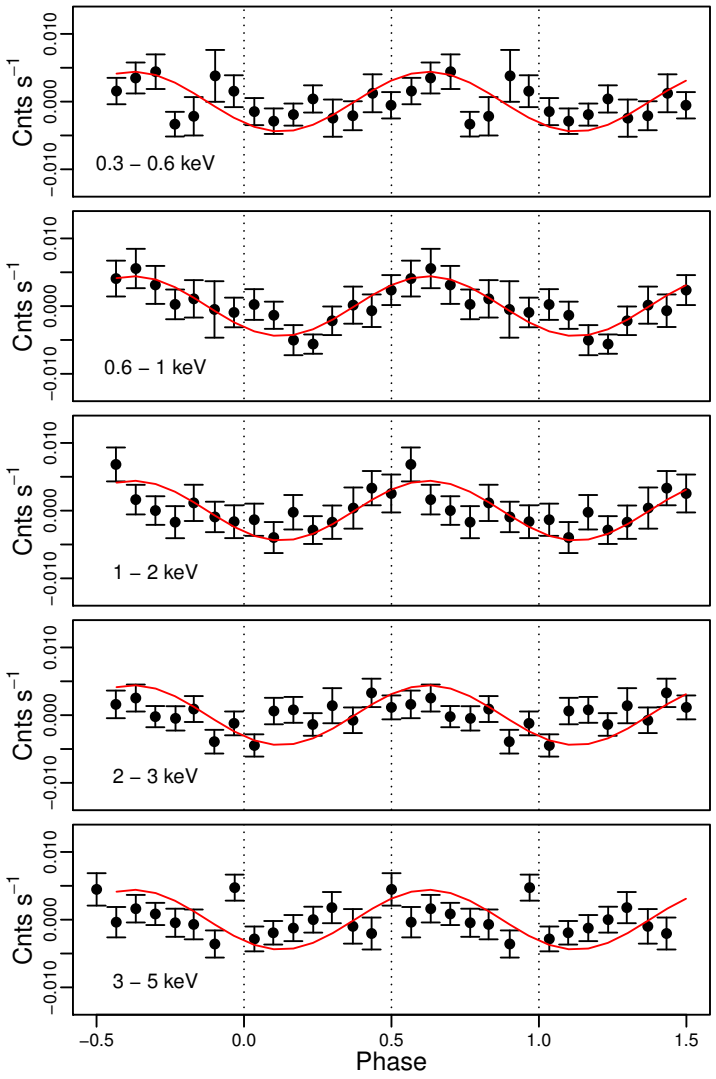

FIGURE 3.6: The *Suzaku* BI light curves of V2491 Cyg in different energy ranges folded with the period of 0.0266 days. The corresponding energy range is indicated in the bottom-left corner of each plot.

shrink even after it reached the size of the WD, instead of becoming cooler at a constant radius like in many other novae.

In our data I found that the blackbody-like component is still present and has a temperature 77^{+7}_{-9} eV. The normalization constant of the blackbody model gives a luminosity of 1.4×10^{35} $D^2_{10.5kpc}$ erg s^{-1} and an emitting radius of 1.2×10^7 $D_{10.5kpc}$ cm. A close emitting radius value was found in the fit with the stellar atmosphere model with a slightly higher temperature. Such a radius of the emitting region is too large for a polar cap on a magnetic WD, but is still more than an order of magnitude smaller than the WD radius. The fit with the WD atmosphere model is statistically indistinguishable from the one with a blackbody and does not allow us to choose between the localized hydrogen burning and the polar cap as a possible source of the soft X-ray radiation.

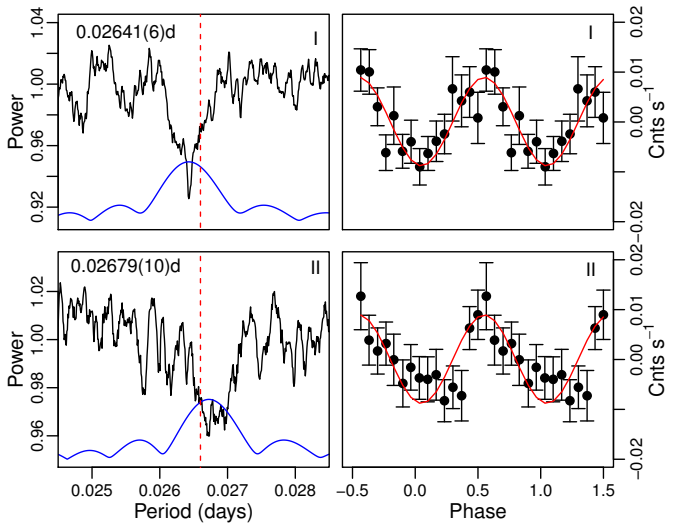

FIGURE 3.7: Left panels: power spectra of the first (top) and the second (bottom) halves of the *Suzaku* XIS BI observation of V2491 Cyg obtained with the PDM method. The red dashed line represents the mean period – 0.0266 days (38.3 min). The period measured in each half is marked. Right panels: the first (top) and the second (bottom) halves of the *Suzaku* XIS BI light curve folded with the 0.0266 days period (38.3 min). I analysed the light curve extracted in the 0.8–3.0 keV energy range and binned every 80 s.

The constant-temperature at decreasing radius, well below the WD radius dimensions, derived by Page et al. [159] was not observed in other novae and contradicts the models. We are intrigued by the possibility that we still observe the same blackbody component after more than two years. Could it be due to residual nuclear burning, possibly continuing in this post-outburst quiescent phase in a smaller region than the whole WD? Orio and Shaviv [166] predicted the possibility of localized thermonuclear burning on a WD. Other authors have argued that the burning would not remain localized and eventually the thermonuclear flash would propagate over the whole WD surface, (e.g. [167]), very differently for instance from helium burning on a neutron star.

On the other hand, a distinct blackbody component with temperature in the range 20–100 eV is observed in many IPs [see 60–62, and references therein]. These objects form a growing group of so-called "soft IPs". Bernardini et al. [62] in their nine objects sample found two new IPs with a blackbody component with T_{bb}=70–80 eV. These authors showed that the WD spot area (the source of a blackbody radiation) is 4.5×10^{14} D^2_{900pc} cm^2 in V2069 Cyg and 6.3×10^{13} D^2_{1kpc} cm^2 in RX J0636. These values are still smaller than the size that I obtained for V2491 Cyg (1.8×10^{15} $D^2{}_{10.5kpc}$ cm^2), but can be comparable taking into account uncertainties in the distance determination for both of them.

It should also be stressed that with the existing data, we cannot rule out that the supersoft flux has more than one origin, for instance that there are unresolved narrow

emission lines merging with the soft continuum and making the source appear more luminous in the supersoft range. In archival data of V2487 Oph and V4743 Sgr (see [168] and section 3.2) we found that the post-outburst RGS spectra, albeit with low signal-to-noise ratio, still show emission lines in the softest range. At this stage, this possibility is only speculative, but it should be taken into account as it may imply a lower supersoft X-ray luminosity that estimated in our broad-band fit with *Suzaku*.

In calculating the luminosity I assumed the widely adopted distance d=10.5 kpc [153]. Munari et al. [169] independently found 14 kpc using the interstellar Na I line to evaluate the reddening. Although these distances have been inferred with the maximum-magnitude rate-of-decay (MMRD) relationship and these values may thus be highly uncertain (the relationship does not hold for RNe and sometimes is not very precise for CNe, moreover the nova had a rare secondary optical maximum), the optical and especially the supersoft X-ray luminosity in the outburst indicate that the distance cannot be much smaller. Especially the large supersoft X-ray flux [155, 159] is evidence of a distance of at least 10 kpc, otherwise the WD would have been underluminous compared with the models of the same high effective temperature (from 9×10^5 to a 10^6 K, see [2, 3]) and also with previous observations of novae in the SSS phase (see [7] for a review).

3.1.4 Optical observations and data analysis

In order to explore the possibility of magnetic nature of V2491 Cyg we proposed photometric and spectroscopic observations in the optical band. I also collected the archival spectroscopic observations of V2491 Cyg obtained in the Special Astronomical Observatory of Russian Academy of Sciences (SAO RAS). The optical flux of IPs is usually modulated with the beat period between the spin and the orbital one due to the reprocession of the X-rays from the surface of the secondary. Optical spectra of IPs are characterized by a prominent He II λ4686 line, which is an indicator of a strong ionizing flux shortward of 228 Å. Silber [170] formulated an empirical criterion for magnetic CVs, according to which the equivalent widths (EWs) ratio of the He II λ4686 to Hβ line should be >0.4 and the EW of the Hβ line should be grater than 20. However, strong He II λ4686 lines are not observed only in IPs and are also typical of post-outburst novae [171, 172][1]. To summarize, if V2491 Cyg is magnetic, we expect to observe a modulation of its optical flux with the period slightly longer than the one detected in the X-rays and a strong He II λ4686 line in its optical spectrum.

[1] for a discussion of He II λ4686 lines in IPs see
http://asd.gsfc.nasa.gov/Koji.Mukai/iphome/issues/heii.html

Table 3.4: Details of the optical observations of V2491 Cyg.

Date and time	Years AO[a]	Instrument	Exposure (s)
	Photometry		
2015 07 16-18	7.2	WIYN 0.9m HDI	120-180[b]
2015 07 17-23	7.2	CRAO 1.25m	120[c]
	Spectroscopy		
2008 06 08 00:11:49–00:53:04	0.17	Zeiss 1000[d]	1200,2400
2009 07 30 22:38:55–23:05:31	1.25	BTA SCORPIO[e]	420–600
2012 08 17 23:03:40–23:20:13	4.3	BTA SCORPIO[f]	2×900
2015 08 23 18:31:25–20:28:43	7.3	BTA SCORPIO[g]	21×300

[a]Years since the outburst maximum, [b]*UBVRI* filters, [c]no filter, [d]UAGS spectrograph, [e]grism VPHG1200G 3900-5700Å, [f]VPHG550G2 3100-7300Å, [g]VPHG1200B 3600-5400Å.

Spectroscopic observations were performed with the 6-m Big Azimutal Telescope (BTA) and the 1-m Zeiss telescope of the Special Astronomical Observatory of SAO RAS. For the dates of observations and the exposure times refer to tab. 3.4. The slit width was 1". All the spectra were flux calibrated. Photometric observations were performed with the 0.9-m WIYN telescope of the Kitt Peak National Observatory (KPNO) and the 1.25-m telescope of the Crimean National Observatory (CRAO). During the KPNO observations I obtained the mean magnitudes of V2491 Cyg in the *U, B, V, R, I* filters and performed a long-term monitoring in the *V* fiter. The position of V2491 Cyg and the comparison stars are presented in fig. 3.8. For better accuracy, the CRAO observations were performed without filter. Fig. 3.9 shows the KPNO light curve of V2491 Cyg in the *V* band and that of the comparison star #8, which has the same mean brightness as V2491 Cyg. For absolute magnitude calibration I used the 112 822 star from the Landolt Equatorial Standards catalog [173]. The mean absolute magnitudes and the errors are in table 3.5.

3.1.4.1 Timing analysis

I combined the KPNO and CRAO photometric observations, removed possible long-term variations from each nightly light curve, using 1–4 orders polynomial fitting (the order of polynomial function was chosen depending on the length of observation at each night) and performed a timing analysis using the Lomb-Scargle algorithm [80]. Fig. 3.10 shows the LSP with the highest peak at 0.0276 d. (top) and the light curve, folded with this period (bottom). I did not find any reliable modulation on longer timescales. Although the signal at 0.0276 d is low, this finding is very important in the context of the magnetic interpretation of V2491 Cyg. If the of 38.3 min period detected in the X-rays is the spin period of the magnetized WD, the modulation observed in the optical band should be

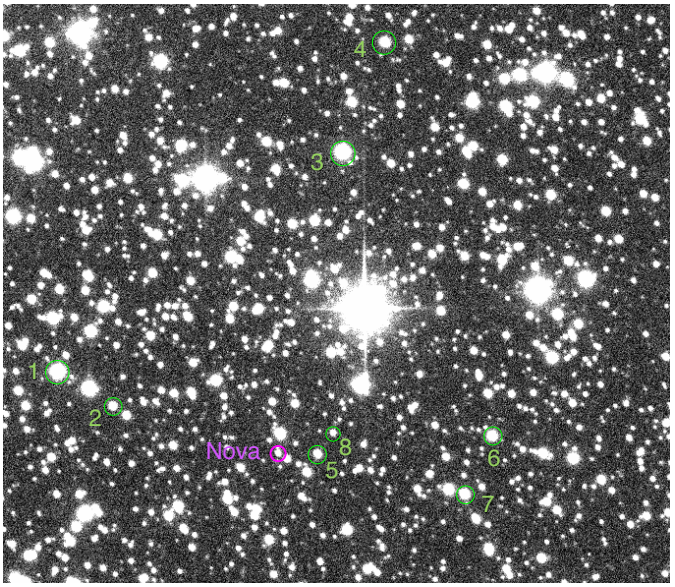

FIGURE 3.8: The V band image of V2491 Cyg obtained with the 0.9-m WIYN KPNO telescope showing the position of the nova (the magenta circle) and the comparison stars (the green circles).

TABLE 3.5: *U,B,V,R,I* magnitudes of V2491 Cyg.

Filter	*U*	*B*	*V*	*R*	*I*
Mag.	18.27±0.07	18.72±0.08	18.03±0.03	17.72±0.03	17.41±0.02

the beat period between the orbital and the spin one. As it is expected, our photometric period is slightly longer than the period detected in the X-rays. Taking into account our measurements, the orbital period should about 0.7 d, too long to be detected in our observations.

3.1.4.2 Spectral analysis

The optical spectra of V2491 Cyg are presented in fig. 3.11, 3.12 and 3.13. All the spectra were flux calibrated, however, in the fig. 3.11 I compare normalized spectra for visibility. The spectral resolution was 8 Å in the observation of 2008, 5.6 Å in 2009, 15.8 Å in 2012 and 6 Å in 2015.

Figure 3.11 shows the evolution of the optical spectrum from the outburst to quiescence. Since the outburst spectra of V2491 Cyg were studied in detail by Ribeiro et al. [174] I will focus mainly on the spectra obtained one year after the explosion and later, when the central source dominates. I just confirm that emission lines measured in the outburst spectrum have a complex saddle-like structure with wings, extended up to 4600 km s^{-1}. Following the discussion of Ribeiro et al. [174] I see that our outburst spectrum is

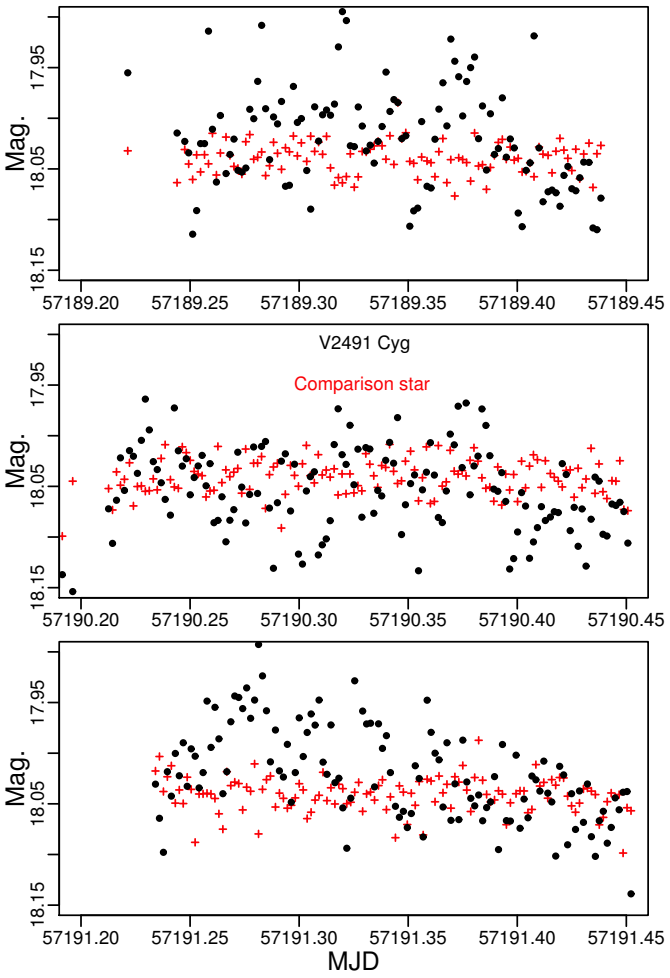

FIGURE 3.9: The V band light curve of V2491 Cyg (black dots) and of the comparison star #8 (red crosses) obtained with the 0.9m KPNO telescope.

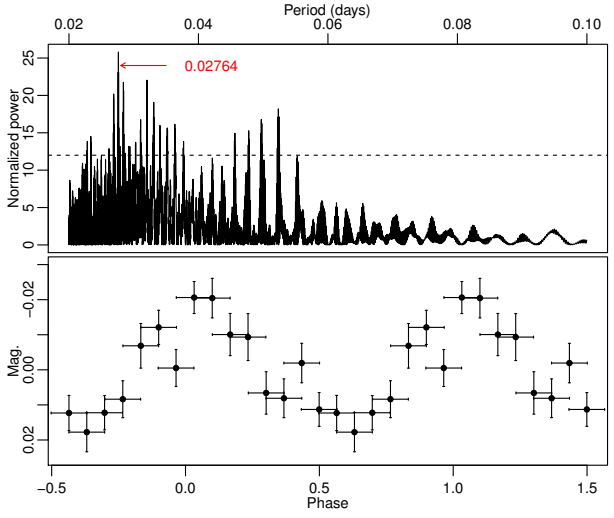

FIGURE 3.10: Top: LSP of the KPNO and CRAO observations of V2491 Cyg. The highest peak marked with the red arrow corresponds to the 0.02764 d. period. The horizontal dashed line represents the 0.3% false alarm probability level. Bottom: the light curve folded with the 0.02764 d. period.

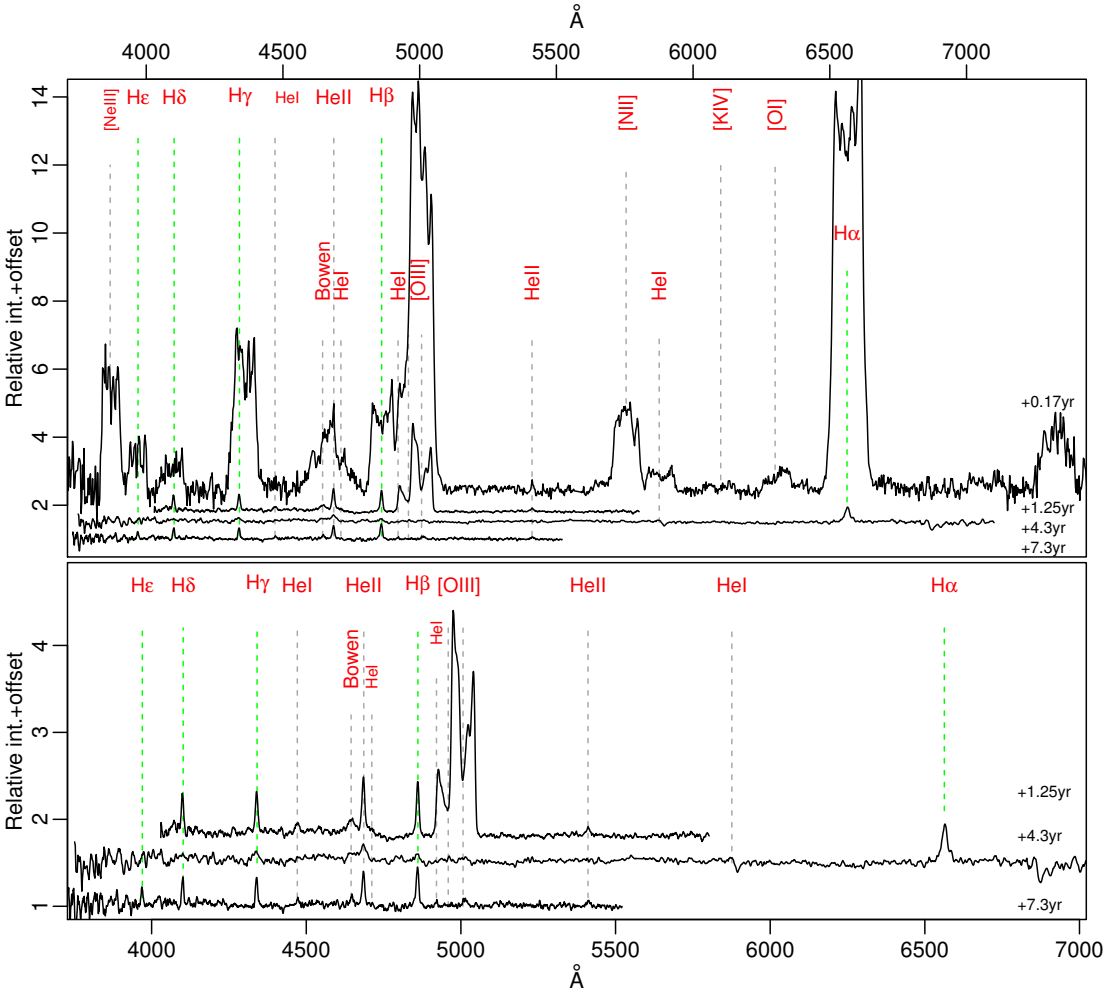

FIGURE 3.11: Top: evolution of the optical spectrum of V2491 Cyg from outburst to quiescence. Years passed after the explosion are marked near each spectrum. Bottom: comparison of the quiescent spectra of V2491 Cyg.

consistent with their model A (polar blobs with an equatorial ring) but has a stronger contribution from the component associated with the equatorial ring.

In the spectrum obtained 4.3 years after the outburst (A0) there are no more signatures of the nova shell emission: the forbidden lines, including the strongest, [O III], have disappeared. The main features of the quiescent spectra are the Balmer lines, the HeII λ4686 line and the Bowen blend $\lambda\lambda$4640 – 4650. The Bowen blend is a combination of high excitation lines, mainly C III, O II, and N III produced by the fluorescence resonance mechanism, which requieres seed photons of He II Lyα at λ303.78 [175]. All the emission lines in the quiescent spectra are single-peaked (excepting the [O III] line, originating in the nova shell), which is most probably due to a low orbital inclination of V2491 Cyg. The orbital period has never been detected in this system, neither spectroscopically nor photometrically, suggesting the inclination lower than $\sim$ 60 degrees. The resolution of the optical spectra, presented in this work, would allow a measurement of line separation

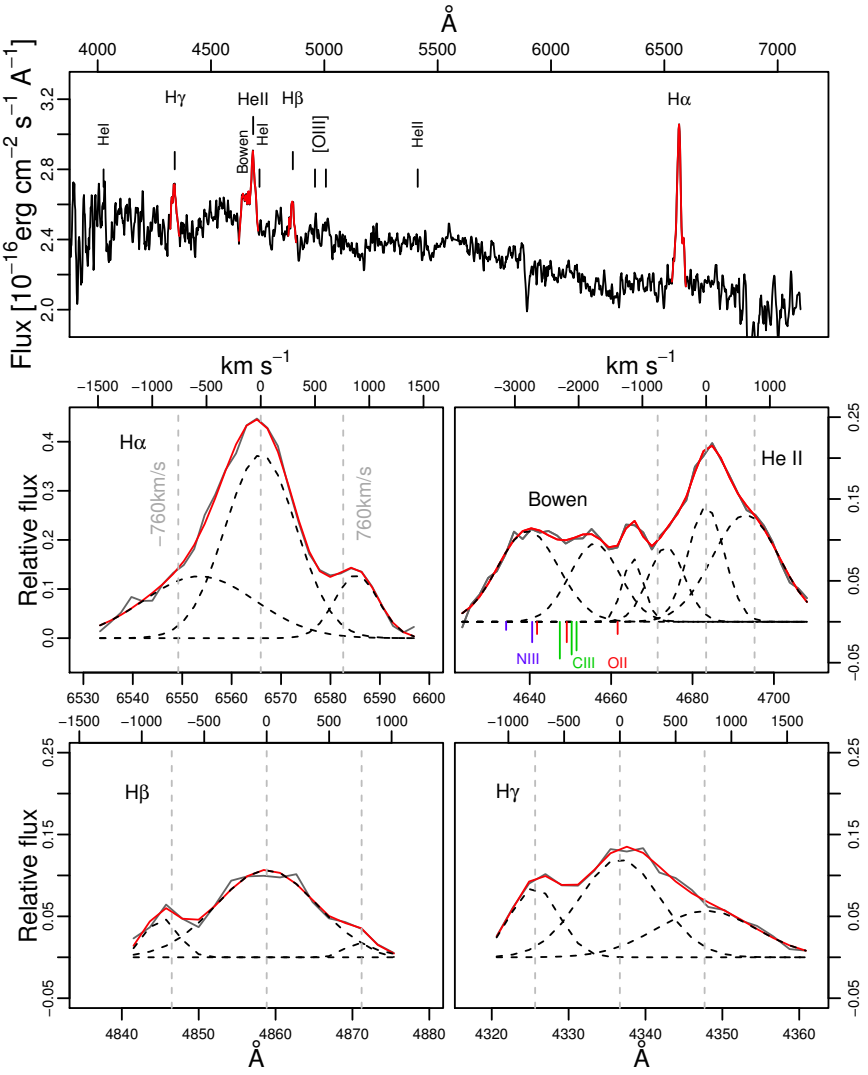

FIGURE 3.12: Top: The flux calibrated spectrum of V2491 Cyg, obtained in 2012. The strongest emission lines are marked. The result of the fit of the emission lines with a number of Gaussians is plotted in red. Bottom: the regions of the Balmer lines, the Bowen blend and the He II line after the subtraction of the continuum. The red lines show the result of the fit and the black-dashed lines show the Gaussian components that were introduced. The table positions of the N III , O II and C III lines that constitute the Bowen blend are marked with blue, red and green vertical lines, respectively. The length of the label depends on the laboratory intensity of the emission line.

of 190 – 360 km s^{-1}, however I did not detect any line splitting, which can be attributed to the Keplerian motion in the accretion disk. If V2491 Cyg is an IP and assuming M_{WD}=1.2 $M_{\odot}$, the Keplerian velocity at the synchronization radius (corresponding to the 38 min rotation period) will be 760 km s^{-1}. In case of non-magnetic accretion, the maximum plasma velocity in the accretion disk will be even higher. If the Balmer lines in the V2491 Cyg spectra originate from the accretion disk, the absence of the double-peaked profiles gives an upper limit for the inclination: arcsin(190/760) = 14 deg.

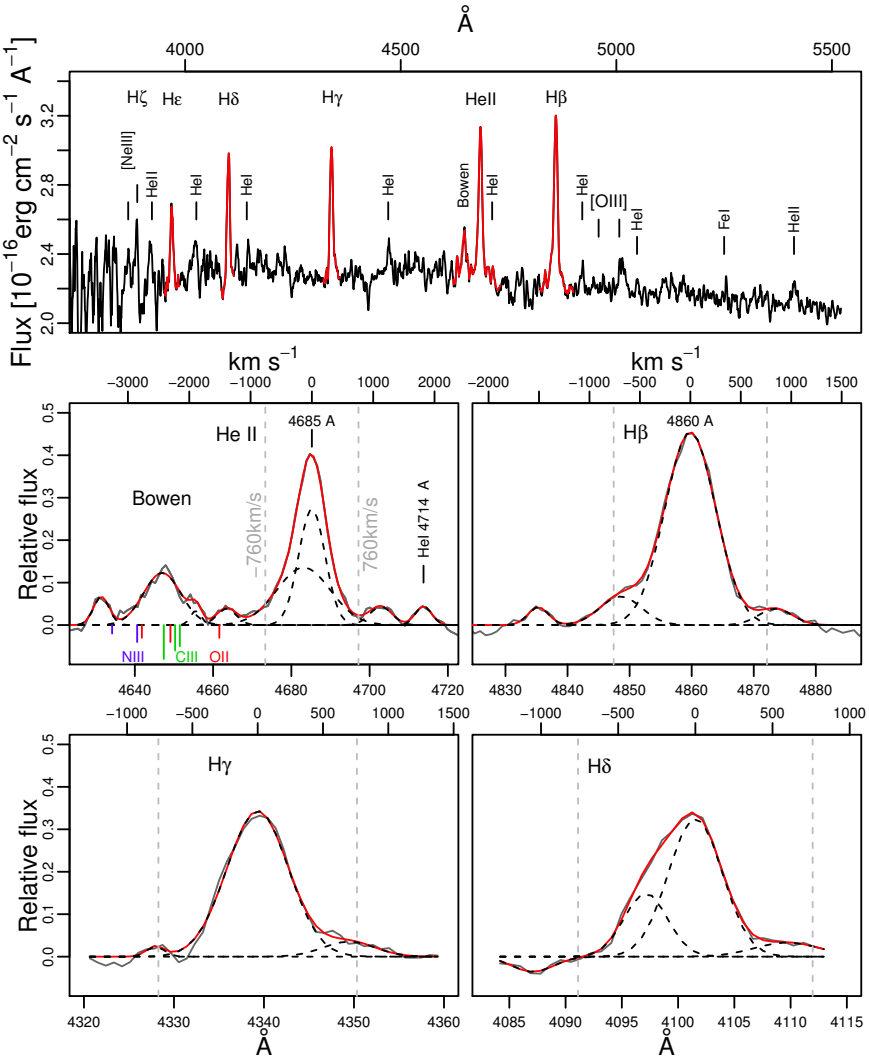

FIGURE 3.13: The same as in fig. 3.12, but for the observations of 2015.

From figure 3.11 we also see that HeII λ4686 line becomes weaker with time, as it is expected from a cooling post-outburst WD. In order to analyse the evolution of the emission lines of V2491 Cyg I localized the regions of the HeII λ4686 and Balmer lines and attempted to fit them with a number of Gaussians after removing the continuum using the `continuum` task in `IRAF`. The result of the fit is marked with the red solid line and the Gaussian components are marked with the black dashed lines in fig. 3.12 and 3.13. The EWs and the fluxes of the emission lines are in table 3.6. From tab. 3.6 we see that the EW of the He II λ4686 line decreased almost by a factor of two between 2009 and 2012. Comparing the flux in the HeII λ4686 with that of Hβ I also noticed a strange behaviour: the EW ratio of the HeII λ4686 to Hβ line was 1.1 in 2009, then 2.5 in 2012 and 0.9 in 2015. From the comparison with other lines I find that these unexpected changes of the flux ratio are due to an unusually weak Hβ line in the 2012 spectrum.

TABLE 3.6: Fluxes and EWs of the emission lines of V2491 Cyg.

Line	Flux ($\times 10^{-16}$ erg cm^{-2} s^{-1})			EW (Å)		
	1.25 yr	4.3 yr	7.3 yr	1.25 yr	4.3 yr	7.3 yr
Hα		15.3			11.7	
Hβ	23.1	3.0	7.1	7.9	2.1	5.5
Hγ	15.3	4.8	4.4	4.9	3.2	3.3
Hδ	17.0		2.7	5.1		2.0
HeIIλ4686	25.7	6.9	6.5	9.0	5.3	4.9
Bowen blend	22.6	5.3	2.8	7.2	4.0	2.0

The He II λ4686 line and the Bowen blend in the BTA spectra of V2491 Cyg obtained up to 7.3 years after the explosion indicate that there is an ionizing component that is strong in the 200–300 Å range. If the ionizing source producing the strong He II λ4686 line in 2009 is the same blackbody-like component, observed with *Suzaku* in 2010 and with *Swift* in late 2008, then the decrease of the EW may be due to a cooling or disappearance of this component. We may speculate that the blackbody-like X-ray component disappeared somewhere between 2010 and 2012. The EWs of the He II λ4686 and Hβ lines are small in comparison to what is usually observed in novae in the first years after explosions [171, 172]. It may imply that the WD photosphere is cooling fast, reducing the number of photons with wavelengths shorter than the 228 Å edge, consequently contributing less to the formation of the He II λ4686 line. Alternatively, the small EWs may be a result of a strong reprocessed continuum due to irradiation of the accretion disk and the secondary.

Almost all the Balmer lines and the HeII λ4686 line in the 2012 and 2015 spectra have two components, red and blue-shifted, with the same velocity $\sim$760 km s^{-1}. This spectrum resembles that of GK Per, a well-known IP, which is the subject of Chapter 4, where similar emission line components were detected during the dwarf nova outburst and were interpreted as emission from the accretion curtain near the magnetized WD [176, 177]. Although some of these line components in V2491 Cyg are weak and are comparable with the noise level, the same velocities and their presence in two spectra, obtained 3 years apart, indicate that they can be real. From the analogy with GK Per, it is reasonable to propose that V2491 Cyg is an IP.

However, we need to explore other possibilities, too. If the nova shell is larger than the slit width, we can loose light with zero radial velocity and detect only the light from the material moving from and towards the observer. The slit width was 1" and assuming the same expansion velocity as was measured during the outburst, 4600 km s^{-1}, and a distance of 10 kpc I find that the upper limit for the shell angular dimension is only 0.38", so we can exclude this possibility. The line components can also be the effect of visibility of the accretion disk at different orbital phases, but since our spectroscopic

observations were shorter than any possibly orbital period (we did not found any reliable modulation with periods in the range 0.05–0.2 d) this explanation cannot be accepted. Another possible explanation is the presence of a wind from the binary system, however we would expect a broad line component, rather than two narrow components with the same velocity. Apart from the magnetic interpretation, a possibility that we cannot exclude is that these components can also be due to some kind of bipolar outflow, like a slow jet.

During the 2015 observations of V2491 Cyg with BTA 21 spectra were obtained (in fig. 3.11 and 3.13 I show the averaged spectrum), however, the data quality did not allow us to study these spectra individually. In order to better explore the possible origin of the red and blue-shifted lines components, I averaged the spectra obtained in 2015 depending on their quality and obtained seven mean spectra covering almost two possible WD spin periods. I then fitted with a number of Gaussians the region of the Hβ line. The result is shown in fig. 3.14. The red and blue dotted lines show the red and blue-shifted line's components and the black dotted line shows the central component. The numbers at the top-right corners of each panel show the chronological order. In the spectrum # 5 and # 7 I had to introduce another component, which is marked with green. It is not clear whether this component is related to the Hβ line emission. Following Morales-Rueda et al. [176] I calculated the V/R ratio, which is the ratio of the flux in the blue-shifted line component to that, of the red-shifted line component. In GK Per a LSP of the time-series of the V/R ratios shows a power at the WD spin period [176]. We have only 7 observations and there is no possibility to perform a timing analysis. However, I attempted to fit the the V/R ratios of the Hβ line with a sine function with a fixed period of 0.0266 d, as measured in the X-ray light curve. The V/R ratios and the result of the fit are shown in the bottom-right panel of fig. 3.14. The variation of the V/R ratio seems to be consistent with the 38 min period. The middle-right panel of fig. 3.14 shows the EW of the central component of the Hβ emission line. In contrast to the V/R ratio the central line does not show variations with the 38 min period. It is consistent with the scenario in which the central line originates from the accretion disk, while the blue and red-shifted components originate from the accretion curtains.

3.1.5 Magnetic driven accretion in V2491 Cyg

Some indications of a magnetic nature of V2491 Cyg can be found in spectral characteristics, also discussed by Takei et al. [156]. These are our main findings favouring the magnetic scenario:

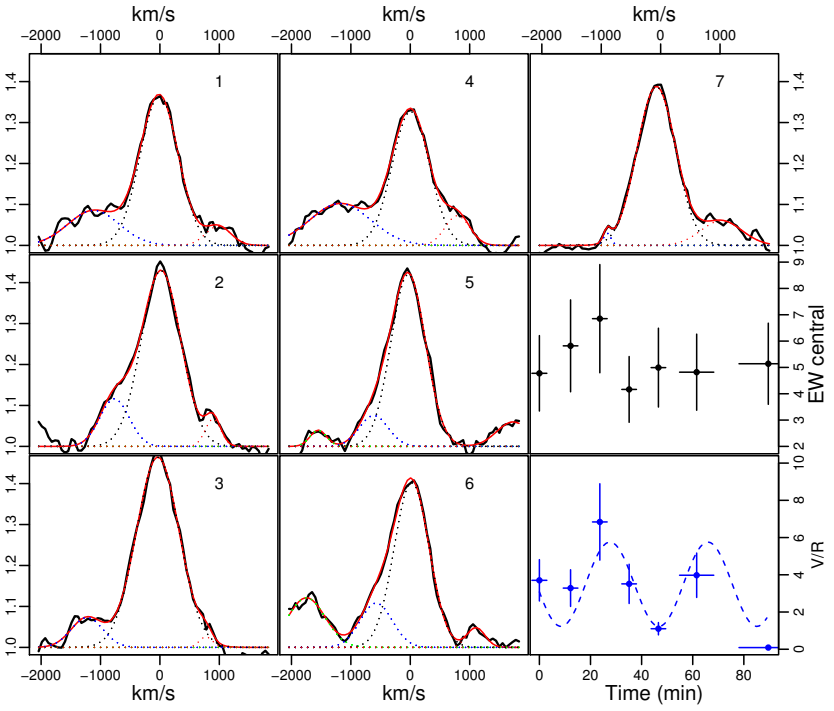

FIGURE 3.14: The evolution of the Hβ line in the 2015 BTA spectrum of V2491 Cyg. The dotted lines show the emission line's components and the red solid line shows the fit. The numbers at the top-right corners of each panel show the chronological order. The last two panels represent the EW of the central Hβ line's component and the V/R ratio as a function of time.

- The hard X-ray band (2.0–10.0 keV) luminosity of V2491 Cyg is $1.82{\times}10^{34}$ erg s^{-1}, which is higher than in most IPs (L_X is usually $\lesssim 10^{33}$ erg s^{-1}, [178, 179]). In IPs the moderately hard X-ray emission mostly originates in high energy plasma produced by the accretion shock on the surface of the WD.

- The observed blackbody-like component may place V2491 Cyg in the group of "soft IPs". The blackbody temperature and the emitting area are comparable with these systems.

- There are two optically thin plasma components with characteristic temperatures ∼0.2 keV and ∼10–20 keV, which may be due to a temperature gradient in the post-shock region.

- We need a complex, partially covering absorber with $N_H{\sim}\ 10^{23}$ cm^{-2} to fit the data, like in many IPs. This phenomenon is usually caused by the accretion curtains crossing the line of sight [60, 61].

- The EW of the Fe Kα line in V2491 Cyg is very large, 246 eV, like usually in IPs (see [180, 181] for the Fe lines in IPs). This is evidence of reflection of the X-ray emitting plasma, most probably from the surface of the WD [163]. It may also

indicate copious X-ray emission above the *Suzaku* XIS detectors' range. However, the observed Compton thin absorber can also contribute to the 6.4 keV line (see [181, 182]).

- The most widely accepted proof of an IP, in which the WD is not synchoronized with the orbital period, is the detection of the spin period in X-rays. The X-ray flux is modulated because the accretion channeled to the pole is shocked, so it is self-occulted and partially absorbed as the WD rotates. I detected an X-ray flux modulation with a period of $\sim$ 38 min that can be attributed to the WD spin. Energy dependence of the amplitude of the pulses supports this assumption and is consistent with the accretion curtain scenario [183, 184].

- The optical flux is modulated with a longer period than the one measured in X-rays. This modulation is likely to arise in the reprocession of the X-rays from the surface of the secondary, which is typical of IPs.

- The prominent He II λ4686 line and the high value of EW(He II λ4686)/EW(Hβ) ratio are also typical of IPs.

- The emission lines detected in the optical spectra have red and blue-shifted components. Similar components were detected in GK Per, a confirmed IP, and are believed to originate in the accretion curtains of the magnetic WD.

On the other hand the IP scenario does not explain the following facts:

- The $\sim$ 38 min period is probably not entirely stable. Also the period detected in the optical light curve may not stable: Shugarov et al. [161] detected a possible 0.02885 d (41 min) period in 2008–2009, while we measured 0.0276 d (40 min).

- According to the empirical criterion for magnetic CVs from Silber [170], the EW of the Hβ line should be grater than 20, while in V2491 Cyg it is $\sim$5. However, as I will show in the next section, this criterion is not always satisfied in IPs.

3.1.6 Conclusions

V2491 Cyg has indeed many characteristics of an IP. We conclude that this system is a strong IP candidate. The most intriguing characteristic of V2491 Cyg is the low-luminosity blackbody-like component in its X-ray spectrum. An important question to answer is whether this component is related to the emission from the irradiated polar cap ("soft IP" scenario) or to the nova explosion. The main difficulties of the "soft IP" scenario are:

- If V2491 Cyg is a "soft IP", the soft X-ray flux emitting region underwent a seamless, early transition from nuclear burning to accretion spot emission, taking into account the observations of Page et al. [159].
- The flux in the He II λ4686 line decreased by a factor of two between 2009 and 2012, which may indicate disappearance of the blackbody-like component somewhere between 2010 and 2012.

A better understanding of this problem was reached after we analyzed observations of another, very similar nova, V4743 Sgr.

3.2 V4743 Sgr

3.2.1 Introduction

Nova V4743 Sgr was discovered by Haseda et al. [185] in outburst in 2002 September 20 close to the 5th magnitude. Kato et al. [186] classified this object as an Fe II-class nova and found that the full width at half maximum (FWHM) of the Hα emission was 2400 km s^{-1}. t_2 and t_3 times for V4743 Sgr are 6 and 12 days, respectively, typical of a very fast nova [187]. Even if the optical light curve decay was fast, the X-ray light curve developed relatively slowly – the nuclear-burning phase lasted at least for 1.5 years after the outburst [188], unlike, for instance, the RNe, which seem to burn the remaining hydrogen very rapidly after the outburst.

V4743 Sgr was the first nova regularly monitored with X-ray gratings in outburst [188–191]. Five additional X-ray grating observations were obtained between 2002 March and 2004 April with *Chandra* and *XMM Newton* and four of them coincided with the supersoft X-ray source (SSS) phase of the nova, when the ejecta became transparent to X-rays from the central source. During the SSS phase the nova was the brightest supersoft X-ray source in the sky and had a continuous spectrum with deep absorption features of O, Ni, and C [190]. Rauch et al. [188] analysed the grating spectra of V4743 Sgr using the NLTE TMAP [79] and found that the nova reached its highest effective temperature of 740 000 K around 2003 April and remained hot for at least 5 months. With such a peak temperature the WD is 1.1 – 1.2 $M_\odot$. van Rossum [192] found a lower value of the effective temperature – 550 000 K, applying a wind-type expanding NLTE model [193]. The difference in the derived effective temperature is not only due to the applied models but also to the higher value of $N_{\rm H}$ inferred by van Rossum [192]. Moreover, the model of van Rossum [192] was developed with solar abundances, which are, however, not suitable for a WD atmosphere.

In addition to offering a view of the WD atmosphere and its composition, the long exposure times in the X-ray grating spectra allowed detection of intense X-ray variability. The nova was in fact very variable, both aperiodically and periodically. Ness et al. [190] detected large-amplitude oscillations with a period of 1325 s (22 minutes) in the first half of their 25 ks *Chandra* exposure but soon after the count rate suddenly dropped to a very low value until the end of the exposure, and only emission lines were observed. Such a low state has never been observed in any of subsequent observations of V4743 Sgr and was probably caused by a temporary obscuration of the central X-ray continuum source by clumpy ejecta [194]. Leibowitz et al. [191] analysed the periodic variability of the X-ray flux in the first two X-ray observations during the outburst, spaced two weeks apart and detected a combination of oscillations represented by a number of discrete frequencies lower than 1.7 mHz. At least five of these frequencies, including the one at 0.75 mHz, were present in both observations. The authors proposed that the 0.75 mHz frequency and its first harmonic in the power spectrum were related to the WD spin period while the other oscillations were due to non-radial pulsations of the WD. Dobrotka and Ness [195] extended the study of the X-ray variability of V4743 Sgr, including three more observations of the nova in outburst, and the two quiescent exposures, proposed by us and discussed in this paper. These authors found that the 0.75 mHz (22 min) feature in the power spectrum was due to different frequencies in outburst, but eventually in the quiescent observations only one frequency remained, which they attributed to the spin period of a magnetized WD in an intermediate polar (IP), following also a suggestion of Leibowitz et al. [191]. Optical observations also strongly support the IP scenario. Kang et al. [196], Richards et al. [197] and Wagner et al. [198] presented measurements of the orbital period ($\sim$ 6.7 h), and detected a much shorter period of $\sim$24 minutes, which seems to be the beat of the orbital period and the one observed in the X-rays, like the period we measured in the optical data of V2491 Cyg.

From their infrared observations Nielbock and Schmidtobreick [199] roughly estimated the distance to V4743 Sgr as 1200$\pm$300 pc, however, the authors pointed out that this value should be taken with caution because of the uncertainties in the estimates of the interstellar extinction towards the nova. The authors also stressed that the maximum possible distance is 6 kpc. Vanlandingham et al. [200] derived a distance of 3.9$\pm$0.3 kpc using the MMRD relationship [9].

In this section I present the *XMM Newton* observations, proposed by PI Orio and performed in quiescence 2 and 3.5 years after the nova explosion and the optical spectra of V4743 Sgr, obtained with the Southern African Large Telescope (SALT) 12 years after the outburst, revealing the evolution of the supersoft X-ray component and the expanding nova shell.

TABLE 3.7: Details of the *XMM Newton* and *SALT* observations of V4743 Sgr.

Date and time	Instrument	Exposure (s)	Count rate (cnts s^{-1})/Mag.[1]
2004-09-30 18:28:25	*XMM Newton* MOS1	22163	0.101 ± 0.002
2004-09-30 18:28:23	*XMM Newton* MOS2	22168	0.103 ± 0.002
2004-09-30 18:27:28	*XMM Newton* RGS1	21295	0.006 ± 0.002
2004-09-30 18:27:36	*XMM Newton* RGS2	21295	0.006 ± 0.002
2004-09-30 18:36:34	*XMM Newton* OM U	4000	14.4019 ± 0.0015
2004-09-30 19:48:21	*XMM Newton* OM B	4000	15.517 ± 0.003
2004-09-30 21:00:09	*XMM Newton* OM UVW1	3998	14.0620 ± 0.0015
2004-09-30 22:11:55	*XMM Newton* OM UVM2	4181	14.156 ± 0.013
2004-09-30 23:26:56	*XMM Newton* OM UVW2	4398	14.27 ± 0.02
2006-03-28 15:28:18	*XMM Newton* MOS1	34164	0.0597 ± 0.0017
2006-03-28 15:28:18	*XMM Newton* MOS2	34168	0.0692 ± 0.0017
2006-03-28 15:27:25	*XMM Newton* RGS1	34418	0.0009 ± 0.0012
2006-03-28 15:27:29	*XMM Newton* RGS2	34410	0.0019 ± 0.0015
2014-03-21 02:54:48	*SALT* RSS[2]	1000	
2014-03-21 03:11:48	*SALT* RSS	1000	

[1] The mean count rate during the exposure for the X-ray observations and the mean magnitude for the *XMM Newton* OM optical monitor (OM) observations. The effective wavelengths of the *XMM Newton* OM filters are: U — 344 nm, B — 450 nm, UVW1 — 291 nm, UVM2 — 231 nm, UVW2 — 212 nm. [2]Robert Stobie Spectrograph

3.2.2 X-ray observations and data analysis

V4743 Sgr was observed with all the instruments onboard *XMM Newton* on September 30 2004 and with the European Photon Imaging Camera (EPIC), and the Reflection Grating Spectrometer (RGS 1 and RGS 2) on March 28 2006 (742 and 1286 days after the nova explosion, respectively). Here I focus mainly on the data of the EPIC Metal Oxide Semi-conductor (MOS) CCD arrays: MOS 1 and MOS 2. The RGS data had a very low signal-to-noise ratio and only the 2004 observation allowed us to marginally detect several emission lines. The data of the EPIC pn camera were not suitable for the analysis, since the source was on a chip gap. The X-ray spectra were fitted with XSPEC v.12.8.2. The dates and exposure times of both X-ray and optical observations are presented in table 3.7.

3.2.2.1 Spectral analysis

The background subtracted 0.2 – 10.0 keV spectra of V4743 Sgr together with the best-fitting models are presented in fig. 3.15. The 2004 data are plotted in black (MOS 1) and red (MOS 2) and the 2006 data in blue (MOS 1) and green (MOS 2). We first analysed the 2004 spectrum because of the higher count rate and found that the best-fitting model consists of a blackbody and two thermal plasma components affected by a partially covering absorber (`pcfabs` model in the `xspec`). Without the complex absorption it was impossible to fit the hard part of the spectra even increasing the temperature. I used the `vapec` model of thermal plasma emission in `xspec`, since it

allows constrains of abundances of different elements and novae have a highly non-solar composition.

In order to compare our results with the outburst *XMM Newton* and *Chandra* X-ray spectra of V4743 Sgr studied in detail by Rauch et al. [188] and van Rossum [192] I attempted a fit of the supersoft component in the 2004 spectrum with the atmospheric model of Rauch et al. [188]. The atmospheric model that I used had the same abundances and $\log g$ as model B in Rauch et al. [188].

The next step was to fit the 2006 data. From fig. 3.15 we see that major changes during one and a half year between observations were in the softest region of the spectrum — the blackbody-like component was no longer measured in the 2006 observation, while the part of the spectrum above 1 keV was almost the same. The data quality did not allow us to fit the 2006 spectrum independently, so I tried a simultaneous fit of the 2004 and 2006 datasets applying the same model and setting the normalization of the blackbody component to zero. I also assumed that the interstellar absorption and the element abundances of the plasma are the same in both observations but let other parameters to vary freely. Although the variable opacity of the nova shell may contribute to the value of the interstellar absorption, I did not expect the absorption to increase, obscuring the soft emission in 2006.

The best fitting parameters of our models are summarised in table 3.8. All the fits required increased abundances of Si and S, but the spectra quality did not allow us to constrain their values. I also did not detect the 6.4 keV Fe Kα reflection line at a significant level.

Rauch et al. [188] fitted the spectrum during the constant bolometric luminosity phase with $T_{eff} \simeq 700\,000$ K and found only evidence of moderate cooling with a temperature of 660 000 K in February of 2004, but the temperature may have been constant within the errors. Eight months later, in the first observation I discuss here, the supersoft flux had decreased by 5 orders of magnitude comparing with the estimates of Rauch et al. [188], but the equivalent blackbody temperature had not decreased, implying shrinking of the emitting region. In other cases, novae have been observed to become fainter at decreasing temperature, consistently with cooling as hydrogen burning turns off (e.g. V1974 Cyg, [201]).

We wanted to assess whether freezing the value of the column density $N_{\rm H}$ at a higher assumed value results in a fit with a lower temperature and higher luminosity, indicating that the whole WD surface may be emitting. The value of the interstellar absorption, derived in our fit is consistent with the estimates of Rauch et al. [188], but is about

TABLE 3.8: The parameters of the best fitting models – wabs×(bb/atm+pcf×(vapec+vapec)) for V4743 Sgr X-ray spectra. The errors represent the 90% confidence region for a single parameter. The luminosity is given assuming a distance of 4 kpc, consistent with the MMRD relation (see discussion in the text).

	Simultaneous fits				Independent fits	
Parameter	2004	2006	2004+atm	2006+atm	2004	2004+atm.
$N_{\rm H}$ [a]	$0.7^{+0.3}_{-0.3}$	$0.7^{+0.3}_{-0.3}$	$0.40^{+0.18}_{-0.16}$	$0.40^{+0.18}_{-0.16}$	$0.4^{+0.4}_{-0.3}$	$0.24^{+0.18}_{-0.17}$
$N_{\rm Hpc}$ [b]	87^{+20}_{-17}	60^{+60}_{-30}	81^{+20}_{-16}	40^{+38}_{-16}	85^{+20}_{-17}	80^{+19}_{-16}
CvrFract[c]	$0.75^{+0.03}_{-0.05}$	$0.46^{+0.14}_{-0.08}$	$0.75^{+0.03}_{-0.05}$	$0.45^{+0.12}_{-0.06}$	$0.75^{+0.03}_{-0.05}$	$0.75^{+0.03}_{-0.03}$
$T_{\rm bb/atm}$ (eV)	53^{+10}_{-9}		63^{+4}_{-3}		64^{+15}_{-15}	67^{+6}_{-4}
T_1 (keV)	$0.21^{+0.03}_{-0.02}$	$0.105^{+0.040}_{-0.018}$	$0.202^{+0.023}_{-0.018}$	$0.13^{+0.03}_{-0.03}$	$0.21^{+0.04}_{-0.03}$	$0.22^{+0.03}_{-0.02}$
T_2 (keV)	13^{+12}_{-3}	>14	14^{+12}_{-4}	>17	13^{+12}_{-3}	$13.3^{+13}_{-3.0}$
Norm$_1$ [d]	$0.33^{+0.26}_{-0.16}$	$0.40^{+1.13}_{-0.29}$	$0.30^{+0.17}_{-0.11}$	$0.10^{+0.35}_{-0.03}$	$0.18^{+0.26}_{-0.14}$	$0.21^{+0.14}_{-0.09}$
Norm$_2$ [d]	$1.49^{+0.16}_{-0.14}$	$1.02^{+0.17}_{-0.16}$	$1.44^{+0.16}_{-0.14}$	$1.03^{+0.14}_{-0.18}$	$1.49^{+0.16}_{-0.14}$	$1.44^{+0.16}_{-0.14}$
Flux$^{e}_{\rm abs}$	$2.28^{+0.07}_{-0.32}$	$1.56^{+0.5}_{-1.5}$	$2.29^{+0.05}_{-2.0}$	$1.6^{+1.2}_{-1.5}$	$2.29^{+0.08}_{-0.3}$	$2.3^{+4.5}_{-1.9}$
Flux$^{e}_{\rm unabs}$	7.62	2.88	5.35	2.13	5.35	4.82
Flux$^{\rm bb/atm\,f}_{\rm abs}$	0.282		0.227		0.306	0.245
Flux$^{\rm bb/atm\,f}_{\rm unabs}$	1.98		0.552		0.981	0.431
χ^2	1.2	1.2	1.2	1.2	0.9	0.9
$L^{g}_{2.0-10.0{\rm keV}}$	4.62	2.76	4.53	2.70	4.60	4.52
$L_{\rm bb}$ [h]	8^{+25}_{-5}		4.9		$3.2^{+12.8}_{-1.6}$	3.84
$R_{\rm bb/atm}$ [i]	8.8		5^{+4}_{-3}		3.8	4^{+3}_{-3}

[a] $\times 10^{21}\,{\rm cm}^{-2}$. [b] $N_{\rm Hpc}$ $\times 10^{21}\,{\rm cm}^{-2}$ for the partial covering absorber. [c] Covering fraction of the partial covering absorber. [d] $\times 10^{-3}$ Normalization constant of the `vapec` model. [e] The X-ray flux ($\times 10^{-12}$ erg cm^{-2} s^{-1}) measured in the range 0.2–10.0 keV. The Flux$_{\rm unabs}$ represents the value of the X-ray flux, corrected for the interstellar and intrinsic absorption. [f] The X-ray flux ($\times 10^{-12}$erg cm^{-2} s^{-1}) of the blackbody component measured in the range 0.2–10.0 keV. [g] The X-ray luminosity ($\times 10^{33}\,{\rm erg\,s^{-1}}$ D$^2_{\rm 4kpc}$) in the range 2.0–10.0 keV. The $L_{2.0-10.0{\rm keV}}$ was calculated from the X-ray flux in the range 2.0–10.0 keV, corrected for the interstellar and intrinsic absorption. [h] The bolometric X-ray luminosity ($\times 10^{33}\,{\rm erg\,s^{-1}}$ D$^2_{\rm 4kpc}$) of the blackbody and atmospheric component. $L_{\rm bb/atm}$ were calculated from the normalization constants of the models. [i] The radius of the emitting region ($\times 10^6$ cm). For the blackbody fit $R_{\rm bb}$ was found from the Stefan-Boltzmann law. The atmospheric model gives the value of the emitting radius $R_{\rm atm} = 10^{-11}\sqrt{\rm norm}\ {\rm D_{4kpc}}$ cm.

two times lower than the one in the direction of V4743 Sgr given by the Leiden/Argentine/Bonn (LAB) Survey of Galactic H I and the Dickey&Lockman H I map in the $N_{\rm H}$ ftool[2] (a column density of 1.05 and $1.41\times10^{21}\,{\rm cm}^{-2}$, respectively). Moreover, van Rossum [192] claimed that the analysis of the red tail slope of the *Chandra* X-ray spectrum of V4743 Sgr in outburst, indicates $N_{\rm H}= 1.36 \pm 0.04 \times 10^{21}\,{\rm cm}^{-2}$. So there are indeed reasons to think that $N_{\rm H}$ may be higher than our best fitting values. We thus set the value of $N_{\rm H}$ to $1.36\times10^{21}\,{\rm cm}^{-2}$ and fitted the 2004 spectrum again with both the blackbody and the atmospheric model. As expected, the increased absorption mainly affected the supersoft component, and returned $T_{\rm bb} = 38.7^{+3.1}_{-2.7}\,{\rm eV}$, $T_{\rm atm} = 662^{+20}_{-21}\,{\rm kK}$, and much higher luminosity — $L_{\rm bb} = 1.1^{+0.7}_{-0.4} \times 10^{35}\ {\rm D^2_{4kpc}\,erg\,s^{-1}}$, $L_{\rm atm} = 2.55 \times 10^{34}\ {\rm D^2_{4kpc}\,erg\,s^{-1}}$, corresponding to the radius of the emitting region of $R_{\rm bb} = 6.2 \times 10^7\ {\rm D_{4kpc}\,cm}$ and $R_{\rm atm} = 1.3 \times 10^7\ {\rm D_{4kpc}\,cm}$, respectively, still smaller than the WD radius (for our calculations I assumed a distance of 4 kpc, since this value

[2] http://heasarc.gsfc.nasa.gov/cgi-bin/Tools/w3nh/w3nh.pl

is close to the mean of the estimates mentioned in section 3.2.1). Another mechanism that should be taken into account is a possible absorption in the accretion curtain of the magnetized WD. In our best fitting model I assumed that the partial covering absorber affects only the thermal plasma emission, however, I will further show that the 2004 soft X-ray light curve is also modulated with the WD spin period, which may be due to the accretion curtain, crossing the line of sight (see fig. 3.18 and section 3.2.2.2). If we assume that the blackbody component is absorbed by the partially covering absorber, the resultant blackbody luminosity is $L_{bb} = 3^{+10}_{-2} \times 10^{35}\ D^2_{4kpc}\,erg\,s^{-1}$ and $R_{bb} = 1.8 \times 10^7\ D_{4kpc}\,cm$.

The 2004 RGS spectra are presented in fig 3.16. Several emission lines are marginally detected: O VII at ∼21.8–22 Å, O VIII at ∼18.9 Å, Fe XVII at 17.2 Å and N VII at ∼25 Å. The spectrum has a very low signal-to-noise ratio and I did not use it to refine the model parameters. In fig. 3.16 I overplot the best-fitting model over the binned RGS 1 and 2 data and present the residuals in order to show that the model is consistent with the RGS data.

3.2.2.2 Timing analysis

I binned the *XMM Newton* light curves every 100 seconds, combined the data of the MOS 1 and MOS 2 detectors and subtracted a possible long-term trend with a third-order polynomial fit. I applied the Lomb-Scargle method [80] for the 2004 and 2006 datasets in order to investigate the X-ray intensity modulations. The resultant LSPs are presented in fig. 3.17. In both light curves the ∼0.75 mHz frequency (the 22 min period) is clearly detected. The dashed horizontal line is the 0.3% false alarm probability and the dashed blue line shows the LSP after the subtraction of the main peak by fitting and removing a sine function. I also applied the bootstrap method, repeatedly scrambling the data 10000 times and calculating the probability that random peaks in LSP in the range 0.1 mHz – 2 mHz exceed the height of the peak at 0.75 mHz in the original LSP. The probability that the peak in the original data occurred by chance is zero for the 2004 dataset and 0.02% for the 2006 one. In order to confirm the values of the frequencies with an independent analysis I applied the PDM method [81] to the same light curves. The values of the frequencies found with different methods are presented in table 3.9.

We investigated the energy dependence of the X-ray modulation. I first extracted the light curves in two energy ranges: 0.3 – 0.8 keV and 0.8 – 10 keV and performed the same methodology as was mentioned above. Fig. 3.18 represents the LSPs for the hard and soft energy ranges of the 2004 and 2006 datasets. While in 2004 the modulation was the same in both energy ranges, in 2006 it was present only in the hard X-rays. The

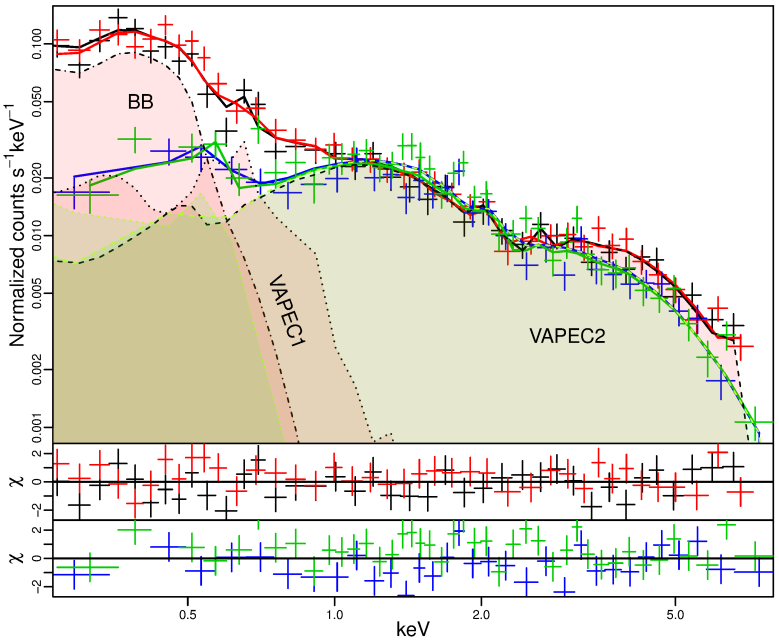

FIGURE 3.15: Top panel: XMM *Newton* spectra of V4743 Sgr. The 2004 data are plotted in black (MOS 1 data) and in red (MOS 2) and the 2006 data in blue (MOS 1) and in green (MOS 2). The solid lines represent the fit with `wabs`×(`bb+pcfabs`×(`vapec+vapec`)) model, where the parameters of the interstellar absorption (`wabs`) and the plasma abundances of the 2004 and 2006 spectra were tight. The normalization of the blackbody component was set to zero in the model of the 2006 spectra. The components of the models are plotted with the dotted (low-temperature `vapec` components), dashed (high-temperature `vapec` components) and the dash-dotted lines (the blackbody component). The model components of the 2004 data were filled with pink and that of the 2006 model – with green. Middle panel: residuals of the 2004 MOS 1 and MOS 2 data fit. Bottom panel: residuals of the 2006 MOS 1 and MOS 2 data fit.

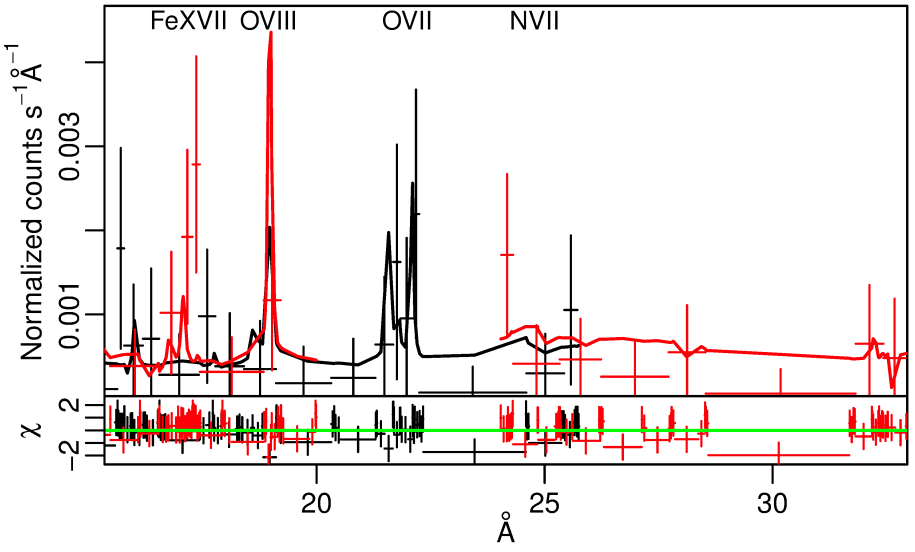

FIGURE 3.16: Top panel: The 2004 XMM *Newton* RGS spectra of V4743 Sgr. The RGS 1 data are plotted in black and RGS 2 — in red. The solid lines represent the best-fitting model of the XMM *Newton* MOS data. The data were binned for visualizing purposes. Bottom panel: residuals from the model.

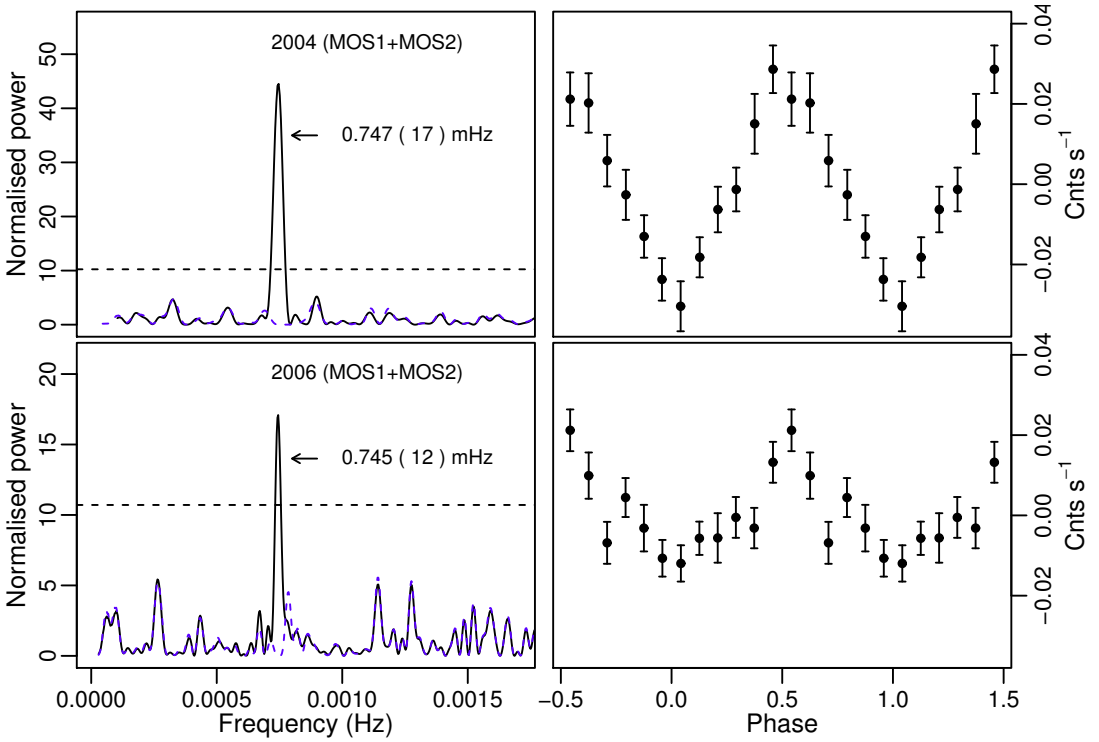

FIGURE 3.17: The Lomb-Scargle periodograms and the phase folded light curves of the 2004 (top) and 2006 (bottom) *XMM Newton* light curves. The data from the MOS 1 and MOS 2 detectors were combined. The values of the frequencies and the 1σ errors, calculated by fitting a Gaussian in the main peak of the LSP, are marked in the plots. The horizontal dashed line represents the 0.3% false alarm probability level. The blue dashed lines are the LSPs of the same datasets after subtraction of the highest peak. The light curves were folded with the same frequency – 0.748 mHz (22.2 min period).

amplitudes of the modulation in 2004 were ∼50% and 30% in the soft an hard ranges, respectively and ∼30% in the hard range in 2006. Aiming to constrain the spectral component, modulated with the spin period in the 2004 dataset, I extracted the MOS 1 and 2 light curves in a narrower range — 0.3 – 0.6 keV, where the blackbody-like emission dominates. The modulation was still present even in this energy range, indicating that the supersoft X-ray emission is modulated with the same period.

Using the spin period found from the PDM analysis of the 2006 hard light curve, I calculated the ephemeris of the pulse maxima. The Modified Barycentric Julian Date of the maxima can be found as:

$$\mathrm{T_{max}(MBJD)} = 53822.6488(25) + 0.0154439(15) * E \tag{3.1}$$

Although the orbital modulation was observed in the optical band [196–198], indicating a moderately high inclination of $\sim 60°$, I find no variability that might represent an orbital modulation in our X-ray data, neither in the soft, nor in the hard ranges.

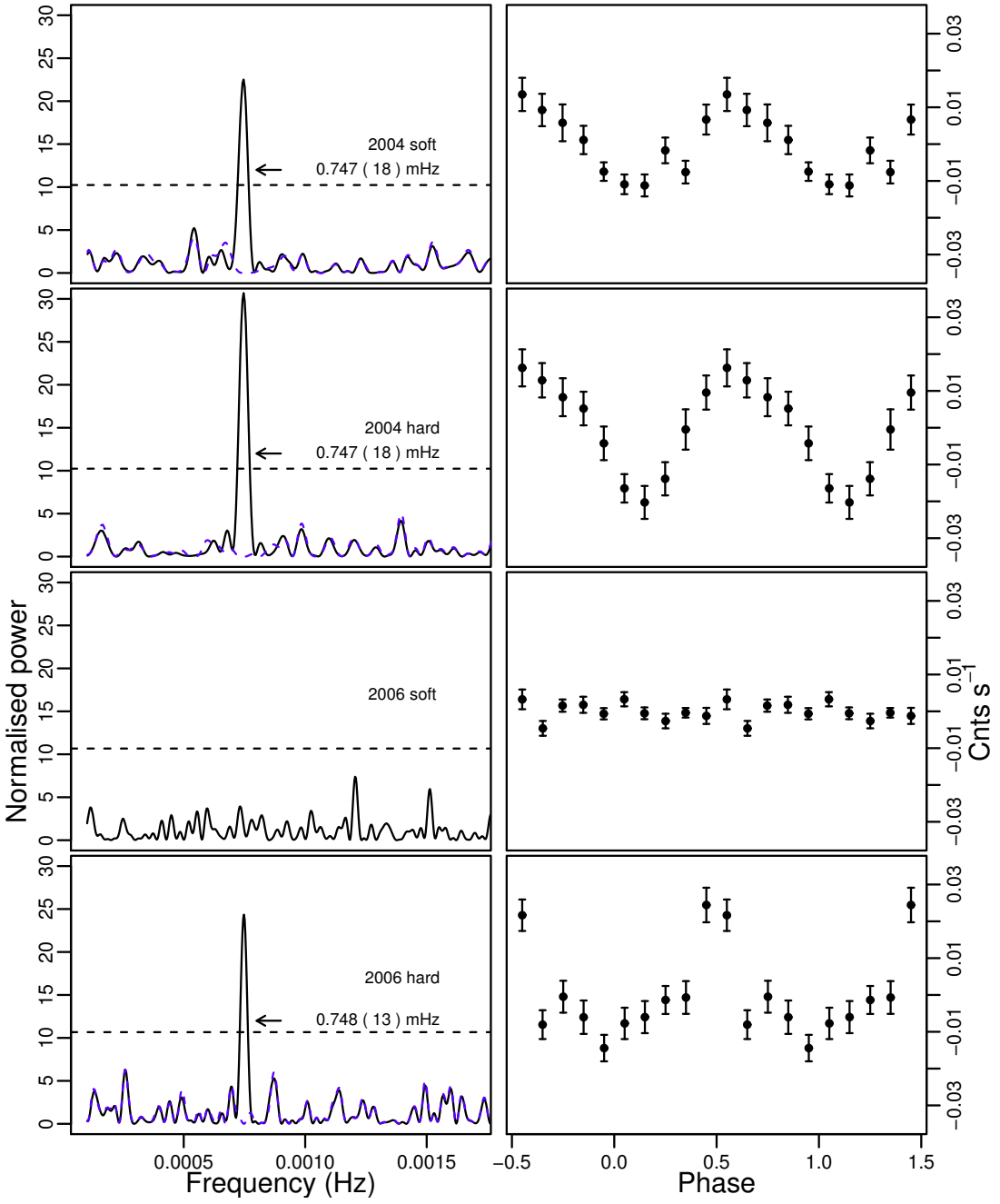

FIGURE 3.18: The same as fig. 3.17, but for energy ranges below (soft) and above (hard) 0.8 keV.

TABLE 3.9: The results of the timing analysis of the *XMM Newton* light curves.

Dataset	Frequency (mHz)		Period (min)	
	LS	PDM	LS	PDM
2004 (MOS1+MOS2)	0.747(17)	0.7424(14)	22.3(5)	22.45(4)
2006 (MOS1+MOS2)	0.745(12)	0.7434(28)	22.4(4)	22.42(8)

Notes LS — Lomb-Scargle method; PDM — Phase Dispersion Minimisation method. The erros in the frequencies found with the LS method correspond to the 1σ level.

3.2.3 Optical observations

3.2.3.1 SALT observations

Optical spectra of V4743 Sgr in the $\lambda\lambda$4500–5600 Å range were obtained on March 21 2014 at the SALT telescope using the Robert Stobie Spectrograph (RSS), grating PG2300, in a long slit mode (single, 8 arcmin long, 1.5 arcsec wide slit)[3]. The instrumental resolution is 110 – 120 km s^{-1}. For the flux calibration I used the standard star Feige 110. This observation was done in the framework of a monitoring program of novae previously observed as SSS as they returned to quiescence (Zemko 2016 in prep).

The flux calibrated and de-reddened optical SALT spectrum is presented in the top panel of fig. 3.19. For dereddening I assumed $N_{\rm H}$=0.71×10^{21} cm^{-2} (see table 3.8), which corresponds to E(B-V)=0.12 [148]. The [O III] λ5007 line is only marginally detected (the rest wavelengths of the [O III] lines are marked on the plot), which is typical of a very fast nova after 10 years [202].

The strongest emission lines are He II λ4686, Hβ and the Bowen blend. I removed the continuum using the `continuum` task in `IRAF` and fitted with Gaussians the main features in these regions (the Hβ, He II λ4686 lines and their components and the Bowen blend) in order to measure their central positions and velocity broadening. The result of the fit is shown with the red line in all the plots of fig. 3.19 and the dashed black lines on the bottom plots show the Gaussian components that were introduced. The central positions of the best fitting Gaussians are also marked. From this fit I found that both Hβ and He II λ4686 emission lines have a narrow and a broad component, just slightly shifted with respect to each other as it is seen from the bottom panels of fig. 3.19. The narrow component of Hβ has a double peaked profile with a separation of only ∼250 km s^{-1} between the two peaks, which is quite small for the accretion disk rotation (assuming M$_{\rm WD}$=1.2 M$_\odot$, P$_{\rm orb}$=6 h and a reasonable value for the mass ratio q∼0.8 the velocity will be about 560 km s^{-1} at the radius of the tidal limit of the accretion disk, which is expected to be the upper limit for the disk radius, see e.g. [203]). The broad component of Hβ has a FWHM of ∼1300 km s^{-1} and the broad component of He II λ4686 — ∼990 km s^{-1}. The Hβ line seems to have another small component at 4876 Å, red-shifted by ∼970 km s^{-1} with respect to the position of the double-peaked central line. Interestingly, similar small components, red and blue-shifted by almost the same velocity of ∼950 km s^{-1} are also observed in the He II λ4686 line. Similar line components were measured in the optical spectra of V2491 Cyg.

[3] Under program 1178-7 2013-2-UW-001 (PI: Marina Orio)

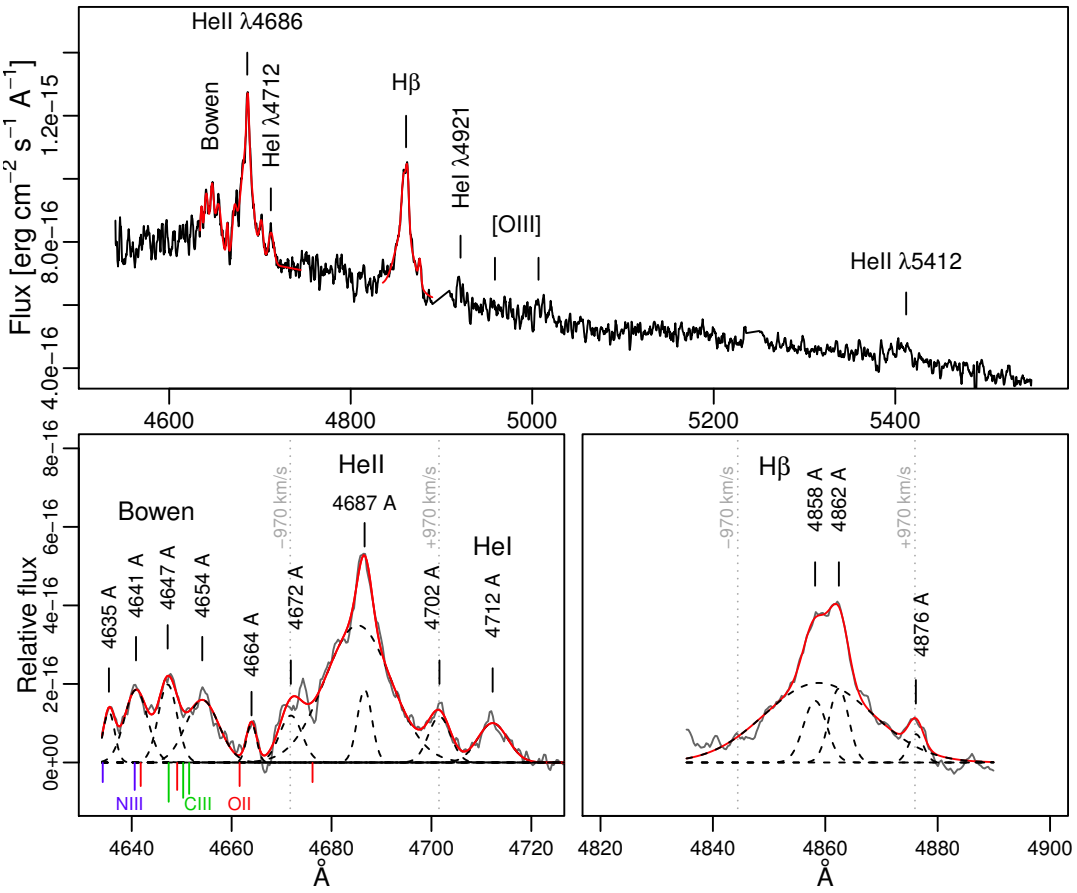

FIGURE 3.19: Top: The SALT spectrum of V4743 Sgr, revealing the strong emission lines of the He II λ4686 and Hβ. Bottom: The regions of the Bowen blend, He II λ4686 and the Hβ lines after the subtraction of the continuum. The red lines show the fit of the He II λ4686, Bowen blend and He I (left) and the Hβ (right) lines. Both the He II λ4686 and Hβ lines have a narrow and a broad component. The central positions of the best fitting Gaussians are marked on the plots (excepting the broad components, since they roughly coincide with the narrow ones). The grey dotted vertical lines show the velocity shifts of $\pm$970 km s^{-1}. The black dashed lines represent the Gaussians that were introduced to the fit. The table positions of the N III , O II and C III lines that constitute the Bowen blend are marked with blue, red and green vertical lines, respectively. The length of the label depends on the laboratory intensity of the emission line.

Another prominent feature of the spectrum is the Bowen blend at $\lambda\lambda$4640–4650 Å. The rest positions of the most intensive lines are indicated in the bottom-left panel of fig. 3.19. The length of the label of each line depends on its laboratory intensity. I see that the λ4641 and λ4647 lines, observed in the spectrum, coincide with the rest positions of the N III and C III lines, respectively. On the other hand, the origin of the λ4654 line is unknown. The EWs of the He II λ4686 and Hβ emission lines are about 10.5 Å and that of the Bowen blend is $\sim$5.2 Å.

3.2.3.2 Kepler observations

The Kepler observations of V4743 Sgr were proposed by us (PI Orio) in the framework of the K2 campaign (field #7). Both short (2 min) and long (30 min) cadence light curves were obtained. The analysis of the short-cadence light curve is now in progress and I will discuss here only the long-cadence light curve. The 30 min cadence light curve of V4743 Sgr was extracted using the K2SFF tool [204][4]. The top-left panel of fig. 3.20 shows this light curve, which is variable on timescale of several days, but with no definite periodicity. I divided the light curve in segments with the length of 1 day and removed the long-term variations with a third-order polynomial fitting from each segment. The de-trended light curve is presented in the top-right panel of fig. 3.20. I then applied the Lomb-Scargle method to search periodic modulations. The middle panels show spikes in the LSPs, which correspond to the orbital period (6.684 h) and to the beat-period between the orbital and the spin one (23.65 min). Taking into account these two periodicities and the period found in the X-ray light curves, we see that a relation $1/P_{spin} - 1/P_{orb} = 1/P_{beat}$ is perfectly satisfied.

3.2.4 Discussion

V4743 Sgr is a bright X-ray source, which emitted both soft (<0.6 keV) and hard X-rays in 2004 and only hard in 2006. Novae shortly after eruption can emit X-rays in the 1–10 keV range originating from the shocked ejected shells [205, 206], but since the source of this emission is spatially extended it cannot be variable on short time scales, in contrast to our observations (figs. 3.18 and 3.17). Based on the fact that the hard X-ray component, which is present in both observations, is modulated with the WD spin period and is also well fitted with the two-temperature thermal plasma emission model, typical of plasma in collisional equilibrium cooling as it settles onto the WD, we argue that this component is due to the resumed accretion.

The disappearance of the soft emission in 2006 indicates that it is, in turn, associated with hydrogen burning and not with accretion. The soft component was also modulated with the WD spin period supporting the idea that the source of this emission is close to the WD surface, like in case of short-period X-ray oscillations of novae in SSS phases found by Ness et al. [207]. Since both *XMM Newton* exposures are longer than the orbital period the disappearance of the supersoft component is also not an effect of different orbital phases.

As in case of V2491 Cyg the He II λ4686 line and the Bowen blend in the *SALT* spectra of V4743 Sgr indicate that there is still an ionizing component that is strong in the 200–300

[4] https://archive.stsci.edu/k2/hlsp/k2sff/search.php

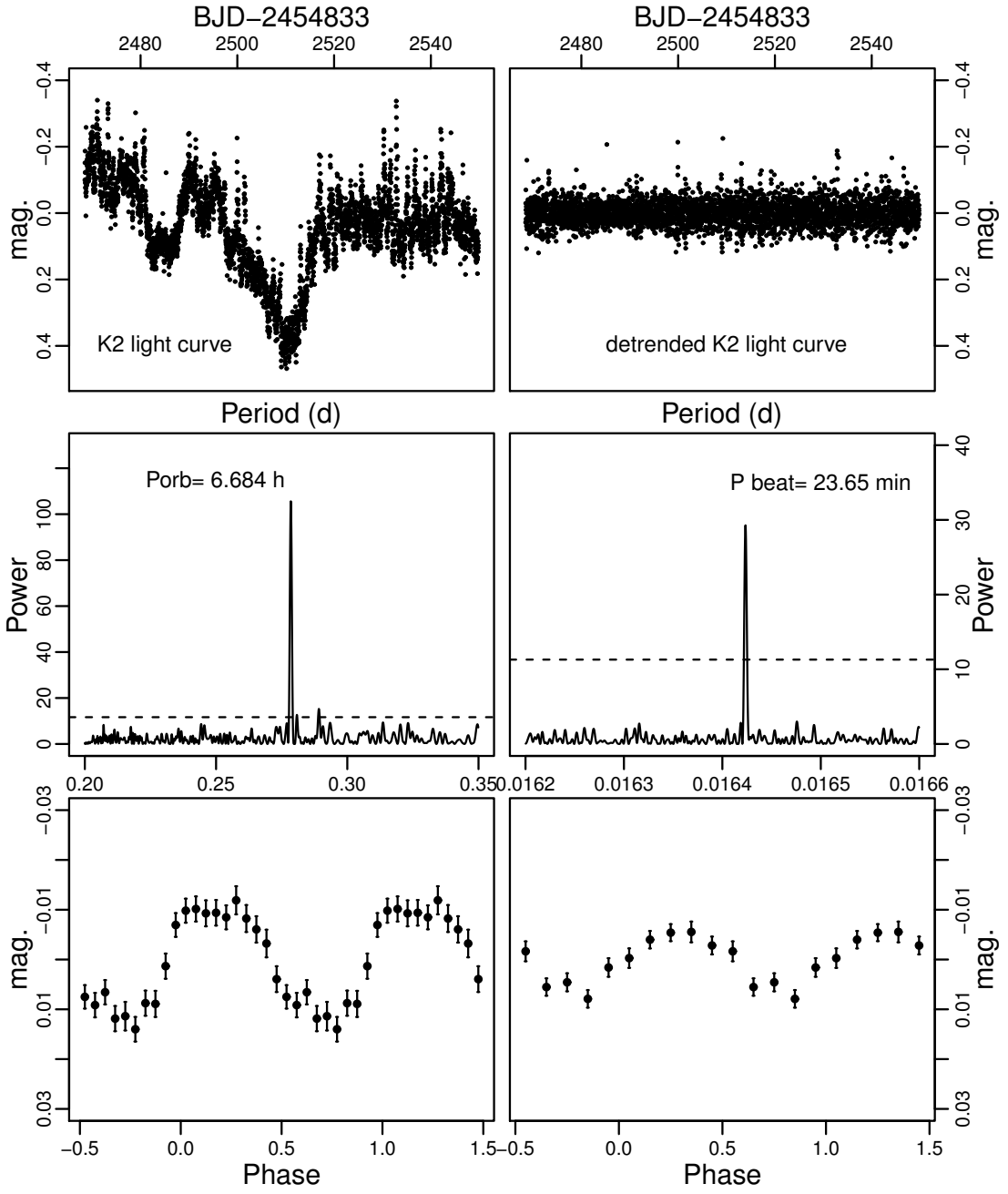

FIGURE 3.20: Top: the original (left) and de-trended Kepler light curves. Middle: LSP of the detrended Kepler light curve showing the orbital (left) and the beat (right) period. The horizontal dashed line shows the 0.3% false alarm probability level. Bottom: the light curve folded with the orbital (left) and the beat (right) periods.

Å range. This component may be the same that was previously emitting the supersoft X-rays and has cooled to a peak temperature in the UV range. If so, the disappearance of the supersoft X-ray emission in 2006 is probably consistent with cooling. The EWs of the He II λ4686 and Hβ lines are larger than in V2491 Cyg but still small in comparison to what is usually observed in novae a decade after explosions [171, 172]. In this section I will discuss possible emitting sites of the soft X-ray component and magnetic nature of V4743 Sgr.

3.2.4.1 The IP scenario

Several observational facts suggest that V4743 Sgr is an intermediate polar.

- Taking into account uncertainty in the distance, discussed above, the hard X-ray luminosity in the 2.0–10 keV range was 2.4×10^{32}–6.2×10^{33} erg s^{-1} in 2006, which is typical of IPs [179].
- The spectra can be fitted only introducing a complex, partially covering absorber, which can be a result of periodic obscuration of the central emitting region by accretion curtains [60, 61].
- The most important indication of a magnetic nature of V4743 Sgr is the presence of the coherent ∼0.75 mHz modulation, observed in X-rays even in quiescence. The frequency was stable from 2004 to 2006, to within measurement limitations. In the Kepler light curves we also detected the orbital period and beat period period between the spin and the orbital one.
- The prominent He II λ4686 line and the high value of EW(He II λ4686)/EW(Hβ) ratio are typical of IPs, however the EW of the Hβ line is small in comparison with the empirical criterion for magnetic CV from Silber [170].
- The emission lines have a complex structure with red and blue-shifted components with the same velocity, which may originate in the accretion curtains in the magnetosphere of the WD.

The only element that seems odd and somehow out of place in the IP scenario is that the soft X-ray modulation disappeared in the 2006 data (see fig. 3.18): the variability was observed only above 0.8 keV. This is in contrast with the usual situation for IPs in which X-ray modulations are more prominent in soft X-rays, since the cross section of photoelectric absorption in the accretion curtain decreases with energy. We also did not detect any modulation of the X-rays related to the orbital period, but this can be due to relatively short exposure times. In fact, during the outburst, there was a marginal

detection of orbital modulation in the supersoft X-rays light curve [191]. The orbital modulation in the X-ray light curve is usually, but not always, observed in IPs with inclination angles exceeding $\sim 60^{\circ}$ [208]. Altogether, many observational facts indicate that V4743 Sgr is an IP and we favour this hypothesis.

3.2.4.2 The soft X-ray component

Taking into account all the measurements of T_{eff} and the luminosity of the supersoft X-ray component in the 2004 *XMM Newton* spectrum (see tab. 3.8 and the section 3.2.2.1) we find that the luminosity decreased at least by two orders of magnitude compared with the values found by van Rossum [192] and Rauch et al. [188] in the last *Chandra* exposure during the SSS phase and the estimates of the emitting region radius lie in the range $4.0 \times 10^6 - 6.2 \times 10^7$ D_{4kpc} cm. Even the largest possible distance of 6 kpc (found by Nielbock and Schmidtobreick [199]) would only increase this value by 50%. It is not consistent with an emitting region as large as the whole WD surface but is close to the estimates of the size of a polar cap in an IP [209].

This low luminosity blackbody component is very similar to that, found in V2491 Cyg more than 2 years after the outburst. Another example is V2487 Oph – a recurrent nova and an IP candidate – which showed blackbody-like emission in X-rays even 8.8 years after the nova explosion [168]. However, in the 2006 observations of V4743 Sgr the blackbody component was not detected and it would be difficult to explain this fact in the context of the soft IP scenario. Irradiation of the polar cap region can indeed depend on the mass transfer rate, but since the hard X-ray component was the same in both datasets – 2004 and 2006 – we do not expect the mass transfer rate to vary significantly. A possible explanation is a temperature gradient on the surface of the WD, which can remain for several years after the nova explosion. It is not clear, however, why in V4743 Sgr this gradient disappear already after 3.5 years, while in V2487 Oph it was observed for almost 9 years.

3.3 Conclusions

I analysed the X-ray and optical observations of the two novae: V2491 Cyg and V4743 Sgr obtained in quiescence. These objects are very similar: their nova explosions were fast, they most probably host massive WDs and are X-ray luminous even in quiescence, indicating high accretion rates. These novae also have very similar optical spectra with the prominent He II λ4686 line, Bowen blend and red and blue-shifted emission line

components. Summarising the findings, V4743 Sgr is an intermediate polar and V2491 Cyg is an intermediate polar candidate.

The most puzzling characteristic of these two novae are the low luminosity blackbody-like components in their X-ray spectra, observed several years after the explosions. These components have temperatures close to the WD temperature during the SSS phase, but a much lower luminosity, indicting the size well below the size of the WD surface. In contrast to the typical behaviour of novae, these systems seem to show a shrinking of the soft X-rays emitting region at almost constant temperature instead of cooling. There is only another such example — V2487 Oph —, which is also an IP candidate and most probably hosts a massive WD [168]. In V4743 Sgr the supersoft X-ray component disappeared by the time of the last *XMM Newton* observation, implying that the source of radiation is not related to accretion and cannot be explained by the irradiated polar cap on the WD, like in "soft IPs". In V2491 Cyg we also detected a sudden decrease of the flux of the He II λ4686 line, which indicates cooling or disappearance of the ionizing source, a similar process to that, observed in V4743 Sgr. We propose that this supersoft emission may be due to a temperature gradient on the surface of the WD, which can be a characteristic of magnetic novae. Another explanation is a residual nuclear burning, possibly continuing in the post-outburst quiescent phase in a smaller region than the whole WD.

The disappearing low-luminosity supersoft component is a very interesting phenomenon. Such components were observed in three novae, and in V2487 Oph it lasted for at least almost 9 years, while in V4743 Sgr only for two years and in V2491 Cyg probably for 2.6–4.3 years. Data on other novae are still missing and further X-ray monitoring is encouraged, since this phenomenon may have profound implications for the secular history of accretion and hydrogen burning.

Chapter 4

Multi-mission observations of the old nova GK Per during the 2015 outburst

GK Per, a classical nova of 1901, is thought to undergo variable mass accretion onto a magnetized WD in an intermediate polar system. We organized a multi-mission observational campaign in the X-ray and UV energy ranges during its dwarf nova (DN) outburst in 2015 March-April. The main goal was to study the effects of increased mass transfer through the disk in a magnetic system.

4.1 Introduction

GK Per underwent a nova explosion on 1901 February 21 [210] and after a long period of irregular fluctuations, in 1948, it started to behave like a DN, with small amplitude (1 – 3 mag.) outbursts lasting for up to two months and recurring at intervals that can be roughly expressed as n×(400 ± 40) days [211]. The widely accepted explanation of these outbursts is a recurring thermal instability in the inner part of the accretion disk [inside-out outbursts; see 212, 213, for the application of the disk instability model to GK Per].

GK Per, at a distance of 470 pc [214], is the second closest nova to us and the best monitored at quiescence. It is surrounded by an expanding nova shell, which emits in the X-rays [215, 216], weakly in UV [217], optical [i.e. 218], infrared [i.e. 219] and radio [220] bands and has a complex structure with numerous knots [221] and a jet-like feature.

The orbital period is 1.9968 d [222, 223]. The secondary is a K2-type subgiant mass of 0.25–0.48 $M_\odot$ [223–225] and the mass of the primary is 0.86±0.02 $M_\odot$ [226]. GK Per has an extended accretion disk ($\sim 10^{11}$ cm) and interpreting the typical duration of DN outbursts in GK Per as the viscous decay time-scale Evans et al. [227] find that only about 10 % of the disk is involved in the outbursts.

King et al. [228] and Bianchini and Sabadin [229] proposed that GK Per hosts a magnetic WD. Watson et al. [225] discovered a modulation with a 351 s period in the X-ray light curve and proposed that this is the WD spin period. Watson et al. [225] also noticed that the pulse fraction is 50 % above 3 keV and up to 80 % below 3 keV, but does not depend on the mean X-ray flux. The pulse profile is single-peaked in outburst and double-peaked, with smaller amplitude in quiescence [230, 231].

Apart from the spin-related modulation, during outbursts GK Per shows quasi periodic oscillations (QPOs) in X-rays and in the optical band with the characteristic timescale of several kiloseconds [e.g 176, 225, 231, 232]. This timescale is exceptionally long comparing to what is typically observed in CVs [233]. QPOs with periods of 360–390 s were also detected in optical observations of GK Per by several authors. Watson et al. [225] noticed that the beat period between the spin period and the shorter-period QPOs is in the kiloseconds range, close to the period of the longer QPOs. Morales-Rueda et al. [176] explored this idea, assuming that the QPOs are due to absorption of the emission from the innermost regions of the accretion disk by blobs of material in the magnetosphere. The 360–380 s period in this model is due to the the Keplerian velocity in the inner disk radius. Hellier et al. [231] argued that this scenario explains the optical data of Morales-Rueda et al. [176], but does not fit the X-ray observations. These authors suggested instead that bulges of material in the inner edge of the accretion disk, high above the disk plane, obscure the WD and the ∼5000s period is due to the slow-moving prograde waves in the innermost region of the disc [234].

Several pieces of evidence indicate that during dwarf nova outbursts the accretion disk in GK Per pushes the magnetosphere towards the surface of the WD [226, 231, 235]. This scenario, first proposed by Hellier et al. [231] in analogy with XY Ari [236], explains the single-peaked pulse profile as a consequence of cutting off the line of sight to the lower accreting pole. The maximum plasma temperature in GK Per in quiescence is higher than in outburst [237], which can also be understood in the context of the shrinking of the accretion disk [238]. However, while the hard X-ray emission can be explained as due to the accretion columns emitting bremsstrahlung radiation that is highly absorbed, the broad-band X-ray spectrum of GK Per and its evolution during outbursts are much more complex. Šimon [239] noticed that the halt of the rise of the hard X-ray luminosity is not modeled only by just assuming increased absorption, and probably involves large

structural changes of the accreting regions. Mukai et al. [78] have shown that the outburst X-ray spectrum of GK Per below 2 keV is not consistent with a "typical" cooling-flow spectrum of an accreting WD and proposed a considerable contribution of photoionization. Vrielmann et al. [235] and Evans and Hellier [60] noticed that the soft X-ray emission of GK Per detected during the 2002 outburst may originate in the heated surface of the WD, like in the case of "soft intermediate polars".

On 2015 March 6.84 Dubovsky (VSNET-ALERT 18388) and Schmeer (VSNET-ALERT 18389) discovered that GK Per has started a new DN outburst and was at a magnitude 12.8. We proposed a multimission observation campaign in order to follow the evolution of the object during the outburst and to obtain X-ray spectra in a broad energy range, revealing the physical processes that take place in this binary system.

4.2 X-ray observations and data analysis

We started the observations of the 2015 DN outburst of GK Per as soon as it became observable with *Swift* on March 12 2015, and we could follow the outburst almost until the optical maximum. We wanted a higher cadence than in the previous 2006 outburst *Swift* monitoring, and obtained two exposures per day for two weeks and one exposure per day in the following two weeks. During the first two weeks of the monitoring the *Swift* X-Ray Telescope (XRT) [240] was in the automatic state [241], choosing the photon counting (PC) or window timing (WT) operating mode depending on the source count rate. During the second two weeks the monitoring was performed only in the WT mode. The *Swift* Ultraviolet Optical Telescope (UVOT) was in the image mode, providing the mean magnitude per exposure in one of the four UVOT filters (U, UVW1, UVM2, UVW2). Coordinated *NuSTAR* and *Chandra* Advanced Imaging Spectrometer High-Energy Transmission Grating (ACIS-S/HETG) observations were performed on April 4 2015, close to the optical maximum. The *Chandra* ACIS-S/HETG consists of two sets of gratings [242], operating in the 31–2.5 Å (Medium Energy Grating) and 15–1.2 Å (High Energy Grating) energy ranges with the resolution better than 0.023 Å. *NuSTAR* has two detectors: FPMA and FPMB, covering the same energy range, from 3 to 79 keV. The time resolution of all the instruments used for the observations is better than 2.5 s, which is much shorter than the periodicities we expected to find. The *Swift* XRT spectra in the 0.3–10 keV energy range and the mean X-ray count rate per snapshot were obtained using the *Swift* XRT data products generator [243, 244], subsequently performing the barycentric correction with an applet[1], created by Eastman et al. [245]. The *Swift* XRT light curves in the WT mode and in the PC mode (the latter excluding

[1] http://astroutils.astronomy.ohio-state.edu/

the central region and subsequently running `xrtlccorr`, because of the pile-up) and the UVOT data were processed with the `ftools` package. The *Swift* XRT light curves were barycentric corrected using `barycorr` tool.

We also used the processed *Swift* Burst Allert Telescope (BAT) data from the *Swift* BAT transient monitor page [246]. The *Chandra* data were reduced with `CIAO v.4.7` and the *NuSTAR* data with the standard `nuproducts` pipeline. The *NuSTAR* and *Chandra* light curves were barycentric corrected. The list of the observations with the exposure times and count rates is presented in table 4.1.

4.3 Development of the outburst

Figure 4.1 shows a comparison between the development of the outburst in the optical, UV and X-rays. The top panel is the optical light curve, which was obtained from The American Association of Variable Star Observers (AAVSO)[2]. The beginning of the outburst in the optical band was taken as a reference and is marked with the red dashed vertical line in all the panels. The maximum of the outburst in the optical band is also marked with the blue line. The second panel shows the *Swift* UVOT data in different filters. All the UVOT light curves showed a gradual rise until almost a week before maximum. The images in the lower energy filter — U — and the last observations in the UVW1 and UVW2 filters were saturated and provide only lower limits for the magnitudes. We analysed also quiescence *Swift* UVOT observations of GK Per obtained in 2012 to find the amplitude of the outburst in the UV range. Table 4.2 shows the quiescent UVOT magnitudes.

The third panel is the *Swift XRT* light curve averaged within a snapshot in the whole energy range: from 0.3 to 10 keV. The count rate varied from 0.7 to 2.8 cnts s^{-1} but did not show any significant increasing or decreasing trend.

We missed the initial steep rise, observed only with the *Swift* BAT, because GK Per was too close to the Sun, and observed only a plateau in the X-ray count rate. In fig. 4.1, the bottom panels show the soft (0.3–2.0 keV) and hard (2.0–10 keV) XRT light curves. The hard count rate is more scattered in comparison with the soft one and decreased as the outburst developed. The soft count rate, in turn, showed a prominent rise, which resulted in a gradual decrease of the hardness ratio (panel 5) with minimum around MJD 57113, 25 days after the beginning of the outburst. The light curve measured with the *Swift* BAT is more stable and only showed a moderate decrease after maximum

[2]https://www.aavso.org/

Table 4.1: Observational log.

Instrument	Date*	Exp.(s)	Count rate
Swift XRT(PC)	57093.15	606.7	1.72±0.10
	57093.58	1268.7	2.10±0.08
	57094.08	1033.0	1.70±0.08
	57094.68	373.6	1.15±0.10
	57095.04	952.8	2.10±0.13
	57095.93	960.3	1.41±0.07
	57096.30	744.7	1.48±0.09
	57096.90	441.3	1.80±0.13
	57097.04	970.3	1.32±0.08
	57097.57	937.7	0.94±0.06
	57098.03	997.9	1.63±0.09
	57098.97	882.6	1.33±0.07
	57099.17	875.0	1.27±0.07
	57099.57	514.0	1.66±0.10
	57100.11	922.7	1.58±0.08
	57100.97	1033.0	1.08±0.06
	57101.10	1133.3	1.11±0.06
	57101.57	925.2	1.64±0.09
	57102.23	1058.0	1.18±0.06
	57102.86	910.1	1.59±0.08
	57103.10	917.7	0.84±0.06
	57103.63	418.7	0.86±0.07
	57104.22	140.4	1.06±0.12
	57104.70	975.3	1.70±0.10
	57105.95	905.1	0.67±0.04
	57106.15	1075.6	1.71±0.09
	57106.76	965.3	1.14±0.07
	57107.29	1110.7	1.71±0.09
	57107.82	1196.0	0.69±0.04
Swift XRT(WT)	57094.68	520.9	2.79±0.08
	57108.75	762.0	1.17±0.04
	57109.62	986.2	1.39±0.04
	57110.51	1145.6	1.23±0.04
	57111.28	1086.9	1.85±0.04
	57111.28	1086.9	1.85±0.04
	57113.34	1228.2	1.78±0.04
	57114.13	1040.9	1.14±0.04
	57115.90	2401.5	1.30±0.03
	57116.07	1078.0	1.34±0.04
	57117.66	974.1	1.40±0.04
	57118.20	903.6	2.14±0.05
	57119.29	1261.4	1.40±0.06
	57120.36	1578.7	1.14±0.04
	57121.06	1049.5	1.11±0.04
Chandra MEG	57116.83	69008	0.0751±0.0010
Chandra HEG	57116.83	69008	0.1214±0.0013
NuSTAR FPMA	57116.12	42340	3.665±0.009
NuSTAR FPMB	57116.12	42340	3.626±0.009

Notes.* Modified Julian Date. The count rates were measured in the following energy ranges: *Swift* XRT — 0.3–10.0 keV, *Chandra* MEG — 0.4–5.0 keV, *Chandra* HEG — 0.8–10.0 keV, *NuSTAR* FPM — 3–79 keV.

TABLE 4.2: *Swift* UVOT magnitudes of GK Per obtained in quiescence.

MJD	Filter	Exposure (s)	Mag.
56115.279	UVM2	413	16.75±0.03
56115.284	UVW1	361	15.691±0.019
56115.274	UVW2	413	16.67±0.02
56117.082	UVM2	316	16.95±0.04
56117.086	UVW1	319	15.85±0.02
56117.078	UVW2	316	16.92±0.03
56118.013	UVM2	112	16.74±0.05
56118.014	UVW1	143	15.67±0.03
56118.012	UVW2	112	16.68±0.04

around day 10 after the outburst. The flux increase started 2 days earlier in the *Swift* BAT energy range than in optical.

4.4 Timing analysis

4.4.1 Broad band power spectra.

For our timing analysis we extracted the *Swift* XRT, *NuSTAR* (the FPMA and FPMB detectors were combined) and *Chandra* light curves and binned them every 10 s. In order to investigate a possible energy dependence of the X-ray variability we split the *Swift* XRT light curve in two ranges: 0.3–2.0 and 2.0–10 keV, the *Chandra* HETG light curve was extracted below 6 Å (1.95 keV) and above 6 Å and the *NuSTAR* one above and below 10 keV. *Chandra* hard and *NuSTAR* data show a strong periodic modulation, which can be seen in fig. 4.2. For visibility in fig. 4.2 the *Chandra* count rate was multiplied by a factor of 20. To study this modulation quantitatively, we constructed Lomb-Scargle periodograms [80] of various data in soft and hard energy bands. The Lomb-Scargle periodograms (LSPs) in a broad range of periods for all the light curves are presented in fig. 3.10. The top-left panel show the LSPs of hard (black) and soft (red) *Swift* XRT light curves. The highest peak of the hard LSP corresponds to the WD spin period — 351.33 s. The spin modulation is not present in the LSP of the soft *Swift* XRT light curve: it shows peaks only at longer time scales with the strongest one at 5736 s. Although QPOs in GK Per on a timescale of ∼5000 were reported by many authors, this period is too close to the *Swift* orbital period of 5754 s to be distinguished from the windowing in the observations. The top-right and bottom-left panels of fig. 3.10 show the LSPs of the *Chandra* HETG and the *NuSTAR* light curves, respectively. There is no peak in the Chandra soft LSP at 5736 s period, which confirms that this peak in the soft *Swift* periodogram does not correspond to a real modulation. On the other hand, the *NuSTAR* and the hard *Chandra* LSPs show peaks at ∼7000 s. These

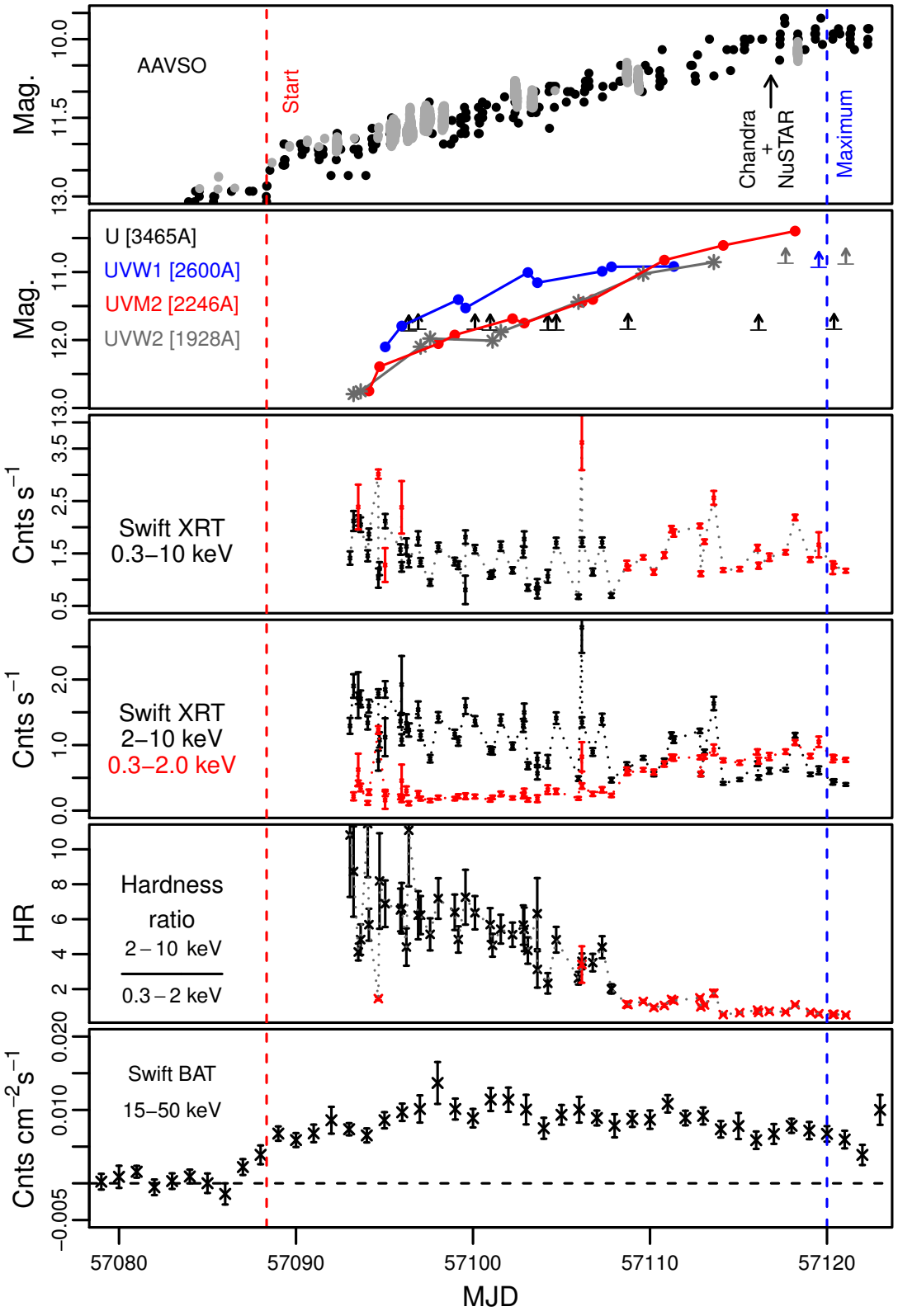

FIGURE 4.1: From top to bottom: AAVSO light curve in the *V* band (grey) and without a filter (black). The red and blue vertical lines in all the panels mark the beginning (MJD 57088.34) and the maximum (MJD 570120) of the outburst in the optical band. The *Swift* UVOT light curves in different filters. The *Swift* XRT light curve in the PC (red) and WT (black) modes. The *Swift* XRT light curves above 2 keV (black) and below 2 keV (red). The X-ray hardness ratio from the data obtained in the WT (red) and PC (black) mode. The *Swift* BAT light curve.

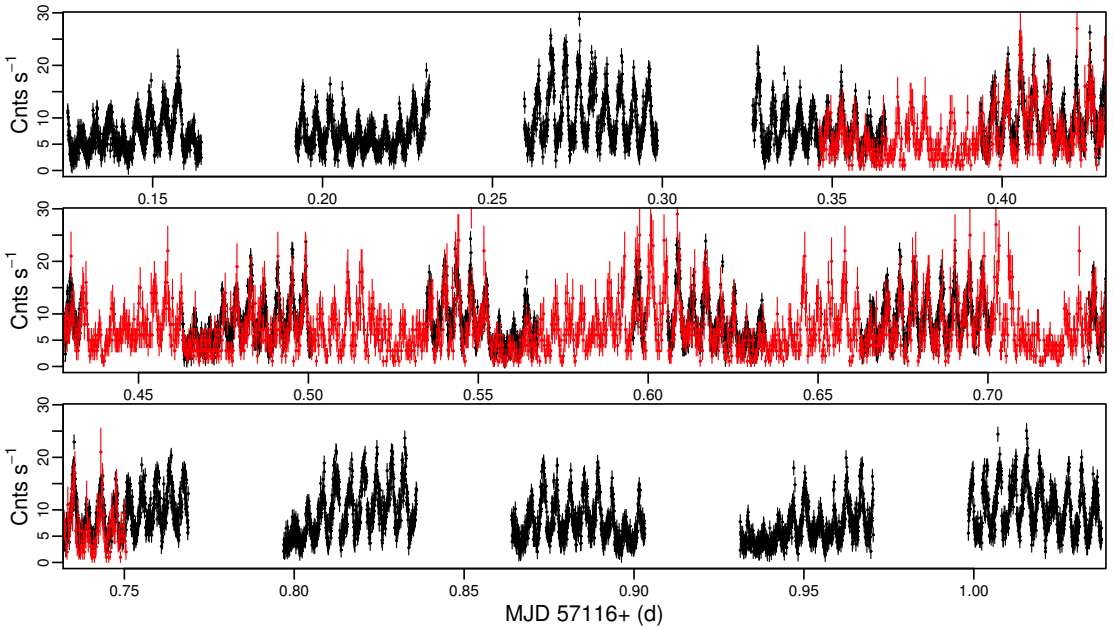

FIGURE 4.2: *NuSTAR* FPMA+FPMB light curve binned every 10 s (black) and the *Chandra* HETG light curve in the 1–6 Å wavelength range, binned every 20 s (red) and multiplied by a factor of 20 for visibility.

light curves are indeed variable on the timescales of kiloseconds with amplitudes up to **10** cnts s^{-1}, as shown by fig. 4.2.

The blue dashed lines in the top-right and bottom-left panels show the LSPs after the subtraction of the peak corresponding to the spin period. We fitted and subtracted a sine function with a fixed period of 351.33 s from the original data, and plotted the LSP again. The peak close to half of the spin period remained in the hard *NuSTAR* and Chandra LSPs.

4.4.2 Energy dependence of the WD spin modulation.

All the LSPs of the light curves extracted above 2 keV show a prominent peak corresponding to the WD spin period, while neither *Chandra* nor *Swift* soft LSPs show any. The absence of the spin modulation in the region of 0.3 – 2 keV may indicate that this emission component has a different origin and is visible during the whole spin cycle. We also extracted the light curves from the *Chandra* HETG data in the regions of the strongest emission lines of Mg, Si and Fe Kα 6.4 keV and checked whether the flux in these lines is modulated with the orbital or with the spin period. Only the Fe Kα line emission showed spin modulation, while the flux in the other emission lines had aperiodic fluctuations.

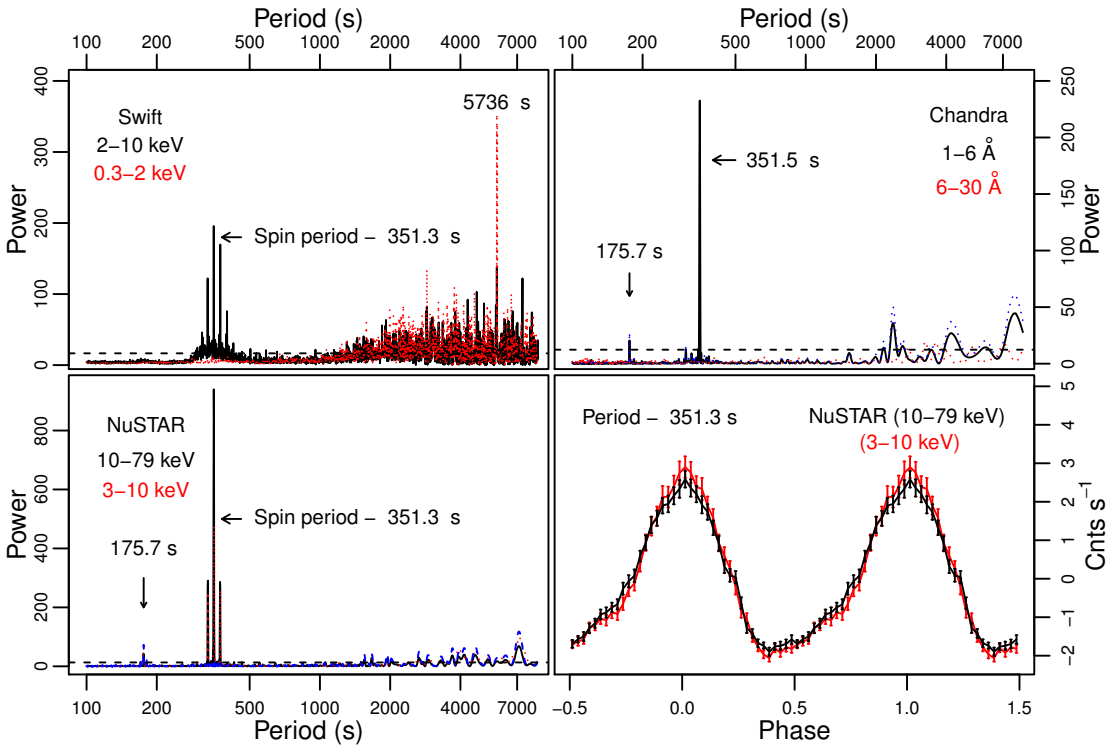

FIGURE 4.3: Top-left: the LSP of the *Swift* XRT data in the 2–10 keV energy range (black) and at 0.3 – 2 keV (red). Top-right: the LSP of the *Chandra* HETG data in the energy range 1–6 Å before (red) and after (blue) subtracting the highest peak, at 351.5 s. The red line shows the LSP of the *Chandra* HETG data in the energy range 6–30 Å. Bottom-left: the LSP of the *NuSTAR* data in the 10 – 79 keV (black) and 3 – 10 keV (red) energy range. The blue line shows the LSP of the *NuSTAR* data in the 10 – 79 keV range after subtracting the peak at 351.3 s. The horizontal dashed lines show the 0.3% false alarm probability level at all the LSPs. Bottom-right: the *NuSTAR* light curve in the 3 – 10 keV (red) and 10 – 79 keV (black) ranges, folded with the WD spin period of 351.3 s

The peak corresponding to the spin period is present even in the LSP of the *NuSTAR* light curve above 10 keV. A large amplitude spin modulation, with the peak-to-peak amplitude ∼10 cnts s^{-1} can be seen fig. 4.2. Typically the spin modulation of IPs is not detected, or only marginally measurable, in the hard X-rays [247, 248], since the cross section of the photoelectric absorption that usually causes the modulation decreases with energy. The effect of photoelectric absorption is not significant above 10 keV, so the observed high energy modulation might originate in a different mechanism than absorption of the accretion column emission. The comparison of the phase folded light *NuSTAR* light curves in two energy ranges (fig. 4.3) confirms that the spin modulation is not energy dependent: the spin profiles are almost identical.

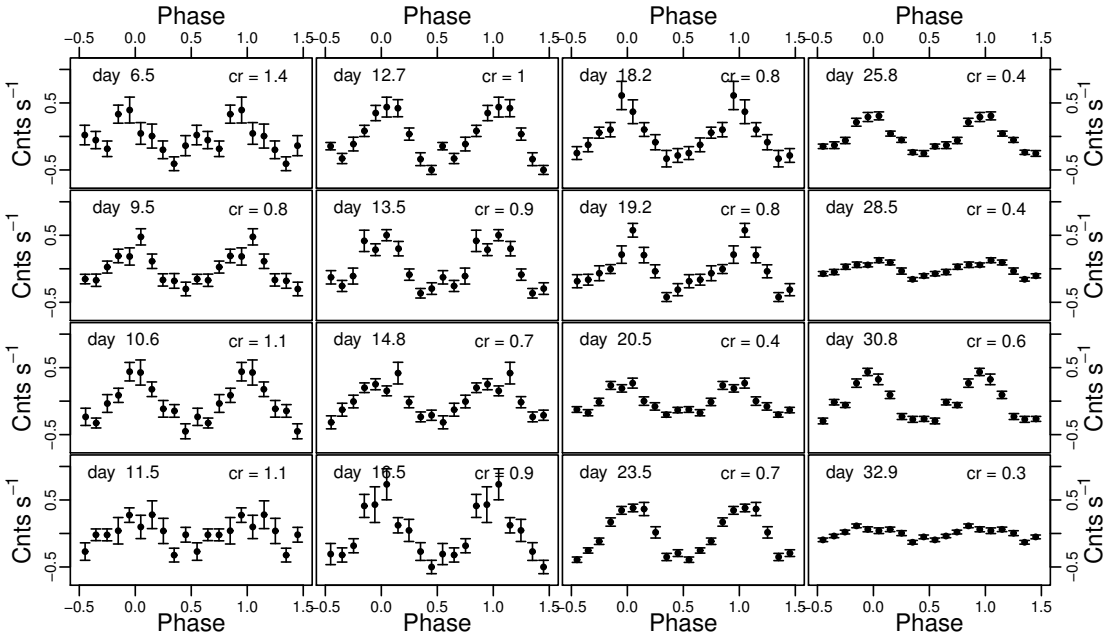

FIGURE 4.4: Evolution of the spin pulse profiles in the *Swift* XRT light curves above 2 keV. We combined every three individual observations and folded them with the 351.33 s period. The mean date of observation and the mean count rate (cr) is marked on each plot.

4.4.3 Evolution of the spin pulse profile.

The next step was to explore the spin modulation of the light curves. We first investigated how the spin pulse profile changed as the outburst developed. Since the modulation is mostly seen in hard X-rays, we combined the *Swift* XRT light curves above 2 keV in groups of three exposures and folded them with the 351.3 s period using a constant number of bins. The result is shown in fig. 4.4: the pulse profile becomes smoother with time and the stabilized by day ∼20 after the beginning of the outburst in optical. The pulse amplitude also depends on the mean value of the count rate. This will be further explored using the *NuSTAR* data.

4.4.4 WD spin-up rate.

We measured the spin period more precisely combining the *NuSTAR*, *Swift* XRT light curve extracted above 2 keV and the *Chandra* HETG light curve in the 1–6 Å wavelength range. Since the spin amplitude in each instrument is a similar fraction of the mean count rate, and the mean count rate is much lower for *Swift* XRT and the *Chandra* HETG, we first normalized the light curve from each instrument to its mean count rate. In order to account for possible long-term variability we removed linear trends from each segment the *NuSTAR* light curve, from the *Chandra* light curve and from each *Swift* observation before applying the phase dispersion minimization method [81]. Fig. 4.5

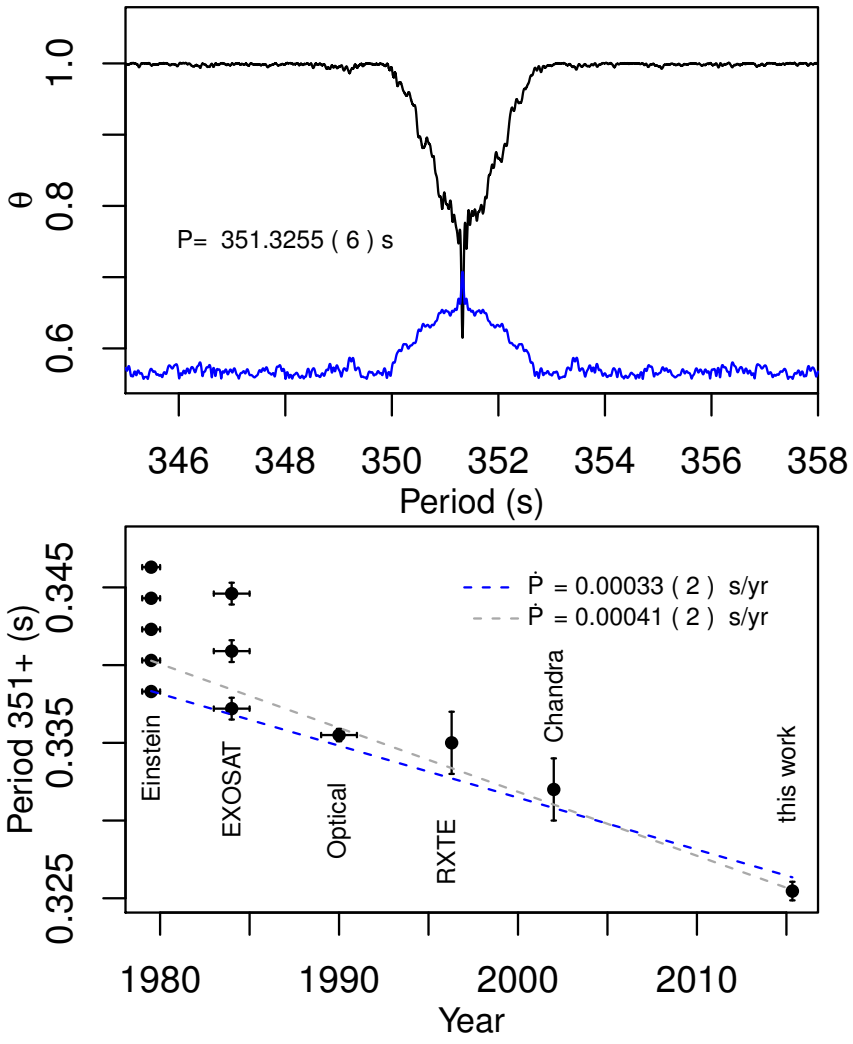

FIGURE 4.5: Top: PDM analysis of the *NuSTAR*, *Chandra* HETG 1–6 Å and hard *Swift* XRT light curves. Bottom: the WD spin period as a function of time and the result of the linear fitting.

shows that the PDM analysis resulted in a value of the spin period P_{spin}= 351.3255(6) s. Combining the WD spin measurements performed by Watson et al. [225], Norton et al. [230], Hellier et al. [231], Eracleous et al. [249], Patterson [250], Mauche [251] and following a discussion by Patterson [250] and Mauche [251], we fitted the trend of P_{spin} as a function of time with a linear function. The uncertainty in spin-up rate is due to the uncertainty in the period derived from the *Einstein* data: two different values, 351.3383 and 351.3403 s, resulted in an acceptable fit, and adopting each of them yields a spin-up rate of 0.00033(2) s yr^{-1} and 0.00041(2) s yr^{-1}, respectively.

Using the new value of the spin period (P_{spin}= 351.3255(6) s), I also calculated the ephemeris of the pulse maxima. The Modified Barycentric Julian Date of the maxima

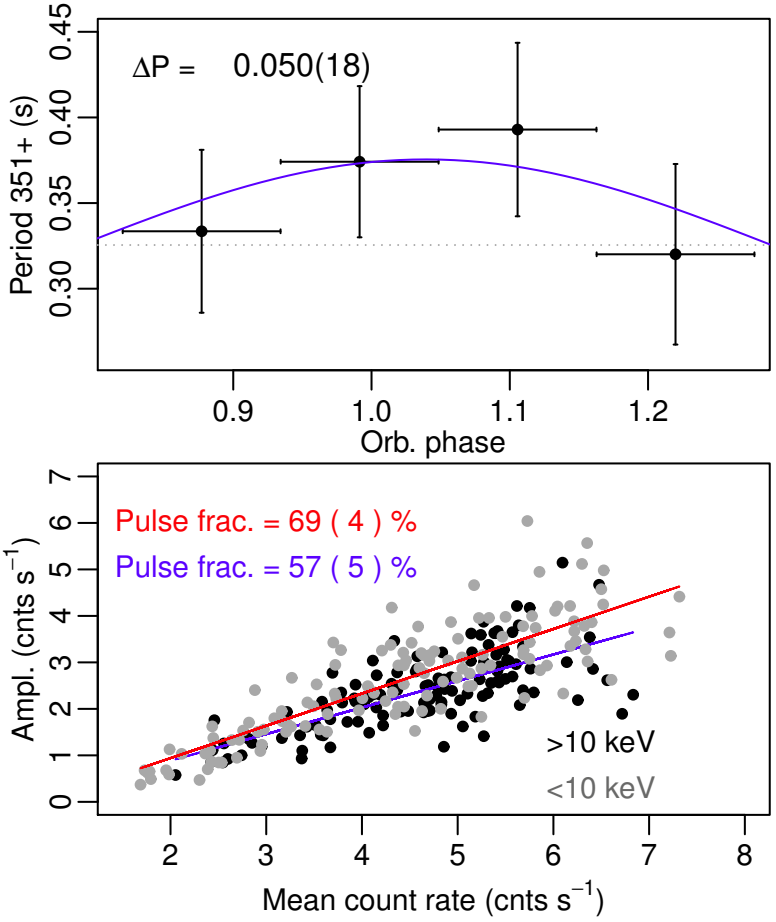

FIGURE 4.6: Top: the WD spin period as a function of orbital phase and the result of the fit with a sine function. The dashed grey line shows the mean period, 351.3255 s. Bottom: the amplitude of pulses, calculated as (maximum-minimum)/2, as a function of the mean count rate per pulse and the result of the linear fit. The grey dots and red line correspond to the *Nustar* light curve, extracted below 10 keV, and black dots and blue line — above 10 keV.

can be found as:

$$\mathrm{T_{max}(MBJD)} = 57093.51666(21) + 0.004066267(7) * E \tag{4.1}$$

4.4.5 Orbital variability of the spin period.

Watson et al. [225] pointed out that the spin period should be modulated with the orbital one (i.e. X-ray radial velocity curve), but taking into account the estimates of the binary parameters of GK Per, the authors concluded that these variations would be below the detection limit. With the most recent measurements of the mass ratio q, WD mass M_{WD}, binary inclination angle i and orbital period P_{orb}, I derived the expected

amplitude of variation of the pulse period $\Delta P_{\rm spin}$ with orbital phase. The semi-major axis of the WD's orbit is:

$$a_x \sin i = \frac{P_{\rm orb}}{2\pi} K_x \tag{4.2}$$

where K_x is the radial velocity semi-amplitude. Assuming a circular orbit [222] I can write:

$$M_2 \sin^3 i = \frac{P_{\rm orb} K_x^3}{2\pi G} \left(1 + \frac{1}{q}\right)^2 \tag{4.3}$$

Using $q = M_2/M_1$ and equation 4.3 we obtain the semi-major axis in light seconds:

$$a_x = \frac{q}{c} \left[\frac{P_{\rm orb}^2}{4\pi^2} \frac{G M_{\rm WD}}{(1+q)^2}\right]^{1/3} \text{ light seconds} \tag{4.4}$$

where c is the speed of light. Thus, we finally obtain $\Delta P_{\rm spin}$ as:

$$\Delta P_{\rm spin} = \frac{2\pi P_{\rm spin}}{P_{\rm orb}} a_x \sin i \text{ s} \tag{4.5}$$

Using the measurements of Morales-Rueda et al. [223] and Suleimanov et al. [226] ($q = 0.55 \pm 0.21$, $M_{\rm WD} \geq 0.86 \pm 0.02$ $M_\odot$, $P_{\rm orb} = 1.9968 \pm 0.0008$ d) we find that $a_x \sin i = 6.1 \pm 1.8 \sin i$ lt-sec and $\Delta P_{\rm spin} = 0.078 \pm 0.023 \sin i$ s. Since the binary inclination lies within the range 50–73° [223], the result is $\Delta P_{\rm spin} = 0.042 - 0.096$ s. Thus, the orbital modulation of the spin period significantly affects the measurements of the latter if the observations last for a shorter time than the orbital period. In fact, in fig. 4.3 I show that the spin period derived from the *Chandra* observation, which is the shortest one, is measured to be longer.

In order to explore a possible spin period variation with the orbital period in our data we combined the *NuSTAR* and the *Chandra* HETG 1–6 Å light curves, both covering half of the orbital period. Since the light curves show also variability on a kilosecond timescale (see fig. 4.2) we fitted and subtracted 5-order polynomial functions from light curve segments lasting 14 rotation periods each. The resultant, "flat" light curve, was then divided in four parts of equal length and the spin period was measured in each part with the PDM method.

Unfortunately, we only have the ephemerides of Morales-Rueda et al. [223], obtained almost 20 years ago, so the error on the phase determination may make it non significant. However, the orbital period itself is precisely measured, and in fig. 4.6 we show that $P_{\rm spin}$ is indeed variable. Fitting its orbital period dependence with a sine function, we find $\Delta P_{\rm spin} = 0.050(18)$ s. This is close to the lower limit of the expected range of

$\Delta P_{\rm spin}$. We note, however, that flickering cannot be removed, so the uncertainty in this measurement is large.

We applied the template fitting method described in Kato et al. [252] to the *NuSTAR* light curves extracted above and below 10 keV in order to measure the pulse fraction. We folded the light curves with the 351.3255 s period, fitted the mean pulse profile with a spline function and then used this spline template to fit individual pulses and to measure the amplitude and the mean count rate per pulse. The pulse amplitude was calculated as (fitted pulse maximum - fitted pulse minimum)/2. The bottom panel of fig. 4.6 shows the result. The correlation between the mean count rate and the amplitude of pulse is very prominent and can be fitted with a linear function, providing values of the pulse fraction of 65 and 57% for the soft and hard light curves, respectively. Variation of the mean count rate reflects the long term variability on the timescale of kiloseconds (QPOs). The spin modulation is due to the geometric effects and the linear dependence between the mean count rate and the pulse amplitude suggests that QPOs in the *NuSTAR* energy range are due to the intrinsic variability of the emitting source.

4.5 Spectral analysis

The X-ray spectrum of GK Per is very complex. The long-term observations with *Swift* showed that it is also quite variable, as demonstrated by the hard and soft X-ray light curves in fig. 4.1. Fig. 4.7 shows the comparison of the *Swift* XRT spectra obtained on different days, including only spectra with at least 14 data points after we binned the PC mode spectra with a minimum of 20 counts per bin, and the WT mode ones with at least 40 counts per bin. We divided the measurements by the response effective area, so the WT and PC mode spectra could be directly compared. Since all the exposures were longer than the spin period, rotation dependent variability is smeared out. In order to look for possible orbital phase dependence of the spectrum we marked the corresponding orbital phase [from the ephemerides in 223] in each panel. We also labeled each panel with the mean count rate. We did not find significant spectral variability dependent on the orbital phase, although all the spectra were different from day to day, sometimes with a narrow minimum around 2 keV, other times with a flatter shape around this value. Because of these variations there was no possibility to perform a simultaneous fit of the *Swift* XRT data and the data from the *Chandra* and *NuSTAR* observations and we will discuss these observations separately.

From the timing analysis we found that there are at least two different sources of X-ray emission in GK Per: one dominates above 2 keV and originates somewhere close to the WD, since the flux in this range is modulated with the WD spin period, and

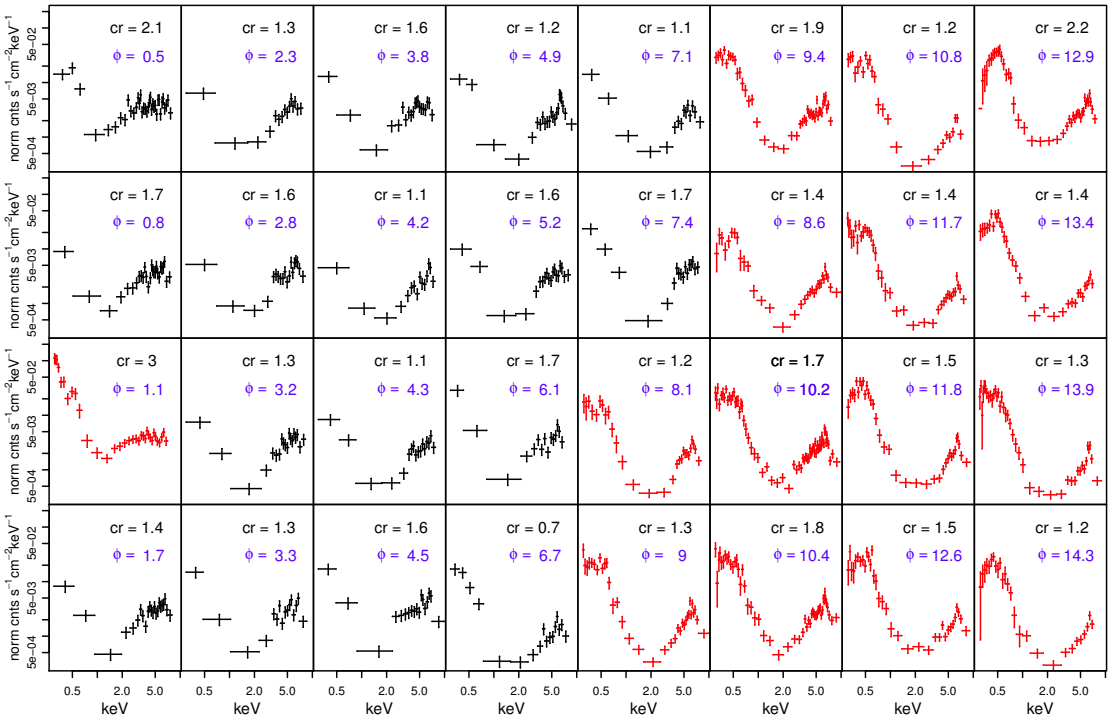

FIGURE 4.7: Evolution of the Swift XRT spectra of GK Per with time. The black points are data obtained in the PC mode and the red ones in the WT mode. The mean count rate and the corresponding orbital phase are marked on each panel.

the second source, dominating below 2 keV, is visible during the whole spin cycle. We first analysed the hard portion of the X-ray spectrum using the *NuSTAR* and *Chandra* HETG observations. The *Chandra* HETG spectra, having higher energy resolution provide better constrain on the metallicity and the structure of the Fe K complex, while the *NuSTAR* data allow to measure the shock temperature.

4.5.1 The hard X-ray spectral component.

Hard X-ray emission of accreting magnetic CVs originates in their accretion columns, where the post-shock plasma is cooling mostly via bremsstrahlung radiation and K and L shell line emission as it settles onto the surface of a WD. Therefore, for the hard continuum we used the cooling flow model `mkcflow`, which calculates a plasma in collisional ionization equilibrium (CIE) with a range of temperatures. `vmcflow` model is a modification of the `mkcflow` with variable abundances of individual elements. The highest plasma temperature (the shock temperature) is an important parameter for magnetic CVs, allowing to estimate the WD mass [63]. In order to investigate the hard X-ray emission, we attempted a simultaneous fit of the *NuSTAR* spectra and the *Chandra* HEG+MEG spectra above 2.5 keV. The *NuSTAR* FPMA and FPMB spectra were fitted together, but the FPMB model was multiplied by a constant to account for a

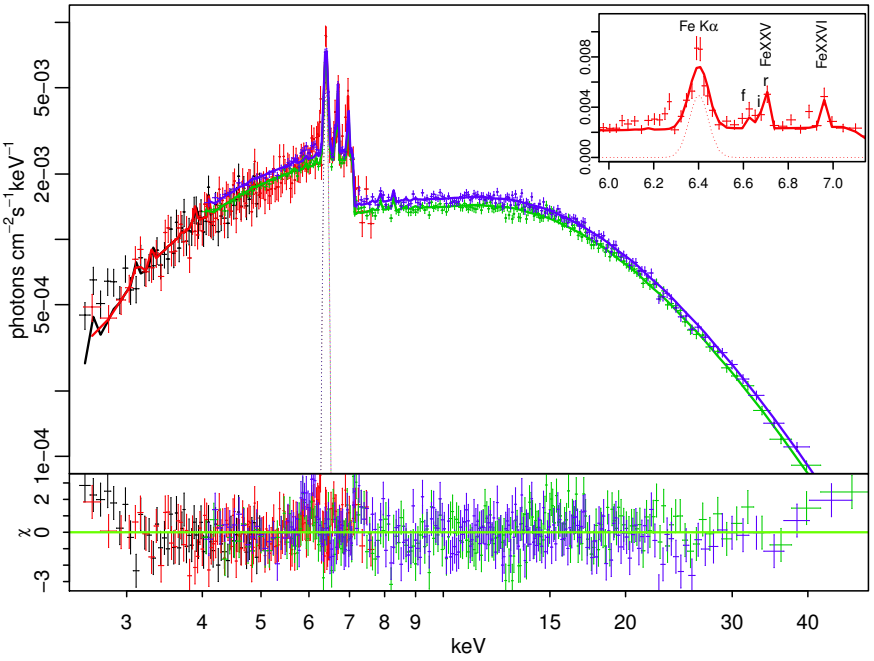

FIGURE 4.8: The *NuSTAR* FPMA (blue) and FPMB (green) and *Chandra* MEG (black) and HEG (red) spectra and the best-fitting model. The model components are marked with the dashed lines. The inset shows the Fe complex in the *Chandra* HEG spectrum.

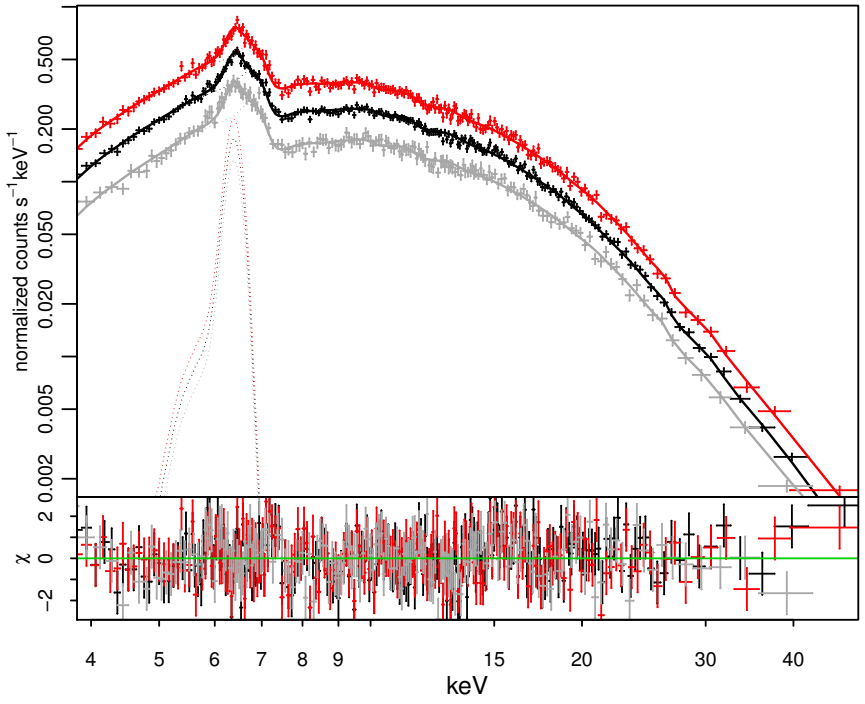

FIGURE 4.9: The *NuSTAR* FPMA mean (black), on-pulse (red) and off-pulse (grey) spectra and the best fitting model. The model components are marked with the dashed lines.

slightly different responses of the two detectors. We used the `vmcflow` model to test the abundances. The value of the interstellar absorption was obtained from the reddening $E(B-V) = 0.3$ [253] and the nH–$E(B-V)$ relation from Bohlin et al. [148]. The shape of continuum above 2 keV indicates that the emission is highly absorbed, but even with partially covering absorber we could not fit the data. A better result was obtained with the `pwab` model [254], in which the fraction of X-rays affected by a given column density N(H) is a power-law function of N(H) with index β. We fix the lower temperature of the `vmcflow` model to the lowest possible value — 0.0808 keV because a heavily absorbed spectrum like that of GK Per does not allow us to determine it accurately, and physically we expect it to be equal to the white dwarf photospheric temperature.

We also added a Gaussian component to fit the Fe Kα fluorescent line at 6.4 keV. The model's parameters of the best fit are in table 4.3. The *NuSTAR* and the hard part of the *Chandra* spectrum together with the described model are presented in fig. 4.8. The inset shows the Fe complex measured in the *Chandra* HEG spectrum. The model slightly underestimates the flux in the forbidden line of the Fe XXV triplet, which may indicate contribution of the photoinization processes. There are also residuals around 6.2–6.3 keV, suggesting Compton-downscattering of photons. A similar "shoulder" of the Fe Kα line was detected in previous *Chandra* HETG observations of GK Per [255].

We used the same procedure of the template fitting, described in the previous section, to find the pulse maxima and to extract the on-pulse and off-pulse *NuSTAR* spectra. Assuming that the pulse maximum is at ϕ=0.5, we chose time intervals corresponding to the 0.3 – 0.7 and 0.8 – 1.2 spin phases and used them to extract the on-pulse and off-pulse *NuSTAR* FPMA spectra. These spectra are shown in fig. 4.9 in comparison with the mean one. All three spectra are remarkably similar. We fitted the on-pulse and off-pulse spectra applying the best-fitting model described above, freezing the maximum plasma temperature, metallicity and the Fe Kα line width. The best-fitting parameters in table 4.3 show that the variation between the on-pulse and off-pulse spectra are due to the normalization of the cooling flow component.

4.5.2 The *Chandra* observation.

We analyzed the spectrum below 2 keV focusing on the *Chandra* HETG data to investigate the emission lines ratio and to derive conclusions about the plasma temperature and density and about the mechanism of ionisation. Useful indexes of the plasma properties are the R=f/i and G=$(f+i)/r$ ratios, where r, i, f are the fluxes in the resonance, intercombination and forbidden line of the He-like triplets and the ratios of H-like to He-like resonance lines in the same triplet [256].

TABLE 4.3: The best fitting-model parameters of the *NuSTAR* mean + *Chandra* HETG, on-pulse and off-pulse *NuSTAR* FPMA spectra. The model is `constant×TBabs×pwab×(vmcflow + gaussian)`. The errors represent the 90% confidence region for a single parameter. We adopted FPMA Constant=1 and FPMB C.=1.089.

Component	Parameter	Value		
		Mean	On-pulse	Off-pulse
TBabs	nH ($\times10^{22}$ cm^{-2})	0.17	0.17	0.17
pwab	nH_{min} ($\times10^{22}$ cm^{-2})	$7.2^{+0.4}_{-0.4}$	$7.4^{+1.1}_{-1.3}$	7.8^{+2}_{-2}
	nH_{max} ($\times10^{22}$ cm^{-2})	520^{+30}_{-30}	550^{+40}_{-40}	530^{+50}_{-50}
	β	$-0.199^{+0.016}_{-0.016}$	$-0.26^{+0.05}_{-0.04}$	$-0.16^{+0.07}_{-0.07}$
vmcflow	T_{low} (keV)	0.0808	0.0808	0.0808
	T_{high} (keV)	$16.2^{+0.5}_{-0.4}$	16.2	16.2
	Fe	$0.105^{+0.012}_{-0.012}$	0.105	0.105
	Ni	0.1	0.1	0.1
	$\dot{m}^a$	$2.6^{+0.2}_{-0.2}$	$3.69^{+0.12}_{-0.11}$	$1.88^{+0.09}_{-0.05}$
Gaussian	E (keV)	6.40	6.40	6.40
	σ (keV)	$0.046^{+0.012}_{-0.008}$	0.046	0.046
	norm ($\times10^{-4}$)	40^{+2}_{-2}	50^{+5}_{-5}	33^{+5}_{-4}
	EW (eV)	210^{+30}_{-20}	191^{+18}_{-19}	250^{+130}_{-200}
Flux	absorbed^b	$7.24^{+0.03}_{-3.07}$	$10.15^{+0.05}_{-0.19}$	$5.1^{+0.6}_{-0.6}$
Flux	unabsorbed^b	$24.2^{+1.0}_{-1.0}$	$34.1^{+1.1}_{-1.0}$	$17.5^{+0.8}_{-0.5}$
L ($\times10^{33}$erg s^{-1})		63^{+3}_{-3}	90^{+3}_{-3}	$46.1^{+2.1}_{-1.3}$
χ^2		1.3		1.0

Notes: [a]mass accretion rate $\times10^{-8}M_\odot$ yr^{-1}. [b]Absorbed and unabsorbed fluxes $\times10^{-10}$ergs cm^{-2} s^{-1} in the 2.5–79 keV energy range. The unabsorbed flux was calculated with the `cflux` command in `xspec`. We assumed a 470 pc distance.

We fitted all the emission lines in the *Chandra* MEG spectrum with Gaussians, assuming that the Ne, Mg and Si lines are absorbed only by the interstellar absorption, and we used a power law to represent the level of continuum. We also assumed that the widths of the lines within a triplet were constant and fixed the distances between these lines to the table values. For the Gaussian fit of the Fe K complex in the *Chandra* MEG spectrum we also introduced the `pwab` model with the parameters of the fit of the mean *NuSTAR* spectrum and a bremsstrahlung component at kT=14 keV for the underlying continuum. We did not find any significant line shifts departing from the laboratory wavelengths. The resulting broadening and flux are presented in table 4.4 and in fig. 4.10. We also measured the R and G ratios for the Si, Mg and Ne triplets, and give them in table 4.5.

The G ratio is around 2, which means that there is no strong photoionizing component (in case of pure photoionized plasma G is ∼4). We either have a collisional-ionization mechanism or a "hybrid plasma", a mixture of collisional and photionization [257]. The He-like triplets of different elements show very different line ratios. The Si XIII triplet has a very strong forbidden line, which cannot be explained solely with collisional ionization,

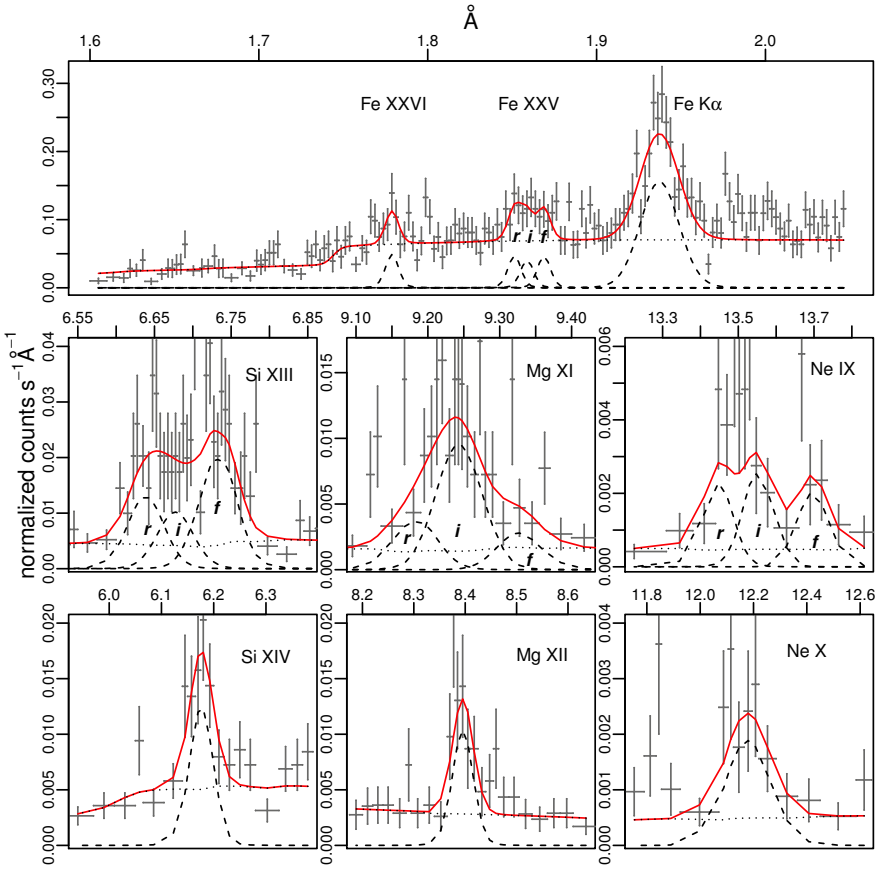

FIGURE 4.10: Gaussian fits of the strongest emission lines of the *Chandra* HEG (top) and MEG spectra. In the fits we assumed that the value of σ is the same within a triplet. The distances between the lines in a triplet were fixed to the table values. The values of σ of the Fe XXVI and Fe $\mathrm{XXV_{r,f,i}}$ lines were fixed to the instrument resolution.

while Mg XI and Ne IX have quite weak forbidden lines, but very strong intercombination lines, which indicates a high density [257].

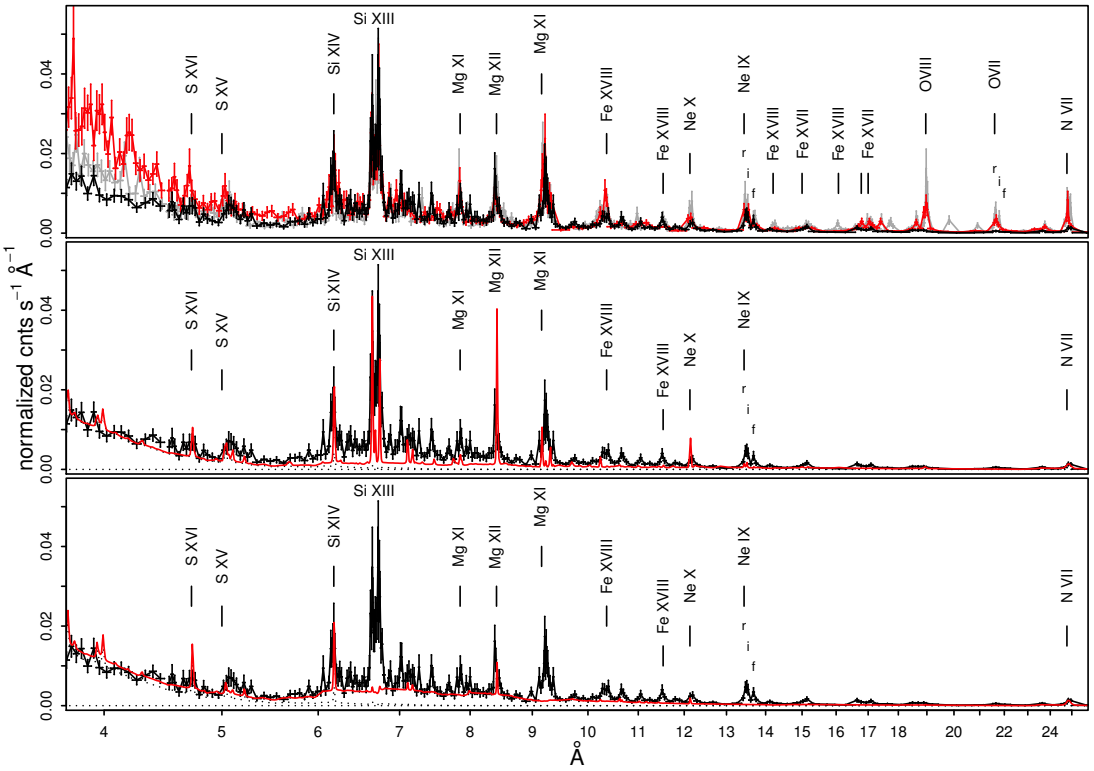

FIGURE 4.11: From top to bottom: comparison of the *Chandra* MEG spectra of GK Per in outbursts in 2015 and 2002. The *Chandra* MEG spectrum discussed in this paper is plotted in black, while the Chandra MEG spectra obtained on March 27 and April 9 2002 (PI C. Mauche) are plotted in red and grey, respectively. All the observations were performed close to the optical maxima. Middle panel: the 2015 *Chandra* MEG spectrum and the `TBabs`×`(pwab`×`(vmcflow + gaussian) + vapec + bb + gaussian)` model (the red line). The temperature of the `vapec` component was fixed to 0.9 keV. Bottom panel: The 2015 *Chandra* MEG spectrum with the same model and the 4.9 keV temperature of the `vapec`.

TABLE 4.4: Emission lines broadening and fluxes in the *Chandra* HETG spectra.

Line	E_{rest} keV	E_{max} keV	Δv km s^{-1}	σ km s^{-1}	$F_{abs}\times10^{-13}$ ergs cm^{-2} s^{-1}	$F_{unabs}\times10^{-5}$ ph cm^{-2} s^{-1}	$F_{unabs}\times10^{-13}$ ergs cm^{-2} s^{-1}
Ne X	1.02195	$1.017^{+0.004}_{-0.004}$	-1400^{+1200}_{-1200}	2100^{+1000}_{-800}	$0.6^{+0.2}_{-0.2}$	5^{+2}_{-2}	$0.9^{+0.3}_{-0.4}$
Ne IX$_r$	0.92200				$0.5^{+0.3}_{-0.3}$	6^{+3}_{-3}	$0.8^{+0.5}_{-0.5}$
Ne IX$_i$	0.91488			800^{+600}_{-300}	$0.6^{+0.3}_{-0.3}$	7^{+4}_{-4}	$1.0^{+0.5}_{-0.5}$
Ne IX$_f$	0.90510				$0.5^{+0.3}_{-0.3}$	6^{+4}_{-4}	$0.9^{+0.5}_{-0.5}$
Mg XII	1.47264	$1.477^{+0.003}_{-0.002}$	900^{+600}_{-400}	700^{+500}_{-300}	$0.25^{+0.08}_{-0.08}$	$1.3^{+0.4}_{-0.4}$	$0.32^{+0.09}_{-0.12}$
Mg XI$_r$	1.35225				$0.15^{+0.18}_{-0.15}$	$0.8^{+0.9}_{-0.8}$	$0.18^{+0.32}_{-0.18}$
Mg XI$_i$	1.34332			1100^{+1800}_{-800}	$0.9^{+0.4}_{-0.3}$	$4.9^{+2.3}_{-1.4}$	$1.1^{+0.5}_{-0.3}$
Mg XI$_f$	1.33121				$0.19^{+0.13}_{-0.18}$	$1.1^{+0.7}_{-0.6}$	$0.24^{+0.16}_{-0.23}$
Si XIV	2.00608	$2.008^{+0.002}_{-0.002}$	300^{+300}_{-300}	800^{+400}_{-300}	$0.51^{+0.16}_{-0.15}$	$1.7^{+0.5}_{-0.5}$	$0.56^{+0.17}_{-0.17}$
Si XIII$_r$	1.86500	$1.8674^{+0.0029}_{-0.0015}$	400^{+500}_{-200}		$0.62^{+0.11}_{-0.25}$	$1.9^{+0.8}_{-0.5}$	$0.7^{+0.2}_{-0.2}$
Si XIII$_i$	1.85423	$1.8566^{+0.0029}_{-0.0015}$	400^{+500}_{-200}	1000^{+1200}_{-700}	$0.34^{+0.2}_{-0.19}$	$1.5^{+0.7}_{-0.8}$	$0.4^{+0.2}_{-0.2}$
Si XIII$_f$	1.83967	$1.8421^{+0.0029}_{-0.0015}$	400^{+500}_{-200}		$0.77^{+0.16}_{-0.2}$	$2.9^{+0.6}_{-0.8}$	$0.69^{+0.18}_{-0.18}$
Fe XXVI	6.97316				8^{+4}_{-4}	50^{+20}_{-20}	49^{+24}_{-24}
Fe XXV$_r$	6.70040				6^{+4}_{-4}	40^{+20}_{-20}	41^{+25}_{-25}
Fe XXV$_i$	6.67000				5^{+4}_{-4}	40^{+20}_{-20}	35^{+26}_{-25}
Fe XXV$_f$	6.63659				6^{+3}_{-3}	40^{+20}_{-20}	40^{+22}_{-22}
Fe K$_\alpha$	6.40384	$6.400^{+0.007}_{-0.007}$	-200^{+300}_{-300}	1600^{+300}_{-300}	48^{+6}_{-6}	350^{+50}_{-50}	355^{+47}_{-48}

Notes: We assumed that the value of σ is the same within a triplet for the Ne, Mg and Si lines. The distances between the lines in a triplet were fixed to the table values. The values of σ of the Fe XXVI and Fe XXV$_{r,f,i}$ lines were frozen to the instrumental spectral resolution. The absorbed and the unabsorbed fluxes in ergs cm^{-2} s^{-1} were calculated using the `cflux` command. The unabsorbed flux in ph cm^{-2} s^{-1} was calculated from the normalization constant of the Gaussian model.

TABLE 4.5: R, G and H-like/He-like$_r$ ratios.

Element	R= f/i	G= $(f+i)/r$	H-like/He-like$_r$
Ne	0.9±0.8	2.2±1.4	0.8±0.5
Mg	0.22±0.16		1.6±1.6
Si	1.9±1.0	2.3±0.9	0.9±0.4
Fe	1.0±0.7	2.0±1.2	1.3±0.8

Notes: the values of R and G were calculated from the values of the unabsorbed flux from table 4.4.

Mukai et al. [78] showed that the *Chandra* HETG spectrum of GK Per obtained during the outburst in 2002 is consistent with the predictions of a photoionization model with a power law as the photoionizing continuum. Although the power law emission gave a good approximation, and could indeed photoionize the plasma in which the soft X-rays emission lines are produced, such a non thermal component in a CV does not seem to have a physical reason. Given also the G ratio and the absence of a clearly non-thermal component in the *NuSTAR* range, we do not favor this explanation for the present set of observations.

The top panel of figure 4.11 shows the comparison of the *Chandra* MEG spectrum obtained in 2015 with *Chandra* MEG data discussed in Mukai et al. [78]. The most recent spectrum of GK Per has much weaker lines in the region above 20 Å, which is due to contaminant build-up of the *Chandra* HETG+ACIS detector. The low energy effective area is reduced in 2015 compared to 2002. The intensities of the lines that are in the 6–11 Å region are almost the same. The *Chandra* spectra in fig. 4.11 give an additional proof that there are several distinct sources of emission: there is no correlation between the 6–11Å emission lines strengths and the hard continua below 5 Å.

The N VII line detected in the *Chandra* MEG 2002 and 2015 spectra showed remarkably different profiles in comparison to the other lines. The N VII line's regions are shown in fig. 4.12. In March 2002 and April 2015 two different emission lines were resolved around the rest-frame position of N VII, while in April 2002 another blue-shifted component could be distinguished. Table 4.6 shows the central positions and the unabsorbed fluxes of all the lines that were resolved in three *Chandra* MEG spectra. Vrielmann et al. [235] in their RGS spectrum of GK Per also noticed that the N VII line had a different structure which could be approximated by three Lorentzian profiles. From the *Chandra* MEG spectra we find that if the lines around 24.8 Å are different components of the central N VII line, this would indicate velocity shifts of 1200 – 1600 km s^{-1}. Similar red and blue-shifted emission line's components, although with smaller velocity shifts, were measured in the optical spectra of GK Per during outbursts [258] and were attributed to the emission from the matter in the magnetosphere, falling onto the WD. A question to answer is why N VII is the only line that shows such a complex profile. Two *Chandra*

MEG spectra obtained near optical maximum of the same outburst (see tab. 4.6) also clearly show that the flux of the different N VII line's components varies with time, while the flux of central line is stable within the errors. Another possibility is that the line around 24.8 Å is indeed the N VII emission, but the line around 24.9 Å is the N VI Heβ line, both with zero velocity. In this case the relative intensities of the two lines can be used as temperature indicator (under the assumption of collisional ionization equilibrium). The different relative intensities in March and April of 2002 would imply that the temperature changes. The very strong N VI Heβ line in comparison to N VII in the 2015 spectrum indicates also a very low plasma temperature: $\lesssim$0.08 keV.

We checked whether the expanding nova shell can contribute to line emission in soft X-rays. Balman [215] showed that the shell has enhancement in the elemental abundances of Ne and N and Vrielmann et al. [235] fitted the quiescence Chandra ACIS-S spectrum of the shell with pure emission lines of N, O and Ne, although the lines could not be resolved. In order to estimate a possible contamination of the N VII line from the central source by the shell emission, we compared the predictions of the shell emission model from Takei et al. [216] with the 2015 *Chandra* MEG spectrum. The model from Takei et al. [216] with the only modification in the N abundance (we assumed $N/N_{\odot}=5$) and a power law to represent the continuum level is shown with the red line in the bottom panel of fig. 4.12. We see that the N VII/N VI line's flux from the entire shell is much smaller than that measured in the 2015 *Chandra* MEG spectrum. We conclude that the N lines around 24.8 Å originate not from the extended shell, but the nature of the different components is unknown.

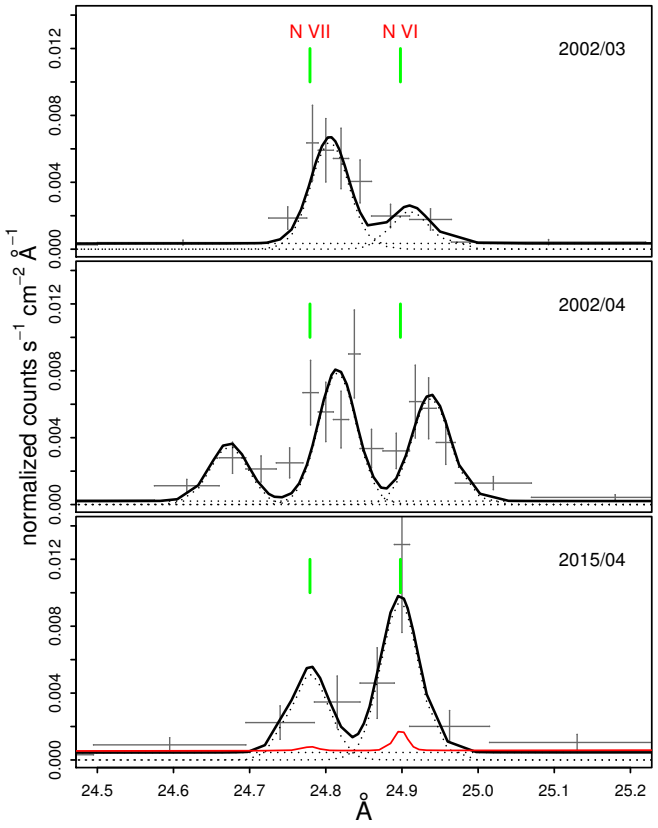

FIGURE 4.12: Comparison of the N VII emission line's profile measured with the *Chandra* MEG in 2015 and 2002 (the datasets are the same as in fig. 4.11). The dates of observations and the rest-frame positions of the N VII and N VI Heβ lines are marked at each panel. All the lines were fitted with two or three Gaussians and a power law to represent the continuum level. In the bottom panel we also show the contribution from the nova shell, based on the model of Takei et al. [216] and a power law to fit the underlying continuum.

TABLE 4.6: N VII emission line fluxes, measured in the *Chandra* MEG spectra of 2002 and 2015.

	central			red-shifted			blue-shifted		
Observation	E max (keV)	Flux*	Ph. flux**	E max	Flux	Ph. flux	E max	Flux	Ph. flux
2002 March 27	$0.4998^{+0.0003}_{-0.0003}$	12±4	1.6±0.4	$0.4977^{+0.0006}_{-0.0008}$	5±2	0.6±0.3			
2002 April 9	$0.5000^{+0.0003}_{-0.0004}$	11±3	1.4±0.4	$0.4973^{+0.0005}_{-0.0003}$	11±3	1.3±0.4	$0.5026^{+0.0002}_{-0.0005}$	5±2	0.6±0.3
2015 April 4	0.50036	9±6	1.1±0.7	0.4980	17±8	1.2±1.0			

Notes: *Unabsorbed flux $\times 10^{-13}$ergs cm^{-2} s^{-1}. **Unabsorbed photon flux $\times 10^{-3}$ photons cm^{-2} s^{-1}. The fluxes were measured from the Gaussian fits, shown in fig. 4.12 using `cflux` and `cpflux` commands. All the line widths were fixed to the value of the instrumental resolution. In these fits we assumed the same value of the interstellar absorption as in the rest of the paper: 0.17×10^{22}cm^{-2}.

The complexity of the spectrum is demonstrated by the ratios of H to He-like lines, which in case of pure collisional-ionization is a signature of the plasma temperature. The He-like lines are stronger than the H-like for all the species. The Si XIII to Si XIV lines ratio indicates a temperature ∼0.9 keV, so the origin of these lines is not in the hotter plasma that explains the *NuSTAR* spectrum. The He to H-like lines ratios of Mg and Ne correspond to even lower plasma temperatures. These lines also cannot be explained by another `mkcflow` component at lower temperature since the cooling flow model always produces H-like lines stronger than the He-like lines [259]. The middle and bottom panels of fig. 4.11 show the comparison of the *Chandra* MEG spectrum with the predictions of the single temperature thermal plasma emission model. We added to the best-fitting model of the *NuSTAR* data a `vapec` component (a single-temperature plasma in CIE with variable abundances of individual elements) and a Gaussian at 0.5 keV to represent the N VII line. Following Vrielmann et al. [235] and Evans et al. [227] we also introduced a blackbody component to represent the thermalized X-ray emission from the WD surface at kT = 66 eV. The choice of the blackbody temperature will be explained in the next section. In the middle panel of fig. 4.11 the temperature of the `vapec` component was fixed to 0.9 keV, in order fit the Si XIII to Si XIV lines ratio. In this case the model underestimates the level of continuum and overestimates the He to H-like lines ratio of Mg and Ne. In the bottom panel the temperature of the `vapec` component corresponds to the best-fitting value — 4.9 keV, which correctly estimates the level of continuum, but cannot reproduce the line ratios. A lower-temperature `vapec` component with higher normalization constant affected by a complex absorber could explain the Si lines and the continuum level, but not the He to H-like lines ratio of Mg and Ne. The emission lines ratios clearly indicate a multi-temperature plasma emission. However, we added another `apec` component to fit the lines at longer wavelengths, but it did not improve the fit significantly. Fig. 4.11 also shows that the `vapec` model underestimates the intercombination and forbidden lines in all the triplets. Thus, the overall spectrum below 2 keV cannot be represented with a model of plasma in CIE, not with a cooling flow, neither with single or two-temperature `vapec` model.

Fig. 8 in Porquet and Dubau [257] shows that the temperature of 0.9 keV and the value of the R ratio of the Si triplet (see table 4.5), which is a density indicator, corresponds to the electron density n_e $\sim 3\times10^{13}$ cm^{-3}. Using these estimates and the value of normalization of the `vapec` component (which gives the emission measure) we find that the radius of the emitting source is $\sim 1.4 R_{WD}$, assuming a spherical distribution of the emitting plasma, M_{WD}=0.86 $M_\odot$ and a WD mass-radius relation from Nauenberg [124]. It should be mentioned, however, that the G and R ratios are measured with large uncertainty (see table 4.5) and we cannot evaluate the contribution of photoionization processes, so this is a qualitative estimate.

TABLE 4.7: Model parameters used for the fit of *Chandra* MEG spectrum apart from that listed in the first column of table 4.3. The model is `TBabs×(pwab×(vmcflow + gaussian) + bb + gaussian)`. The fit was performed for two different temperatures. The parameters without errors were fixed to the values in this table. The Fe and Ni abundances were fixed to 0.106 and 0.1, respectively.

Component	Parameter	Value	
vapec	T (keV)	0.9	$4.9^{+1.4}_{-0.8}$
	norm ($\times 10^{-3}$)	$1.1^{+0.1}_{-0.1}$	$2.6^{+1.5}_{-1.5}$
bb	T (eV)	66	66
	norm ($\times 10^{-4}$)	13^{+2}_{-2}	12^{+2}_{-2}
Gaussian	E (keV)	$0.4988^{+0.0011}_{-0.0009}$	$0.4988^{+0.0011}_{-0.0009}$
	σ (keV)	$0.0019^{+0.0011}_{-0.0009}$	$0.0019^{+0.0011}_{-0.0009}$
	norm ($\times 10^{-4}$)	28^{+13}_{-12}	29^{+13}_{-12}

4.5.3 *Swift* XRT observations

Fig. 4.13 shows the comparison of the average *Swift* XRT spectra in the first two weeks and in the following two weeks. The soft flux increased with time, while the hard flux decreased. We fitted the average spectra with the model described in section 4.5.2 in order to estimate the changes of the flux in different spectral regions. There was no possibility to measure the Fe Kα line width in the *Swift* spectra, so we fixed its central position and the σ to the values from tab. 4.3. We assumed that the metallicity did not change with time and the corresponding parameters in the `vapec` component were constrained to be the same in the two datasets. The best-fitting parameters are listed in the table 4.8. Here and in the following sections we refer to the spectral regions as soft (blackbody-like, below 0.8 keV), intermediate (between 0.8 and 2 keV) and hard (cooling flow component, above 2 keV). There are significant residuals in the part of the spectra below 2 keV and in particular below 0.4 keV in the spectrum obtained in the later period. There is also an excess around 0.9 keV, where the Ne IX line is.

Although the model is quite approximate, we concluded that the hard X-ray flux decreased mostly because of the increased absorption. The soft X-ray flux increased, first of all because of the increased normalization of the blackbody component and the `vapec` components. The blackbody emitting area increased by a factor of 3, but it remained of of the order of $10^{-5} - 10^{-6}$ the area of the WD surface, which is the typical size of a heated polar region in soft IPs [see e.g. 62].

TABLE 4.8: The best fitting model parameters of the *Swift XRT* data. `TBabs×(pwab×(vmcflow + gaussian) + vapec + bb)`. The Fe and Ni abundances of the `vmcflow` and `vapec` components were fixed to 0.105 and 0.1, respectively. The errors represent the 90% confidence region for a single parameter.

Component	Parameter	Value	
		first two weeks	second two weeks
TBabs	$nH^{a,b}$	0.17	0.17
pwab	$nH_{min}{}^{b}$	$2.7^{+0.6}_{-1.2}$	$5.0^{+1.1}_{-1.0}$
	$nH_{max}{}^{b}$	75^{+18}_{-14}	90^{+20}_{-20}
	β^{a}	0	0
vmcflow	T_{high} (keV)	17^{+10}_{-4}	17^{+15}_{-4}
	$\dot{m}^{c}$	$0.7^{+0.5}_{-0.3}$	$0.6^{+0.3}_{-0.3}$
Gaussian	E (keV)	6.4	6.4
	σ (keV)	0.04	0.04
	norm ($\times10^{-4}$)	6^{+2}_{-2}	15^{+2}_{-2}
vapec	T (keV)	>1.9	$0.80^{+0.20}_{-0.10}$
	norm ($\times10^{-3}$)	$2.5^{+3.1}_{-0.5}$	$3.7^{+0.3}_{-0.3}$
bb	T (eV)	75^{+3}_{-3}	63^{+3}_{-2}
	norm ($\times10^{-4}$)	$6.2^{+1.0}_{-0.8}$	36^{+5}_{-5}
$Flux_{0.3-2keV}{}^{d}$	abs.	$4.6^{+0.3}_{-1.0}$	$11.9^{+0.2}_{-0.5}$
	unabs.	420	430
$Flux_{2-10keV}{}^{d}$	abs.	165^{+2}_{-60}	117^{2}_{-50}
	unabs.	507	451
L_{bb} ($\times10^{33}$erg s^{-1})		$1.33^{+0.20}_{-0.17}$	$8.6^{+0.7}_{-0.7}$
$R_{bb}{}^{g}$ ($\times10^{6}$cm)		$1.70^{+0.13}_{-0.12}$	$5.3^{+0.5}_{-0.3}$
$L_{2-10keV}$ ($\times10^{33}$erg s^{-1})		13.4	11.9
χ^2			1.7

Notes: [a]Frozen parameter. [b]$\times10^{22}$ cm^{-2}.
[c]Mass accretion rate $\times10^{-8}M_{\odot}$ yr^{-1}. [d]$\times10^{-12}$erg cm^{-2} s^{-1}.
[g] Radius of the emitting region. We assumed a 470 pc distance.

4.6 Discussion

4.6.1 The WD spin and the long-term variations.

The *NuSTAR* observations of GK Per provided the first detection of a high amplitude modulation due to the WD spin period in X-rays above 10 keV in an IP (only XY Ari in outbursts is known to show a comparable amplitude of modulation). The fact that the spin modulation is so strong in hard X-rays and that the pulse amplitude is not energy dependent indicate that the modulation is a geometric effect rather than due to absorption as in the majority of IPs. This modulation can be partially explained by an obscuration of the lower accretion pole by the inner disk [231, 236]. However, the obscuration of the lower pole alone, does not explain the pulse profile. A small shock region with a low shock height will either be completely visible or completely

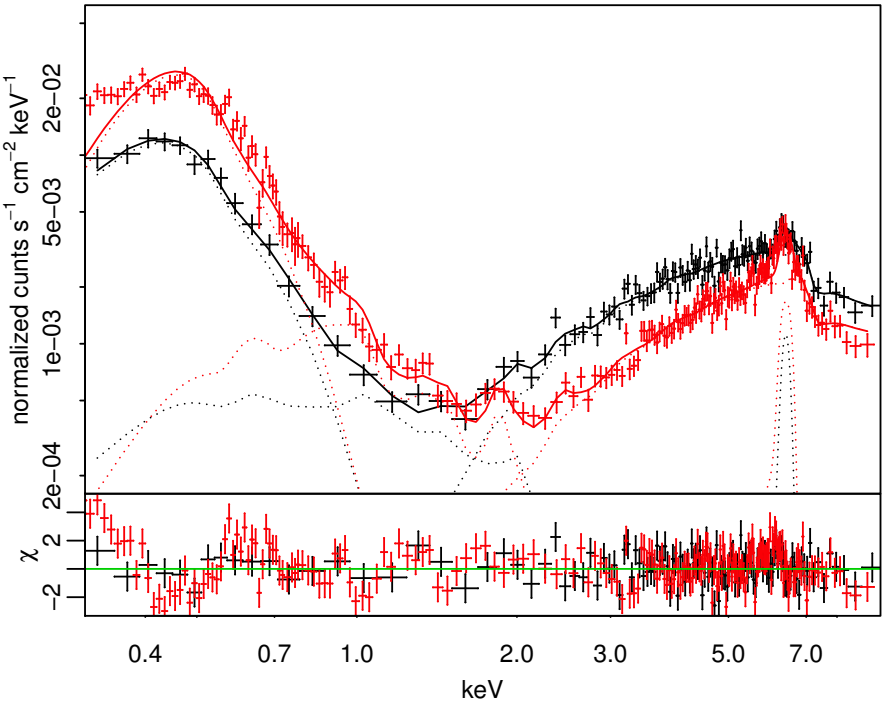

FIGURE 4.13: The averaged *Swift XRT* spectra obtained during the first (black) and the second two weeks (red) of the observations and the best-fitting model. The model parameters are plotted with the dotted lines.

behind the white dwarf with very little transition in between, resulting in a square wave spin modulation. In case of GK Per the modulation is not a square wave but quasi-sinusoidal and about 40% of the total flux is always visible, suggesting a large shock height or an extended shock region. In the first case the soft X-rays, originating closer to the WD surface, will show more prominent modulation, while the hardest X-rays — just moderate eclipses. In GK Per the pulse profiles are not energy dependent, and the pulse fraction is almost the same above and below 10 keV, so we can reject this possibility. In GK Per we most probably deal with an accretion curtain whose footprint is very extended and forms an arc that covers 180 deg. The fraction of the arc that is visible can vary smoothly, resulting in only moderate energy dependence of pulses. It is consistent with the idea proposed by Hellier et al. [231] and Vrielmann et al. [235] that in outburst accretion flows to the poles from all azimuths.

Variability on the timescale of 7000 s was also detected even above 10 keV and this cannot be explained by the model of Hellier et al. [231], in which the QPOs are due to absorption by bulges of material in the accretion disk. These variations are most probably intrinsic variability of the accretion column emission due to inhomogeneous accretion. This is supported by the linear dependence between the mean X-ray count rate and the pulse amplitude.

We have also shown that, although the hard X-ray emission shows a very prominent and high-amplitude spin modulation, precise measurements of the period are not so straightforward due to the presence of the flickering and the quasi-periodic variability. The *NuSTAR* and Chandra data alone did not allow us to measure the spin period precisely, and only the long monitoring with *Swift* allowed an estimate the spin-up rate.

4.6.2 Hard X-ray component.

The spectrum above 2 keV can be well fitted with the cooling flow model with maximum temperature of 16.2 keV, representing the emission from the WD accretion column. The continuum indicates that the source is highly absorbed, and this is also supported by the fact that the contribution of the cooling flow component to the observed line emission below 2 keV should be negligible. The source of this absorption most probably is the pre-shock material. Since, depending on the spin phase there will be different amount of absorption in our line of sight, the overall picture is very complex, and is best approximated be the `pwab` model.

The shock temperature derived from the fit is lower than that observed in quiescence and at the beginning of the outburst, which is about 26–27 KeV [237, 260, 261]. When the inner radius of the accretion disk shrinks, the shock temperature is reduced by a factor of:

$$f = T_{\rm o}/T_{\rm q} = (1 - r_{\rm Mo}^{-1})/(1 - r_{\rm Mq}^{-1}) \tag{4.6}$$

[238], because the approximation of the free fall velocity cannot be used anymore (here $r_{\rm Mo}$ and $r_{\rm Mq}$ are the outburst and quiescent radii of the magnetosphere in the units of the WD radius). The magnetospheric radius is defined by a balance between the ram pressure in the disk, which depends on mass transfer, and the magnetic pressure. As long as the optical flux is increasing, we expect the mass transfer to be constantly increasing as well, since the optical probes the portion of the disk involved in the outburst. This should result into gradual shrinking of the inner disk radius and lowering of the shock temperature. The observations in the very first days of the outburst [261] demonstrate that the decrease of the temperature indeed does not happen immediately. However, the spectral resolution of the short *Swift* exposures and the uncertainty in the intrinsic absorption did not allow us to trace this process. Even in the fit to the averaged *Swift* XRT spectra the errors of the plasma temperature are too high to measure the difference.

4.6.3 Intermediate energy X-ray spectrum

These are the key points of the analysis of the intermediate X-ray spectral component (0.8–2.0 keV):

- There are very prominent emission lines of Si, Mg, Ne and Fe XVII–Fe XVIII.
- The emission lines did not show any systematic velocity shift or broadening.
- The emission line ratios do not allow to clearly distinguish between collisional and photoionization mechanisms.
- Assuming collisional ioinzation equilibrium, the continuum below 2 keV is produced in a medium with a higher temperature than the emission line ratios indicate.
- The spectrum in the 0.8–2 keV range cannot be represented with a model of plasma in CIE, not with a cooling flow, neither with single or two-temperature `vapec` model.
- Neither the continuum, nor the emission lines show any spin modulation in this energy range.

Vrielmann et al. [235] claimed that the emission lines in the X-ray spectrum of GK Per originate in the magnetosphere of the WD, because they show no rotation-related modulations. We found that not only the lines, but also the underlying continuum is not modulated, indicating that the source of emission is not confined to the WD polar regions. This conclusion is also supported by the estimates of the size of the emitting region, which is of the same order of magnitude as the estimated magnetospheric radius of GK Per by Suleimanov et al. [226] (1.4 R_{WD} and 2.8 R_{WD}). We propose that the magnetospheric boundary is the emission site of the intermediate spectral component and the intermediate energy X-ray flux is related to the decrease of the shock temperature. If the shock temperature during outbursts is 2/3 of that in quiescence [226, 237], half of the remaining energy is radiated away in the Keplerian disk. Where is the remaining 1/6th irradiated and how do we explain the energy budget? The site of emission may thus be the magnetospheric boundary, producing this intermediate X-ray spectral component, in the 0.8–2 keV range, even if the exact mechanism of emission is not clear yet. This idea partially explains the anticorrelation of the soft and hard X-rays during the outburst: the lower the shock temperature, the more energy is released in the magnetospheric boundary as moderately soft X-ray emission. Additionally, Suleimanov et al. [226] measured the magnetospheric radius using the the observed break frequency in

the power spectrum and found $\nu_{\rm break} = 0.0225 \pm 0.004$, corresponding to the Keplerian velocity of ~ 2500 km s^{-1}, much faster than at the co-rotation radius, suggesting that the material in the disk must lose energy in order to decelerate and follow the field lines.

4.6.4 The soft component.

The spectral fits and the comparison of the *Chandra* data obtained at different epochs (see fig. 4.11) indicate at least two distinct sources of emission below 2 keV. However, since there is no proper model for the intermediate energy X-ray spectrum of GK Per, it is quite difficult to disentangle the spectral components. The softest part of the spectrum can indeed be blackbody-like and originate on the surface of the WD, heated by the accretion column. Such blackbody-like component in an X-ray spectrum is a distinct property of "soft intermediate polars" [see e.g 60, 61]. The size of the blackbody emitting region was 0.0026 and 0.0083 $R_{\rm WD}$ (using the mass-radius relation from Nauenberg 124 and M=0.86 $M_\odot$), in the first and the second halves of the observations and the temperature was 60 – 70 eV, which is within the range of typical values for soft IPs. The increase of the luminosity of the blackbody-like component indicates that more material is penetrating deeper in the WD photosphere, producing thermalized X-rays emission, which may be an effect of the increased mass accretion rate. The latter reaches maximum around the maximum of the optical light. This is supported by the findings of Šimon [239], who analyzed a sequence of outbursts in GK Per and noticed a discrepancy between the mass transfer through the disk and X-ray emission from the accretion column, which is largest around of optical maximum; this can be explained by a buried shock.

On the other hand, the are significant residuals from the blackbody fit of the *Swift* XRT spectra (fig. 4.13). Following the discussion from Evans et al. [227] we attempted to estimate the upper limit to the temperature of the accretion disk in order check whether it can contribute to the soft X-ray range. The the upper limit to the temperature can be found as:

$$T(R) = \left(\frac{3GM\dot{M}}{8\pi R^3 \sigma} \right)^{1/4} \tag{4.7}$$

[262]. Using the WD mass-radius relation from Nauenberg [124], the values of $\dot{m}$ from table 4.3, M=0.86 $M_\odot$ and inner disk radius R= 2.8$R_{\rm WD}$ [226] we find that the disk temperature can be as high as 90 000 K. This peak temperature corresponds to a blackbody peak wavelength of 320 Å. The inner disk region significantly contributes to the FUV and UV ranges, however, this temperature is still low to be detected with the *Swift* XRT (should be at least 150 000 K) and the disk emission cannot explain the very soft-X-ray excess, seen in fig. 4.13.

Strong emission lines were measured in the *Chandra* HETG spectra obtained in 2002 in a range as soft as 0.5 keV, where the blackbody component dominates, indicating a significant contribution from the low-temperature thin plasma emission. N VII at 0.5 keV additionally shows a completely different profile with two-three components, separated by ∼1200–1600 km s^{-1}.

4.7 Conclusions

We have presented the long-term monitoring of GK Per in a broad energy range, from UV to hard X-rays, during the dwarf nova outburst in March-April 2015. The *NuSTAR* observations allowed to detect a large-amplitude WD spin modulation in the very hard X-rays, which is unusual for an IP.

The spectral and timing analysis of our data has revealed three distinct spectral components, evolving during the outburst. The spectrum above 2 keV can be well explained by a cooling post-shock plasma in the accretion column, highly absorbed by a pre-shock material. The spectrum below ∼0.8 keV probably represents the thermalized X-ray emission from the heated WD surface. The emission line spectrum between 0.8 and 2 keV is the most mysterious, since it cannot be represented by any existing model of plasma in collisional ionization equilibrium. We propose that it originates in the magnetospheric boundary around the WD.

Therefore, as the outburst develops and the mass transfer through the disk grows, there are three simultaneous processes affecting the X-ray spectrum:

- The ram pressure increases at the magnetospheric boundary, pushing the accretion disk towards the WD surface and causing the decrease of the shock temperature.
- The lower the shock temperature with respect to the quiescence level, the more energy is released in the magnetospheric boundary in the ∼0.8 – 2.0 keV range.
- Increased specific mass accretion rate in the accretion column results in a higher amount of material that penetrates deeper in the WD photosphere, causing the increase of the blackbody-like radiation.

The complexity of the X-ray spectrum, the behaviour in different energy ranges and the discrepancy between the spectra we obtained and some predictions of the existing models makes GK Per a challenging target for future studies. We propose that the observational strategy should be to monitor GK Per before the outburst and at different stages of its outburst evolution, in order to disentangle the spectral components and to

reveal the contribution from different sources. Even high resolution data, obtained at a single stage of its outburst, do not allow to reveal the mechanisms that take place in this system.

Chapter 5

Conclusions

Accreting and hydrogen burning WDs are an important class of astrophysical objects. In this thesis I addressed several issues related to these systems, which are important for our understanding of their evolution and possible relation to type Ia SNe.

I investigated a group of CVs, VY Scl-type stars, which accrete at high rate, but with occasional interruptions of the high mass-transfer regime. I explored the idea that VY Scl-type stars undergo quiescent hydrogen burning during their "low states". The possibility of hydrogen burning and the absence of detected nova explosions in these systems imply that at some point of their evolution they may reach the Chandrasekhar limit and explode as type Ia SNe.

I analyzed archival observations of four such objects, BZ Cam, MV Lyr, TT Ari, and V794 Aql, obtained with *Suzaku*, *Chandra* HETG, *ROSAT*, *Swift*, and *GALEX*. Comparing their "high" and "low" state X-ray spectra I found no supersoft X-ray emission, which should be associated with the hydrogen burning. The hydrogen burning may still occur at low temperatures (below 150 000 K), outside the SSS window, but this would imply very low WD masses: below 0.6 M_{WD}. The absence of the supersoft X-ray emission in VY Scl-type stars suggests that they cannot be considered as type Ia SN progenitors. If they burn hydrogen quietly, without triggering nova explosions the mass of the WD must be too low to reach the Chandrasekhar limit. If there is no hydrogen burning the estimated range of mass transfer rate indicate that they must undergo rare nova explosions, expelling more material than was accreted.

All the X-ray spectra of VY Scl-type stars I analyzed were complex, indicating more than one component. We propose that part of the emission originates in circumstellar material, shocked by a wind, possibly at a large distance from the WD. The second component of the X-ray emission is due to the accretion. There are indications of

magnetic-driven accretion in these systems, but we are not able to prove nor clearly disprove the IP scenario.

I aslo studied novae with massive WDs as they return to quiescence. I chose two novae with indications of high WD mass and mass transfer rate, V2491 Cyg and V4743 Sgr, and analyzed their X-ray and optical observations. The X-ray observations were performed with *Suzaku* and *XMM Newton* 2–4 years after the explosions. The timing analysis of the X-ray data revealed that V4743 Sgr is an IP and V2491 Cyg is a strong IP candidate. In order to better explore the possibility of magnetic accretion, I analyzed optical photometric data (obtained with the 0.9-m KPNO, 1.25-m CRAO, and Kepler telescopes) and optical spectra (obtained with the 10-m SALT, 6-m BTA and 1-m Zeiss SAO RAS telescopes). The results of the optical observations also suggest the presence of a strong magnetic field: almost all the emission lines have red and blue-shifted satellite components, which can originate in the accretion curtains, and strong He II λ4686 lines. Additionally, the optical fluxes of both novae are modulated at periods longer than that, detected in the X-rays, indicating reprocession of the X-rays from the surface of the secondaries.

Both novae had a very peculiar characteristic: a blackbody-like component in the X-ray spectrum at temperature close to that, observed during the SSS phase, but with much lower luminosity, suggesting a smaller emitting region. Similar blackbody-like components are also observed in IPs and originate in the heated by the accretion columns WD polar caps. However, in V4743 Sgr the supersoft X-ray component disappeared by the time of the last *XMM Newton* observation, implying that the source of radiation is not related to accretion and cannot be explained by the irradiated polar cap. In V2491 Cyg we also detected a sudden decrease of the flux of the He II λ4686 line, which indicates cooling or disappearance of the ionizing source, a similar process to that, observed in V4743 Sgr.

There is another old nova and an IP candidate, V2487 Oph, which most probably hosts a massive WD and shows similar low-luminosity blackbody-like component in its X-ray spectrum for at least 8 years. One possibile explanation is that this supersoft emission may be due to a temperature gradient on the surface of the WD, which can be a characteristic of magnetic novae. Another explanation is residual nuclear burning, possibly continuing in the post-outburst quiescent phase in a smaller region than the whole WD, a process that has never been observed before. Theoretical studies have shown that once ignited, hydrogen burning will spread along the whole WD surface. However, these studies were related to the beginning of a nova explosion, while we detected possible localization of the burning in quiescence, when the hydrogen fuel is being consumed. This finding may have profound implications for the secular history of

accretion and hydrogen burning and implies that the return to quiescence of magnetic novae may differ from that of non-magnetic systems.

In the last chapter of the thesis I present the results of the long-term monitoring of an intermediate polar, GK Per, in a broad energy range, from UV to hard X-rays, during the dwarf nova outburst in March-April 2015. The observations, performed with *NuSTAR*, *Chandra* HETG, and *Swift*, revealed three distinct spectral components, which evolve during the outburst. We associate the soft component, below 0.8 keV with the emission from the heated WD polar cap and the hard component, above 2 keV, with the thermal plasma emission from the accretion column. The intermediate energy component, dominating in the 0.8–2.0 keV energy range, is the most puzzling, since it cannot be represented by any existing model of plasma in collisional ionization equilibrium. We propose that it originates in the magnetospheric boundary around the WD. The long-term monitoring allowed us to study how does the X-ray spectrum of a magnetic system change as the mass accretion rate increases. We found that there are three simultaneous processes affecting the X-ray spectrum:

- The ram pressure increases at the magnetospheric boundary, pushing the accretion disk towards the WD surface and causing the decrease of the shock temperature.
- The lower the shock temperature with respect to the quiescence level, the more energy is released in the magnetospheric boundary in the $\sim$0.8 – 2.0 keV range.
- Increased specific mass accretion rate in the accretion column results in a higher amount of material that penetrates deeper in the WD photosphere, causing the increase of the blackbody-like radiation.

The *NuSTAR* light curve revealed a large-amplitude WD spin modulation of the hard X-ray flux, which has never been observed before. This modulation of the hard X-rays and the moderate energy dependence of the pulse fraction indicates that the accretion curtain's footprint is very extended and forms an arc that covers 180 deg.

Usually in the models of nova explosion and evolution mass accretion rate is assumed to be constant, while GK Per shows that it is not always the case. A possible next step in the theoretical studies is to account for non-continues mass accretion.

Bibliography

[1] T. Kato, M. Uemura, R. Ishioka, D. Nogami, C. Kunjaya, H. Baba, and H. Yamaoka. Variable Star Network: World center for transient object astronomy and variable stars. *PASJ*, 56:S1–S54, 2004.

[2] S. Starrfield, C. Iliadis, F. X. Timmes, W. R. Hix, W. D. Arnett, C. Meakin, and W. M. Sparks. Theoretical studies of accretion of matter onto white dwarfs and the single degenerate scenario for supernovae of Type Ia. *Bulletin of the Astronomical Society of India*, 40:419, September 2012.

[3] W. M. Wolf, L. Bildsten, J. Brooks, and B. Paxton. Hydrogen Burning on Accreting White Dwarfs: Stability, Recurrent Novae, and the Post-nova Supersoft Phase. *ApJ*, 777:136, November 2013. doi: 10.1088/0004-637X/777/2/136.

[4] M. Henze, M. J. Darnley, F. Kabashima, K. Nishiyama, K. Itagaki, and X. Gao. A remarkable recurrent nova in M 31: The 2010 eruption recovered and evidence of a six-month period. *A&A*, 582:L8, October 2015. doi: 10.1051/0004-6361/201527168.

[5] M. Orio, J. Covington, and H. Ögelman. X-ray emission from classical and recurrent novae observed with ROSAT. *A&A*, 373:542–554, July 2001. doi: 10.1051/0004-6361:20010537.

[6] J. Krautter. The Super-soft Phase in Novae. In A. Evans, M. F. Bode, T. J. O'Brien, and M. J. Darnley, editors, *RS Ophiuchi (2006) and the Recurrent Nova Phenomenon*, volume 401 of *Astronomical Society of the Pacific Conference Series*, page 139, December 2008.

[7] M. Orio. Observations of classical and recurrent novae with X-ray gratings. *Bulletin of the Astronomical Society of India*, 40:333, September 2012.

[8] C. H. P. Gaposchkin. *The Galactic Novae*. New York, Interscience Publishers, 1957.

[9] M. della Valle and M. Livio. The Calibration of Novae as Distance Indicators. *ApJ*, 452:704, October 1995. doi: 10.1086/176342.

[10] F. Verbunt and C. Zwaan. Magnetic braking in low-mass X-ray binaries. *A&A*, 100:L7–L9, July 1981.

[11] S. Rappaport, F. Verbunt, and P. C. Joss. A new technique for calculations of binary stellar evolution, with application to magnetic braking. *ApJ*, 275:713–731, December 1983. doi: 10.1086/161569.

[12] J. Faulkner. Ultrashort-Period Binaries, Gravitational Radiation, and Mass Transfer. I. The Standard Model, with Applications to WZ Sagittae and Z Camelopardalis. *ApJ*, 170:L99, December 1971. doi: 10.1086/180848.

[13] B. Paczynski and R. Sienkiewicz. Gravitational radiation and the evolution of cataclysmic binaries. *ApJ*, 248:L27–L30, August 1981. doi: 10.1086/183616.

[14] B. T. Gänsicke, M. Dillon, J. Southworth, J. R. Thorstensen, P. Rodríguez-Gil, A. Aungwerojwit, T. R. Marsh, P. Szkody, S. C. C. Barros, J. Casares, D. de Martino, P. J. Groot, P. Hakala, U. Kolb, S. P. Littlefair, I. G. Martínez-Pais, G. Nelemans, and M. R. Schreiber. SDSS unveils a population of intrinsically faint cataclysmic variables at the minimum orbital period. *MNRAS*, 397:2170–2188, August 2009. doi: 10.1111/j.1365-2966.2009.15126.x.

[15] H. Ritter and U. Kolb. Catalogue of cataclysmic binaries, low-mass X-ray binaries and related objects (Seventh edition). *A&A*, 404:301–303, June 2003. doi: 10.1051/0004-6361:20030330.

[16] S. Mineshige. Accretion disk instabilities. *Ap&SS*, 210:83–103, December 1993. doi: 10.1007/BF00657876.

[17] N. I. Shakura and R. A. Sunyaev. Black holes in binary systems. Observational appearance. *A&A*, 24:337–355, 1973.

[18] J. K. Cannizzo. A brief overview of dwarf novae and x-ray novae. *New A Rev.*, 44:41, 2000.

[19] Y. Osaki. The disk instability model for dwarf nova outbursts. *Proceeding of the Japan Academy, Series B*, 81:291–305, 2005.

[20] T. Ohshima, T. Kato, H. Itoh, E. de Miguel, T. Krajci, H. Akazawa, K. Shiokawa, W. Stein, E. Pavlenko, A. Baklanov, D. Samsonov, O. Antonyuk, M. Andreev, K. Imamura, F.-J. Hambsch, H. Maehara, J. Ruiz, S. Nakagawa, K. Kasai, B. Boitnott, J. Virtanen, and I. Miller. Discovery of Negative Superhumps during a superoutburst of January 2011 in ER Ursae Majoris. *PASJ*, 64:L3, August 2012.

[21] Y. Osaki and T. Kato. The Cause of the Superoutburst in SU UMa Stars is Finally Revealed by Kepler Light Curve of V1504 Cygni. *PASJ*, 65:50, June 2013. doi: 10.1093/pasj/65.3.50.

[22] P. Zemko, T. Kato, and S. Y. Shugarov. Detection of Change in Supercycles in ER Ursae Majoris. *PASJ*, 65:54, June 2013. doi: 10.1093/pasj/65.3.54.

[23] Y. Osaki. A Model for a Peculiar SU Ursae Majoris-Type Dwarf Nova ER Ursae Majoris. *PASJ*, 47:L11–L14, April 1995.

[24] M. Otulakowska-Hypka and A. Olech. On supercycle lengths of active SU UMa stars. *MNRAS*, 433:1338–1343, August 2013. doi: 10.1093/mnras/stt815.

[25] T. Kato, R. Ishioka, K. Isogai, M. Kimura, A. Imada, I. Miller, K. Masumoto, H. Nishino, N. Kojiguchi, M. Kawabata, D. Sakai, Y. Sugiura, H. Furukawa, K. Yamamura, H. Kobayashi, K. Matsumoto, S.-Y. Wang, Y. Chou, C.-C. Ngeow, W.-P. Chen, N. Panwar, C.-S. Lin, H.-Y. Hsiao, J.-K. Guo, C.-C. Lin, C. Omarov, A. Kusakin, M. Krugov, D. R. Starkey, E. P. Pavlenko, K. A. Antonyuk, A. A. Sosnjvskij, O. I. Antonyuk, N. V. Pit, A. V. Baklanov, J. V. Babina, H. Itoh, S. Padovan, H. Akazawa, S. Kafka, E. de Miguel, R. D. Pickard, S. Kiyota, S. Y. Shugarov, D. Chochol, V. Krushevska, M. Sekeras, O. Pikalova, R. Sabo, P. A. Dubovsky, I. Kudzej, J. Ulowetz, S. Dvorak, G. Stone, T. Tordai, F. Dubois, L. Logie, S. Rau, S. Vanaverbeke, T. Vanmunster, A. Oksanen, Y. Maeda, K. Kasai, N. Katysheva, E. Morelle, V. V. Neustroev, and G. Sjoberg. RZ Leonis Minoris Bridging between ER Ursae Majoris-Type Dwarf Nova and Novalike System. *ArXiv e-prints*, September 2016.

[26] R. Whitehurst. Numerical simulations of accretion disks. i - superhumps - a tidal phenomenon of accretion disks. *MNRAS*, 232:35, 1988.

[27] Y. Osaki. A model for the superoutburst phenomenon of SU Ursae Majoris stars. *PASJ*, 41:1005–1033, 1989.

[28] Y. Osaki and T. Kato. The Cause of the Superoutburst in SU UMa Stars is Finally Revealed by Kepler Light Curve of V1504 Cygni. *PASJ*, 65:50, June 2013. doi: 10.1093/pasj/65.3.50.

[29] T. Kato and Y. Osaki. Analysis of Three SU UMa-Type Dwarf Novae in the Kepler Field. *PASJ*, 65:97, October 2013. doi: 10.1093/pasj/65.5.97.

[30] Y. Osaki and T. Kato. A further study of superoutbursts and superhumps in SU UMa stars by the Kepler light curves of V1504 Cygni and V344 Lyrae. *PASJ*, 66: 15, February 2014. doi: 10.1093/pasj/pst015.

[31] D. W. Hoard, A. P. Linnell, P. Szkody, R. E. Fried, E. M. Sion, I. Hubeny, and M. A. Wolfe. The Hot White Dwarf in the Cataclysmic Variable MV Lyrae. *ApJ*, 604:346–356, March 2004. doi: 10.1086/381777.

[32] B. T. Gänsicke, E. M. Sion, K. Beuermann, D. Fabian, F. H. Cheng, and J. Krautter. TT Arietis: the low state revisited. *A&A*, 347:178–184, July 1999.

[33] R. G. M. Rutten, J. van Paradijs, and J. Tinbergen. Reconstruction of the accretion disk in six cataclysmic variable stars. *A&A*, 260:213–226, July 1992.

[34] G. T. Bath and J. E. Pringle. The evolution of viscous discs. I - Mass transfer variations. *MNRAS*, 194:967–986, March 1981.

[35] D. W. Hoard, K. S. Long, S. B. Howell, S. Wachter, C. S. Brinkworth, C. Knigge, J. E. Drew, P. Szkody, S. Kafka, K. Belle, D. R. Ciardi, C. S. Froning, G. T. van Belle, and M. L. Pretorius. Nova-like Cataclysmic Variables in the Infrared. *ApJ*, 786:68, May 2014. doi: 10.1088/0004-637X/786/1/68.

[36] D. W. Hoard, P. Szkody, C. S. Froning, K. S. Long, and C. Knigge. Observations of the SW Sextantis Star DW Ursae Majoris with the Far Ultraviolet Spectroscopic Explorer. *AJ*, 126:2473–2486, November 2003. doi: 10.1086/378605.

[37] A. S. Oliveira, H. J. F. Lima, J. E. Steiner, B. W. Borges, and D. Cieslinski. The orbital period of the V Sge star candidate QU Carinae. *MNRAS*, 444:2692–2699, November 2014. doi: 10.1093/mnras/stu1624.

[38] P. Rodríguez-Gil, J. Casares, I. G. Martínez-Pais, P. Hakala, and D. Steeghs. Evidence of Magnetic Accretion in an SW Sextantis Star: Discovery of Variable Circular Polarization in LS Pegasi. *ApJ*, 548:L49–L52, February 2001. doi: 10.1086/318922.

[39] P. Rodríguez-Gil, J. Casares, I. G. Martínez-Pais, and P. J. Hakala. Detection of variable circular polarization in the SW Sex star V795 Herculis. In B. T. Gänsicke, K. Beuermann, and K. Reinsch, editors, *The Physics of Cataclysmic Variables and Related Objects*, volume 261 of *Astronomical Society of the Pacific Conference Series*, page 533, January 2002.

[40] J. Patterson, J. R. Thorstensen, T. Vanmunster, R. E. Fried, B. Martin, T. Campbell, J. Robertson, J. Kemp, D. Messier, and E. Armstrong. Rapid Oscillations in Cataclysmic Variables. XVI. DW Cancri. *PASP*, 116:516–526, June 2004. doi: 10.1086/421034.

[41] R. K. Honeycutt and S. Kafka. Characteristics of High-State/Low-State Transitions in VY Sculptoris Stars. *AJ*, 128:1279–1293, September 2004. doi: 10.1086/422737.

[42] M. Livio and J. E. Pringle. Star spots and the period gap in cataclysmic variables. *ApJ*, 427:956–960, June 1994. doi: 10.1086/174202.

[43] K. Wu, D. T. Wickramasinghe, and B. Warner. Feedback Mass Transfer in Cataclysmic Variables - an Explanation of the Behaviour of Vy-Sculptoris. *PASA*, 12: 60, April 1995.

[44] A. R. King and J. K. Cannizzo. Low States in Cataclysmic Variables. *ApJ*, 499: 348–354, May 1998. doi: 10.1086/305630.

[45] R. Leach, F. V. Hessman, A. R. King, R. Stehle, and J. Mattei. The light curves of VY Scl stars. *MNRAS*, 305:225–230, May 1999. doi: 10.1046/j.1365-8711.1999.02450.x.

[46] J.-P. Lasota and J.-M. Hameury. VY Sculptoris stars are Magnetic Cataclysmic Variables. In S. Vrielmann and M. Cropper, editors, *IAU Colloq. 190: Magnetic Cataclysmic Variables*, volume 315 of *Astronomical Society of the Pacific Conference Series*, page 46, December 2004.

[47] V. Stanishev, Z. Kraicheva, H. M. J. Boffin, V. Genkov, C. Papadaki, and S. Carpano. Accretion disc evolution in DW Ursae Majoris: A photometric study. *A&A*, 416:1057–1067, March 2004. doi: 10.1051/0004-6361:20034145.

[48] J. Shears, B. Gaensicke, P. Rodriguez-Gil, D. Boyd, G. Darlington, and I. Miller. Faint-state transitions in the SW Sextantis nova-like variable, HS 0455+8315. *ArXiv e-prints*, March 2015.

[49] P. Zemko and T. Kato. Photometric analysis of TT Arietis in the high and low states during 2004 - 2013. *Contributions of the Astronomical Observatory Skalnate Pleso*, 43:487–489, March 2014.

[50] J. R. Thorstensen, F. A. Ringwald, R. A. Wade, G. D. Schmidt, and J. E. Norsworthy. PG0027 + 260 - an example of a class of cataclysmic binaries with mysterious, but consistent, behavior. *AJ*, 102:272–283, July 1991. doi: 10.1086/115874.

[51] P. Rodríguez-Gil, L. Schmidtobreick, and B. T. Gänsicke. Spectroscopic search for new SW Sextantis stars in the 3-4 h orbital period range - I. *MNRAS*, 374: 1359–1376, February 2007. doi: 10.1111/j.1365-2966.2006.11245.x.

[52] D. W. Hoard, T.-N. Lu, C. Knigge, L. Homer, P. Szkody, M. Still, K. S. Long, V. S. Dhillon, and S. Wachter. Simultaneous X-ray and Ultraviolet Observations of the SW Sextantis Star DW Ursae Majoris. *AJ*, 140:1313–1320, November 2010. doi: 10.1088/0004-6256/140/5/1313.

[53] J. E. Steiner and M. P. Diaz. The V Sagittae Stars. *PASP*, 110:276–282, March 1998. doi: 10.1086/316139.

[54] J. Patterson, J. Kemp, A. Shambrook, J. R. Thorstensen, D. R. Skillman, J. Gunn, L. Jensen, T. Vanmunster, S. Shugarov, J. A. Mattei, T. Shahbaz, and R. Novak. Two Galactic Supersoft X-Ray Binaries: V Sagittae and T Pyxidis. *PASP*, 110: 380–395, April 1998. doi: 10.1086/316147.

[55] D. M. Townsley and B. T. Gänsicke. Cataclysmic Variable Primary Effective Temperatures: Constraints on Binary Angular Momentum Loss. *ApJ*, 693:1007–1021, March 2009. doi: 10.1088/0004-637X/693/1/1007.

[56] L. Schmidtobreick. The SW Sex Phenomenon as an Evolutionary Stage of Cataclysmic Variables. *Central European Astrophysical Bulletin*, 37:361–368, 2013.

[57] L. Schmidtobreick and C. Tappert. Old Novae and the SW Sextantis Phenomenon. In P. A. Woudt and V. A. R. M. Ribeiro, editors, *Stell Novae: Past and Future Decades*, volume 490 of *Astronomical Society of the Pacific Conference Series*, page 29, December 2014.

[58] P. Mróz, A. Udalski, R. Poleski, I. Soszyński, M. K. Szymański, G. Pietrzyński, Ł. Wyrzykowski, K. Ulaczyk, S. Kozłowski, P. Pietrukowicz, and J. Skowron. OGLE Atlas of Classical Novae. I. Galactic Bulge Objects. *ApJS*, 219:26, August 2015. doi: 10.1088/0067-0049/219/2/26.

[59] L. Ferrario, D. de Martino, and B. T. Gänsicke. Magnetic White Dwarfs. *Space Sci. Rev.*, 191:111–169, October 2015. doi: 10.1007/s11214-015-0152-0.

[60] P. A. Evans and C. Hellier. Why Do Some Intermediate Polars Show Soft X-Ray Emission? A Survey of XMM-Newton Spectra. *ApJ*, 663:1277–1284, July 2007. doi: 10.1086/518552.

[61] G. Anzolin, D. de Martino, J.-M. Bonnet-Bidaud, M. Mouchet, B. T. Gänsicke, G. Matt, and K. Mukai. Two new intermediate polars with a soft X-ray component. *A&A*, 489:1243–1254, October 2008. doi: 10.1051/0004-6361:200810402.

[62] F. Bernardini, D. de Martino, M. Falanga, K. Mukai, G. Matt, J.-M. Bonnet-Bidaud, N. Masetti, and M. Mouchet. Characterization of new hard X-ray cataclysmic variables. *A&A*, 542:A22, June 2012. doi: 10.1051/0004-6361/201219233.

[63] K. Aizu. X-Ray Emission Region of a White Dwarf with Accretion. *Progress of Theoretical Physics*, 50:344–344, July 1973. doi: 10.1143/PTP.50.344.

[64] V. Suleimanov, M. Revnivtsev, and H. Ritter. RXTE broadband X-ray spectra of intermediate polars and white dwarf mass estimates. *A&A*, 435:191–199, May 2005. doi: 10.1051/0004-6361:20041283.

[65] S. N. Shore, M. Livio, E. P. J. van den Heuvel, H. Nussbaumer, and A. Orr, editors. *Interacting binaries*, 1994.

[66] M. Livio, A. Shankar, and J. W. Truran. Nova outbursts on magnetic white dwarfs. *ApJ*, 330:264–273, July 1988. doi: 10.1086/166470.

[67] M. Orio, E. Trussoni, and H. Oegelman. Classical novae as fast magnetic rotators. *A&A*, 257:548–556, April 1992.

[68] F. Hoyle and W. A. Fowler. Nucleosynthesis in Supernovae. *ApJ*, 132:565, November 1960. doi: 10.1086/146963.

[69] D. Kushnir, B. Katz, S. Dong, E. Livne, and R. Fernández. Head-on Collisions of White Dwarfs in Triple Systems Could Explain Type Ia Supernovae. *ApJ*, 778: L37, December 2013. doi: 10.1088/2041-8205/778/2/L37.

[70] E. Chiosi, C. Chiosi, P. Trevisan, L. Piovan, and M. Orio. Exploring an alternative channel of evolution towards SNa Ia explosion. *MNRAS*, 448:2100–2125, April 2015. doi: 10.1093/mnras/stv084.

[71] J. Bramante. Dark Matter Ignition of Type Ia Supernovae. *Physical Review Letters*, 115(14):141301, October 2015. doi: 10.1103/PhysRevLett.115.141301.

[72] J. Whelan and I. Iben, Jr. Binaries and Supernovae of Type I. *ApJ*, 186:1007–1014, December 1973. doi: 10.1086/152565.

[73] K. Nomoto. Accreting white dwarf models for type I supernovae. I - Presupernova evolution and triggering mechanisms. *ApJ*, 253:798–810, February 1982. doi: 10.1086/159682.

[74] R. F. Webbink. Double white dwarfs as progenitors of R Coronae Borealis stars and Type I supernovae. *ApJ*, 277:355–360, February 1984. doi: 10.1086/161701.

[75] I. Iben, Jr. and A. V. Tutukov. The evolution of low-mass close binaries influenced by the radiation of gravitational waves and by a magnetic stellar wind. *ApJ*, 284: 719–744, September 1984. doi: 10.1086/162455.

[76] A. Kashi and N. Soker. A circumbinary disc in the final stages of common envelope and the core-degenerate scenario for Type Ia supernovae. *MNRAS*, 417:1466–1479, October 2011. doi: 10.1111/j.1365-2966.2011.19361.x.

[77] R. F. Mushotzky and A. E. Szymkowiak. Einstein Observatory solid state detector observations of cooling flows in clusters of galaxies. In A. C. Fabian, editor, *NATO Advanced Science Institutes (ASI) Series C*, volume 229 of *NATO Advanced Science Institutes (ASI) Series C*, pages 53–62, 1988.

[78] K. Mukai, A. Kinkhabwala, J. R. Peterson, S. M. Kahn, and F. Paerels. Two Types of X-Ray Spectra in Cataclysmic Variables. *ApJ*, 586:L77–L80, March 2003. doi: 10.1086/374583.

[79] T. Rauch and J. L. Deetjen. Handling of Atomic Data. In I. Hubeny, D. Mihalas, and K. Werner, editors, *Stellar Atmosphere Modeling*, volume 288 of *Astronomical Society of the Pacific Conference Series*, page 103, January 2003.

[80] J. D. Scargle. Studies in astronomical time series analysis. II - Statistical aspects of spectral analysis of unevenly spaced data. *ApJ*, 263:835–853, December 1982. doi: 10.1086/160554.

[81] R. F. Stellingwerf. Period determination using phase dispersion minimization. *ApJ*, 224:953–960, 1978.

[82] J. D. Fernie. Uncertainties in period determinations. *PASP*, 101:225–228, February 1989. doi: 10.1086/132426.

[83] T. Kato, H. Maehara, M. Uemura, A. Henden, E. D. Miguel, I. Miller, P. A. Dubovsky, I. Kudzej, S. Kiyota, F.-J. Hambsch, K. Tanabe, K. Imamura, N. Kunitomi, R. Takagi, M. Nose, H. Akazawa, G. Masi, S. Nakagawa, E. Iino, R. Noguchi, K. Matsumoto, D. Fujii, H. Kobayashi, K. Ogura, S. Ohtomo, K. Yamashita, H. Yanagisawa, H. Itoh, G. Bolt, B. Monard, T. Ohshima, J. Shears, J. Ruiz, A. Imada, A. Oksanen, P. Nelson, T. L. Gomez, B. Staels, D. Boyd, I. B. Voloshina, T. Krajci, T. Crawford, C. Stockdale, M. Richmond, E. Morelle, R. Novák, D. Nogami, R. Ishioka, S. Brady, M. Simonsen, E. P. Pavlenko, F. A. Ringwald, T. Kuramoto, A. Miyashita, R. D. Pickard, T. Hynek, S. Dvorak, R. Stubbings, and E. Muyllaert. Survey of Period Variations of Superhumps in SU UMa-Type Dwarf Novae. II The Second Year (2009-2010). *PASJ*, 62:1525–1584, December 2010. doi: 10.1093/pasj/62.6.1525.

[84] P. Zemko, M. Orio, K. Mukai, and S. Shugarov. X-ray observations of VY Scl-type nova-like binaries in the high and low state. *MNRAS*, 445:869–880, November 2014. doi: 10.1093/mnras/stu1783.

[85] J. Greiner, G. H. Tovmassian, R. Di Stefano, A. Prestwich, R. González-Riestra, L. Szentasko, and C. Chavarría. Transient supersoft X-ray emission from V 751 Cygni during the optical low-state. *A&A*, 343:183–196, March 1999.

[86] J. Greiner and A. Teeseling. On the x-ray properties of v sge and its relation to the supersoft x-ray binaries. *A&A*, 339:L21, 1998.

[87] J. Greiner, G. Tovmassian, M. Orio, H. Lehmann, V. Chavushyan, A. Rau, R. Schwarz, R. Casalegno, and R. Scholz. BZ Camelopardalis during its 1999/2000 optical low state. *A&A*, 376:1031–1038, 2001.

[88] I. Hachisu and M. Kato. A Limit Cycle Model For Long-Term Optical Variations of V Sagittae: The Second Example of Accretion Wind Evolution. *ApJ*, 598: 527–544, November 2003. doi: 10.1086/378848.

[89] R. K. Honeycutt. Similarities between Stunted Outbursts in Nova-like Cataclysmic Variables and Outbursts in Ordinary Dwarf Novae. *PASP*, 113:473–481, April 2001. doi: 10.1086/319543.

[90] F. A. Ringwald and T. Naylor. High-speed optical spectroscopy of a cataclysmic variable wind – BZ Camelopardalis. *AJ*, 115:286–295, 1998.

[91] J. Patterson, R. Patino, J. R. Thorstensen, D. Harvey, D. R. Skillman, and F. A. Ringwald. Periods and quasiperiods in the cataclysmic variable BZ Camelopardalis. *AJ*, 111:2422–2430, 1996.

[92] D. R. Skillman, J. Patterson, and J. R. Thorstensen. Superhumps in cataclysmic binaries. iv. mv lyrae. *PASP*, 107:545, 1995.

[93] P. Godon and E. M. Sion. FUSE Observational Evidence of the Boundary Layer of MV Lyrae in the High State. *PASP*, 123:903–913, 2011.

[94] A. P. Linnell, P. Szkody, B. Gänsicke, K. S. Long, E. M. Sion, D. W. Hoard, and I. Hubeny. MV Lyrae in Low, Intermediate, and High States. *ApJ*, 624:923–933, 2005.

[95] J. R. Thorstensen, J. Smak, and F. V. Hessman. The two periods of TT Arietis. *PASP*, 97:437–445, 1985.

[96] K. V. Belyakov, V. F. Suleimanov, E. A. Nikolaeva, and N. V. Borisov. Modeling of the spectral energy distribution of the cataclysmic variable TT Ari and evaluation of the system parameters. In K. Werner and T. Rauch, editors, *American Institute of Physics Conference Series*, volume 1273 of *American Institute of Physics Conference Series*, pages 342–345, November 2010.

[97] P. Godon, E. M. Sion, P. Barrett, and P. Szkody. A far-ultraviolet study of the nova-like V794 Aquilae. *ApJ*, 656:1092–1103, 2007.

[98] R. K. Honeycutt and J. W. Robertson. Multiyear photometry and a spectroscopic orbital period search for the VY Sculptoris type cataclysmic variable V794 Aquilae. *AJ*, 116:1961–1965, 1998.

[99] J. B. Hutchings and A. P. Cowley. Far-ultraviolet spectra of TT Arietis. *AJ*, 133: 1204–1207, 2007.

[100] J. Greiner, R. Schwarz, C. Tappert, R. E. Mennickent, K. Reinsch, and G. Sala. On the relation between supersoft X-ray sources and VY Scl stars: The cases of V504 Cen and VY Scl. *Astronomische Nachrichten*, 331:227–230, 2010.

[101] A. Baykal, A. Esendemir, Ü. Kiziloglu, M. A. Alpar, H. Ögelman, N. Ercan, and G. İkis. X-ray variability and 1mHz oscillations in TT Arietis. *A&A*, 299:421–426, 1995.

[102] A. van Teeseling, K. Beuermann, and F. Verbunt. The x-ray source in non-magnetic cataclysmic variables. *A&A*, 315:467, 1996.

[103] R. K. Honeycutt, J. Shears, S. Kafka, J. W. Robertson, and A. A. Henden. The 1991-2012 Light Curve of the Old Nova HR LYRAE. *AJ*, 147:105, May 2014. doi: 10.1088/0004-6256/147/5/105.

[104] R. Hudec, H. Huth, and B. Fuhrmann. Long-term photographic photometry of TT ARIETIS. *The Observatory*, 104:1–5, February 1984.

[105] A. W. Shafter, P. Szkody, J. Liebert, W. R. Penning, H. E. Bond, and A. D. Grauer. TT Arietis – the low state. *ApJ*, 290:707–720, 1985.

[106] R. Hudec, W. Wenzel, W. Goetz, B. Valníček, R. Peřestý, G. A. Richter, G. Hacke, H. Huth, A. Mrkos, and J. Tremko. X-ray and optical observations of the X-ray source EX0020528+1454.8. *Ap&SS*, 131:697–700, March 1987. doi: 10.1007/BF00668161.

[107] A. Baykal and Ü. Kiziloğlu. Low frequency flickering of TT Arietis: hard and soft X-ray emission region. *Ap&SS*, 246:29–38, 1996.

[108] D. Porquet and J. Dubau. X-ray photoionized plasma diagnostics with helium-like ions. Application to warm absorber-emitter in active galactic nuclei. *A&AS*, 143: 495–514, May 2000. doi: 10.1051/aas:2000192.

[109] K. Mukai, A. Kinkhabwala, J. R. Peterson, S. M. Kahn, and F. Paerels. Two types of x-ray spectra in cataclysmic variables. *ApJ*, 586:L77, 2003.

[110] I. L. Andronov, A. V. Baklanov, A. Liakos, and P. Niarchos. Optical Photometry of TT Ari Simultaneous with the Suzaku Satellite Observations: QPOs in the Negative Superhump State. *The Astronomer's Telegram*, 2122, July 2009.

[111] K. Mukai, J. Patterson, B. Koff, E. Morelle, W. Stein, and A. Oksanen. Swift and CBA Observations of TT Ari on 2009 October 16. *The Astronomer's Telegram*, 2254, October 2009.

[112] P. Garnavich and P. Szkody. Observed low states in DQ Herculis systems. *PASP*, 100:1522–1528, 1988.

[113] G. L. Ellis, E. T. Grayson, and H. E. Bond. A search for faint planetary nebulae on Palomar Sky Survey prints. *PASP*, 96:283–286, 1984.

[114] J. Krautter, G. Radons, and U. Klaas. On the nature of 623+71 – a cataclysmic binary surrounded by a bow-shock-like emission nebula. *A&A*, 181:373–377, 1987.

[115] J. M. Hollis, R. J. Oliversen, R. M. Wagner, and W. A. Feibelman. The 0623+71 bow shock nebula. *ApJ*, 393:217–224, 1992.

[116] R. K. Honeycutt, S. Kafka, and J. W. Robertson. Wind Variability in BZ Camelopardalis. *AJ*, page 45, 2013.

[117] A. van Teeseling and F. Verbunt. ROSAT X-ray observations of ten cataclysmic variables. *A&A*, 292:519–533, 1994.

[118] J. Greiner. Soft X-ray emission of VY Sculptoris stars during optical high state. *A&A*, 336:626–636, 1998.

[119] L. Rosino, G. Romano, and P. Marziani. Photometric and spectroscopic observations of mv lyrae from 1968 to 1991. *PASP*, 105:51, 1993.

[120] W. Wenzel and B. Fuhrmann. Semiregular variations of brightness of the cataclysmic star MV Lyrae. *Zentralinstitut fuer Astrophysik Sternwarte Sonneberg Mitteilungen ueber Veraenderliche Sterne*, 9:175–180, 1983.

[121] I. L. Andronov and S. Y. Shugarov. A Photometric Study of Mv-Lyrae. *Astronomicheskij Tsirkulyar*, 1218:3, 1982.

[122] E. P. Pavlenko and S. Y. Shugarov. MV Lyrae - Since Parenago to the Present Time. *Astronomical and Astrophysical Transactions*, 15:89–100, 1998. doi: 10.1080/10556799808201755.

[123] R. K. Honeycutt and E. M. Schlegel. The very low state of V794 Aquilae. *PASP*, 97:1189–1191, 1985.

[124] M. Nauenberg. Analytic Approximations to the Mass-Radius Relation and Energy of Zero-Temperature Stars. *ApJ*, 175:417, July 1972. doi: 10.1086/151568.

[125] Y. Hillman, D. Prialnik, A. Kovetz, and M. M. Shara. Growing White Dwarfs to the Chandrasekhar Limit: The Parameter Space of the Single Degenerate SNIa Channel. *ApJ*, 819:168, March 2016. doi: 10.3847/0004-637X/819/2/168.

[126] R. Popham and R. Narayan. Accretion disk boundary layers in cataclysmic variables. 1: Optically thick boundary layers. *ApJ*, 442:337–357, March 1995. doi: 10.1086/175444.

[127] R. Popham. A boundary layer origin for dwarf nova oscillations. *MNRAS*, 308: 979–983, October 1999. doi: 10.1046/j.1365-8711.1999.02782.x.

[128] G. W. Pratt, K. Mukai, B. J. M. Hassall, T. Naylor, and J. H. Wood. An XMM-Newton observation of the nova-like variable UX UMa: spatially and spectrally resolved two-component X-ray emission. *MNRAS*, 348:L49–L53, March 2004. doi: 10.1111/j.1365-2966.2004.07574.x.

[129] J. Greiner, A. Iyudin, M. Jimenez-Garate, V. Burwitz, R. Schwarz, R. DiStefano, and N. Schulz. Resonant Scattering and Recombination in CAL 87. In G. Tovmassian and E. Sion, editors, *Revista Mexicana de Astronomia y Astrofisica Conference Series*, volume 20 of *Revista Mexicana de Astronomia y Astrofisica, vol. 27*, pages 18–20, July 2004.

[130] M. Orio, K. Ebisawa, J. Heise, and J. Hartmann. A New View of the Supersoft X-Ray Source Cal 87 Observed with XMM-Newton. In G. Tovmassian and E. Sion, editors, *Revista Mexicana de Astronomia y Astrofisica Conference Series*, volume 20 of *Revista Mexicana de Astronomia y Astrofisica, vol. 27*, pages 210–210, July 2004.

[131] E. L. Robinson. Detection of mass loss from the dwarf nova Z Camelopardalis. *ApJ*, 186:347–356, November 1973. doi: 10.1086/152504.

[132] F. A. Cordova and K. O. Mason. High-velocity winds from a dwarf nova during outburst. *ApJ*, 260:716–721, September 1982. doi: 10.1086/160291.

[133] K. S. Long and C. Knigge. Modeling the Spectral Signatures of Accretion Disk Winds: A New Monte Carlo Approach. *ApJ*, 579:725–740, November 2002. doi: 10.1086/342879.

[134] Y. Ueda, K. Asai, K. Yamaoka, T. Dotani, and H. Inoue. Discovery of an Iron K Absorption Line in the Low-Mass X-Ray Binary GX 13+1. *ApJ*, 556:L87–L90, August 2001. doi: 10.1086/323007.

[135] W. N. Brandt and N. S. Schulz. The Discovery of Broad P Cygni X-Ray Lines from Circinus X-1 with the Chandra High-Energy Transmission Grating Spectrometer. *ApJ*, 544:L123–L127, December 2000. doi: 10.1086/317313.

[136] D. S. Baskill, P. J. Wheatley, and J. P. Osborne. ASCA X-ray observations of the disc wind in the dwarf nova Z Camelopardalis. *MNRAS*, 328:71–78, November 2001. doi: 10.1046/j.1365-8711.2001.04880.x.

[137] K. Saitou, M. Tsujimoto, K. Ebisawa, and M. Ishida. Suzaku X-Ray Observation of the Dwarf Nova Z Camelopardalis at the Onset of an Optical Outburst. *PASJ*, 64:88, August 2012. doi: 10.1093/pasj/64.4.88.

[138] J.-M. Hameury and J. Lasota. Vy sculptoris stars as magnetic cvs. *A&A*, 394: 231, 2002.

[139] P. Rodríguez-Gil, B. T. Gänsicke, H.-J. Hagen, S. Araujo-Betancor, A. Aungwerojwit, C. Allende Prieto, D. Boyd, J. Casares, D. Engels, O. Giannakis, E. T. Harlaftis, J. Kube, H. Lehto, I. G. Martínez-Pais, R. Schwarz, W. Skidmore, A. Staude, and M. A. P. Torres. SWSextantis stars: the dominant population of cataclysmic variables with orbital periods between 3 and 4h. *MNRAS*, 377: 1747–1762, June 2007. doi: 10.1111/j.1365-2966.2007.11743.x.

[140] J. Patterson, W. H. Fenton, J. R. Thorstensen, D. A. Harvey, D. R. Skillman, R. E. Fried, B. Monard, D. O'Donoghue, E. Beshore, B. Martin, P. Niarchos, T. Vanmunster, J. Foote, G. Bolt, R. Rea, L. M. Cook, N. Butterworth, and M. Wood. Superhumps in Cataclysmic Binaries. XXIII. V442 Ophiuchi and RX J1643.7+3402. *PASP*, 114:1364–1381, December 2002. doi: 10.1086/344587.

[141] P. Rodríguez-Gil, L. Schmidtobreick, K. S. Long, B. T. Gänsicke, M. A. P. Torres, M. M. Rubio-Díez, and M. Santander-García. The fight for accretion: discovery of intermittent mass transfer in BB Doradus in the low state. *MNRAS*, 422:2332–2340, May 2012. doi: 10.1111/j.1365-2966.2012.20783.x.

[142] P. Zemko, K. Mukai, and M. Orio. Suzaku Observation of the Classical Nova V2491 Cyg in Quiescence. *ApJ*, 807:61, July 2015. doi: 10.1088/0004-637X/807/1/61.

[143] P. Zemko, M. Orio, K. Mukai, A. Bianchini, S. Ciroi, and V. Cracco. V4743 Sgr, a magnetic nova? *MNRAS*, 460:2744–2751, August 2016. doi: 10.1093/mnras/stw1199.

[144] S. Nakano, J. Beize, Z.-W. Jin, X. Gao, H. Yamaoka, K. Haseda, E. Guido, G. Sostero, G. Klingenberg, and K. Kadota. V2491 Cygni. *IAU Circ.*, 8934:1, April 2008.

[145] T. Tomov, M. Mikolajewski, T. Brozek, E. Ragan, E. Swierczynski, P. Wychudzki, and C. Galan. V2491 Cyg - a possible recurrent nova? *The Astronomer's Telegram*, 1485:1, April 2008.

[146] T. Tomov, M. Mikolajewski, E. Ragan, E. Swierczynski, and P. Wychudzki. Optical observations of the fast nova V2491 Cyg. *The Astronomer's Telegram*, 1475: 1, April 2008.

[147] R. J. Rudy, D. K. Lynch, R. W. Russell, C. E. Woodward, and K. Covey. V2491 Cygni. *IAU Circ.*, 8938:2, April 2008.

[148] R. C. Bohlin, B. D. Savage, and J. F. Drake. A survey of interstellar H I from L-alpha absorption measurements. II. *ApJ*, 224:132–142, August 1978. doi: 10.1086/156357.

[149] R. Jurdana-Sepic and U. Munari. Plate archive photometry of the progenitors of Nova Cyg 2008 N.2 and Nova Sgr 2008. *Information Bulletin on Variable Stars*, 5839:1, July 2008.

[150] M. Hernanz and G. Sala. A Classical Nova, V2487 Oph 1998, Seen in X-rays Before and After Its Explosion. *Science*, 298:393–395, October 2002. doi: 10.1126/science.298.5592.393.

[151] P. Schmeer and C. Gualdoni. V679 Carinae = Nova Carinae 2008. *IAU Circ.*, 8999:4, December 2008.

[152] A. Ibarra, E. Kuulkers, J. P. Osborne, K. Page, J. U. Ness, R. D. Saxton, W. Baumgartner, V. Beckmann, M. F. Bode, M. Hernanz, K. Mukai, M. Orio, G. Sala, S. Starrfield, and G. A. Wynn. Pre-nova X-ray observations of V2491 Cygni (Nova Cyg 2008b). *A&A*, 497:L5–L8, April 2009. doi: 10.1051/0004-6361/200911710.

[153] L. A. Helton, C. E. Woodward, K. Vanlandingham, and G. J. Schwarz. V2491 Cygni. *Central Bureau Electronic Telegrams*, 1379:1, May 2008.

[154] I. Hachisu and M. Kato. Optical and Supersoft X-Ray Light-Curve Models of Classical Nova V2491 Cygni: A New Clue to the Secondary Maximum. *ApJ*, 694: L103–L106, April 2009. doi: 10.1088/0004-637X/694/2/L103.

[155] J.-U. Ness, J. P. Osborne, A. Dobrotka, K. L. Page, J. J. Drake, C. Pinto, R. G. Detmers, G. Schwarz, M. F. Bode, A. P. Beardmore, S. Starrfield, M. Hernanz, G. Sala, J. Krautter, and C. E. Woodward. XMM-Newton X-ray and Ultraviolet Observations of the Fast Nova V2491 Cyg during the Supersoft Source Phase. *ApJ*, 733:70, May 2011. doi: 10.1088/0004-637X/733/1/70.

[156] D. Takei, J.-U. Ness, M. Tsujimoto, S. Kitamoto, J. J. Drake, J. P. Osborne, H. Takahashi, and K. Kinugasa. X-Ray Study of Rekindled Accretion in the Classical Nova V2491 Cygni. *PASJ*, 63:729, November 2011. doi: 10.1093/pasj/63.sp3.S729.

[157] E. Kuulkers, A. Ibarra, K. L. Page, A. Beardmore, P. Evans, J. P. Osborne, M. Bode, J. J. Drake, K. Mukai, J.-U. Ness, M. Orio, R. Saxton, S. Starrfield, S. P. S. Eyres, T. J. O'Brien, and T. W. B. Muxlow. Swift and MERLIN observations of Swift J194302.1+321913 during the nova outburst of V2491 Cyg. *The Astronomer's Telegram*, 1480:1, April 2008.

[158] J. P. Osborne, K. Page, P. Evans, A. Beardmore, E. Kuulkers, A. Ibarra, J.-U. Ness, S. Starrfield, M. Bode, J. J. Drake, M. Orio, J. Krautter, G. S. M. Tsujimoto, and D. Takei. Nova V2491 Cyg has become a bright super-soft source. *The Astronomer's Telegram*, 1542:1, May 2008.

[159] K. L. Page, J. P. Osborne, P. A. Evans, G. A. Wynn, A. P. Beardmore, R. L. C. Starling, M. F. Bode, A. Ibarra, E. Kuulkers, J.-U. Ness, and G. J. Schwarz. Swift observations of the X-ray and UV evolution of V2491 Cyg (Nova Cyg 2008 No. 2). *MNRAS*, 401:121–130, January 2010. doi: 10.1111/j.1365-2966.2009.15681.x.

[160] A. Baklanov, E. Pavlenko, and E. Berezina. Discovery of the optical variability of Nova V2491 Cyg. *The Astronomer's Telegram*, 1514:1, May 2008.

[161] S. Y. Shugarov, D. Chochol, I. M. Volkov, and P. O. Zemko. Photometric Investigation of the X-ray Nova V2491 Cyg. In C. Sterken, N. Samus, and L. Szabados, editors, *Variable Stars, the Galactic halo and Galaxy Formation*, page 198, February 2010.

[162] M. J. Darnley, V. A. R. M. Ribeiro, M. F. Bode, and U. Munari. On the progenitor system of Nova V2491 Cygni. *A&A*, 530:A70, June 2011. doi: 10.1051/0004-6361/201016038.

[163] I. M. George and A. C. Fabian. X-ray reflection from cold matter in active galactic nuclei and X-ray binaries. *MNRAS*, 249:352–367, March 1991.

[164] C. Hellier and K. Mukai. On the iron Kα complex in magnetic cataclysmic variables. *MNRAS*, 352:1037–1040, August 2004. doi: 10.1111/j.1365-2966.2004.07995.x.

[165] E. M. Schlegel, H. V. Shipley, V. R. Rana, P. E. Barrett, and K. P. Singh. X-Ray Emission Line Spectroscopy of Cataclysmic Variables. II. Temperatures and Densities from Line Ratios in the Chandra HETG Band. *ApJ*, 797:38, December 2014. doi: 10.1088/0004-637X/797/1/38.

[166] M. Orio and G. Shaviv. Local thermonuclear runaways among classical novae. *Ap&SS*, 202:273–288, April 1993. doi: 10.1007/BF00626882.

[167] S. A. Glasner, E. Livne, and J. W. Truran. Convective overshoot mixing in Nova outbursts - the dependence on the composition of the underlyingwhitedwarf. *MNRAS*, 427:2411–2419, December 2012. doi: 10.1111/j.1365-2966.2012.22103.x.

[168] M. Hernanz. V2487 Oph 1998: a post nova in an intermediate polar. In *European Physical Journal Web of Conferences*, volume 64 of *European Physical Journal Web of Conferences*, page 7002, January 2014. doi: 10.1051/epjconf/20136407002.

[169] U. Munari, A. Siviero, S. Dallaporta, G. Cherini, P. Valisa, and L. Tomasella. An extensive optical study of V2491 Cyg (Nova Cyg 2008 N.2), from maximum brightness to return to quiescence. *New Astr.*, 16:209–219, April 2011.

[170] A. D. Silber. *Studies of an X-Ray Selected Sample of Cataclysmic Variables.* PhD thesis, MASSACHUSETTS INSTITUTE OF TECHNOLOGY., January 1992.

[171] F. A. Ringwald, T. Naylor, and K. Mukai. The optical spectra of old novae. *MNRAS*, 281:192–210, July 1996. doi: 10.1093/mnras/281.1.192.

[172] T. Tomov, E. Swierczynski, M. Mikolajewski, and K. Ilkiewicz. SALT observations of southern post-novae. *A&A*, 576:A119, April 2015. doi: 10.1051/0004-6361/201424709.

[173] A. U. Landolt. UBVRI photometric standard stars in the magnitude range 11.5-16.0 around the celestial equator. *AJ*, 104:340–371, July 1992. doi: 10.1086/116242.

[174] V. A. R. M. Ribeiro, M. J. Darnley, M. F. Bode, U. Munari, D. J. Harman, I. A. Steele, and J. Meaburn. The morphology of the expanding ejecta of V2491 Cygni (2008 N.2). *MNRAS*, 412:1701–1709, April 2011. doi: 10.1111/j.1365-2966.2010.18006.x.

[175] J. E. McClintock, C. R. Canizares, and C. B. Tarter. On the origin of 4640-4650 A emission in X-ray stars. *ApJ*, 198:641–652, June 1975. doi: 10.1086/153642.

[176] L. Morales-Rueda, M. D. Still, and P. Roche. Solving the kilosecond quasi-periodic oscillation problem of the intermediate polar GK Persei. *MNRAS*, 306:753–765, July 1999. doi: 10.1046/j.1365-8711.1999.02484.x.

[177] A. Bianchini, R. Canterna, S. Desidera, and C. Garcia. Evidence for Magnetic Accretion during the 2002 Optical Outburst of the Old Nova GK Persei (1901). *PASP*, 115:474–478, April 2003. doi: 10.1086/374347.

[178] B. Warner. *Cataclysmic Variable Stars.* September 2003.

[179] M. L. Pretorius and K. Mukai. Constraints on the space density of intermediate polars from the Swift-BAT survey. *MNRAS*, 442:2580–2585, August 2014. doi: 10.1093/mnras/stu990.

[180] A. J. Norton, M. G. Watson, and A. R. King. Iron Kα lines and the absorption structure of intermediate polars. In A. Treves, G. C. Perola, and L. Stella, editors, *Iron Line Diagnostics in X-ray Sources*, volume 385 of *Lecture Notes in Physics, Berlin Springer Verlag*, page 155, 1991. doi: 10.1007/BFb0031289.

[181] H. Ezuka and M. Ishida. Iron line diagnostics of the postshock hot plasma in magnetic cataclysmic variables observed with ASCA. *ApJS*, 120:277–298, 1999.

[182] R. N. C. Eze. Suzaku observations of Fe K α line in some Magnetic Cataclysmic Variables. *New Astr.*, 37:35–41, May 2015. doi: 10.1016/j.newast.2014.11.006.

[183] S. R. Rosen, K. O. Mason, and F. A. Cordova. Exosat x-ray observations of the eclipsing magnetic cataclysmic variable ex hya. *MNRAS*, 231:549, 1988.

[184] C. Hellier, M. Cropper, and K. O. Mason. Optical and x-ray observations of ao piscium and the origin of the spin pulse in intermediate polars. *MNRAS*, 248:233, 1991.

[185] K. Haseda, D. West, H. Yamaoka, and G. Masi. Another nova in Sagittarius. *IAU Circ.*, 7975:1, September 2002.

[186] T. Kato, M. Fujii, and K. Ayani. Another Nova in Sagittarius. *IAU Circ.*, 7975: 2, September 2002.

[187] R. J. Strope, B. E. Schaefer, and A. A. Henden. Catalog of 93 Nova Light Curves: Classification and Properties. *AJ*, 140:34–62, July 2010. doi: 10.1088/0004-6256/140/1/34.

[188] T. Rauch, M. Orio, R. Gonzales-Riestra, T. Nelson, M. Still, K. Werner, and J. Wilms. Non-local Thermal Equilibrium Model Atmospheres for the Hottest White Dwarfs: Spectral Analysis of the Compact Component in Nova V4743 Sgr. *ApJ*, 717:363–371, July 2010. doi: 10.1088/0004-637X/717/1/363.

[189] S. Starrfield, J.-U. Ness, J. J. Drake, and M. Orio. V4743 Sagittarii. *IAU Circ.*, 8107:1, April 2003.

[190] J.-U. Ness, S. Starrfield, V. Burwitz, R. Wichmann, P. Hauschildt, J. J. Drake, R. M. Wagner, H. E. Bond, J. Krautter, M. Orio, M. Hernanz, R. D. Gehrz, C. E. Woodward, Y. Butt, K. Mukai, S. Balman, and J. W. Truran. A Chandra Low Energy Transmission Grating Spectrometer Observation of V4743 Sagittarii: A

Supersoft X-Ray Source and a Violently Variable Light Curve. *ApJ*, 594:L127–L130, September 2003. doi: 10.1086/378664.

[191] E. Leibowitz, M. Orio, R. Gonzalez-Riestra, Y. Lipkin, J.-U. Ness, S. Starrfield, M. Still, and E. Tepedelenlioglu. Variability and multiperiodic oscillations in the X-ray light curve of the classical nova V4743 Sgr. *MNRAS*, 371:424–430, September 2006. doi: 10.1111/j.1365-2966.2006.10684.x.

[192] D. R. van Rossum. A Public Set of Synthetic Spectra from Expanding Atmospheres for X-Ray Novae. I. Solar Abundances. *ApJ*, 756:43, September 2012. doi: 10.1088/0004-637X/756/1/43.

[193] D. R. van Rossum and J.-U. Ness. Expanding atmosphere models for SSS spectra of novae. *Astronomische Nachrichten*, 331:175, February 2010. doi: 10.1002/asna.200911321.

[194] J.-U. Ness, J. P. Osborne, M. Henze, A. Dobrotka, J. J. Drake, V. A. R. M. Ribeiro, S. Starrfield, E. Kuulkers, E. Behar, M. Hernanz, G. Schwarz, K. L. Page, A. P. Beardmore, and M. F. Bode. Obscuration effects in super-soft-source X-ray spectra. *A&A*, 559:A50, November 2013. doi: 10.1051/0004-6361/201322415.

[195] A. Dobrotka and J.-U. Ness. Multifrequency nature of the 0.75 mHz feature in the X-ray light curves of the nova V4743 Sgr. *MNRAS*, 405:2668–2682, July 2010. doi: 10.1111/j.1365-2966.2010.16654.x.

[196] T. W. Kang, A. Retter, A. Liu, and M. Richards. Nova V4743 Sagittarii 2002: An Intermediate Polar Candidate. *AJ*, 132:608–613, August 2006. doi: 10.1086/505174.

[197] M. T. Richards, T. W. Kang, A. Retter, and A. Liu. Nova Sagittarii 2002: An Intermediate Polar Candidate. In *American Astronomical Society Meeting Abstracts*, volume 37 of *Bulletin of the American Astronomical Society*, page 1277, December 2005.

[198] R. M. Wagner, J. Steinfadt, H. E. Bond, E. Hooper, A. Karam, J. Rohrbach, G. Schwarz, and S. Starrfield. Photometry and Spectroscopy of the Classical Nova V4743 Sgr 2002 in Outburst and Decline. In *American Astronomical Society Meeting Abstracts*, volume 37 of *Bulletin of the American Astronomical Society*, page 1277, December 2005.

[199] M. Nielbock and L. Schmidtobreick. Looking for dust and molecules in nova v4743 sagittarii. *A&A*, 400:L5, 2003.

[200] K. M. Vanlandingham, G. Schwarz, S. Starrfield, C. Woodward, M. Wagner, J. Ness, and A. Helton. Optical And GALEX Observations Of V4743 Sgr. In *American Astronomical Society Meeting Abstracts #210*, volume 39 of *Bulletin of the American Astronomical Society*, page 99, May 2007.

[201] Ş. Balman, J. Krautter, and H. Ögelman. The X-Ray Spectral Evolution of Classical Nova V1974 Cygni 1992: A Reanalysis of the ROSAT Data. *ApJ*, 499:395–406, May 1998. doi: 10.1086/305600.

[202] R. A. Downes, H. W. Duerbeck, and C. E. Delahodde. Luminosities of [O III] and Hydrogen Balmer lines in nova shells years and decades after outburst. *Journal of Astronomical Data*, 7, December 2001.

[203] B. Warner. Cataclysmic variable stars. *Cambridge Astrophysics Series*, 28, 1995.

[204] A. Vanderburg and J. A. Johnson. A Technique for Extracting Highly Precise Photometry for the Two-Wheeled Kepler Mission. *PASP*, 126:948–958, October 2014. doi: 10.1086/678764.

[205] K. Mukai, M. Orio, and M. Della Valle. Novae as a Class of Transient X-Ray Sources. *ApJ*, 677:1248-1252, April 2008. doi: 10.1086/529362.

[206] J.-U. Ness, J. P. Osborne, M. Henze, A. Dobrotka, J. J. Drake, V. A. R. M. Ribeiro, S. Starrfield, E. Kuulkers, E. Behar, M. Hernanz, G. Schwarz, K. L. Page, A. P. Beardmore, and M. F. Bode. Obscuration effects in super-soft-source X-ray spectra. *A&A*, 559:A50, November 2013. doi: 10.1051/0004-6361/201322415.

[207] J.-U. Ness, A. P. Beardmore, J. P. Osborne, E. Kuulkers, M. Henze, A. L. Piro, J. J. Drake, A. Dobrotka, G. Schwarz, S. Starrfield, P. Kretschmar, M. Hirsch, and J. Wilms. Short-period X-ray oscillations in super-soft novae and persistent super-soft sources. *A&A*, 578:A39, June 2015. doi: 10.1051/0004-6361/201425178.

[208] T. L. Parker, A. J. Norton, and K. Mukai. X-ray orbital modulations in intermediate polars. *A&A*, 439:213–225, August 2005. doi: 10.1051/0004-6361:20052887.

[209] C. Hellier. The size of the accretion region in intermediate polars: eclipses of XY ARIETIS observed with RXTE. *MNRAS*, 291:71–80, October 1997. doi: 10.1093/mnras/291.1.71.

[210] A. S. Williams. New Variable Star 68. 1901 Persei. *Astronomische Nachrichten*, 155:29, March 1901. doi: 10.1002/asna.19011550107.

[211] F. Sabbadin and A. Bianchini. The old-nova GK Per (1901). IV - The light curve since 1901. *A&AS*, 54:393–403, December 1983.

[212] A. Bianchini, F. Sabbadin, G. C. Favero, and I. Dalmeri. Phenomenology of the optical outbursts of the classical old-nova gk persei (1901). *A&A*, 160:367, 1986.

[213] S.-W. Kim, J. C. Wheeler, and S. Mineshige. Disk instability and outburst properties of the intermediate polar GK Persei. *ApJ*, 384:269–283, January 1992. doi: 10.1086/170870.

[214] D. B. McLaughlin. The Spectra of Novae. In J. L. Greenstein, editor, *Stellar Atmospheres*, page 585, January 1960.

[215] Ş. Balman. Chandra Observation of the Shell of Nova Persei 1901 (GK Persei): Detection of Localized Nonthermal X-Ray Emission from a Miniature Supernova Remnant. *ApJ*, 627:933–952, July 2005. doi: 10.1086/430392.

[216] D. Takei, J. J. Drake, H. Yamaguchi, P. Slane, Y. Uchiyama, and S. Katsuda. X-Ray Fading and Expansion in the Miniature Supernova Remnant of GK Persei. *ApJ*, 801:92, March 2015. doi: 10.1088/0004-637X/801/2/92.

[217] A. Evans, M. F. Bode, H. W. Duerbeck, and W. C. Seitter. IUE observations of the shells of RR PIC and GK Per. *MNRAS*, 258:7P–13P, September 1992. doi: 10.1093/mnras/258.1.7P.

[218] M. M. Shara, D. Zurek, O. De Marco, T. Mizusawa, R. Williams, and M. Livio. GK Per (Nova Persei 1901): Hubble Space Telescope Imagery and Spectroscopy of the Ejecta, and First Spectrum of the Jet-like Feature. *AJ*, 143:143, June 2012. doi: 10.1088/0004-6256/143/6/143.

[219] S. P. S. Eyres, A. Salama, A. Evans, M. Bode, S. Dougherty, B. F. M. Waters, and J. C. Rawlings. The extended emission around GK Per - stranger and stranger. In P. Cox and M. Kessler, editors, *The Universe as Seen by ISO*, volume 427 of *ESA Special Publication*, page 309, March 1999.

[220] G. C. Anupama and N. G. Kantharia. A multiwavelength study of the remnant of nova GK Persei. *A&A*, 435:167–175, May 2005. doi: 10.1051/0004-6361:20042371.

[221] T. Liimets, R. L. M. Corradi, M. Santander-García, E. Villaver, P. Rodríguez-Gil, K. Verro, and I. Kolka. A Three-dimensional View of the Remnant of Nova Persei 1901 (GK Per). *ApJ*, 761:34, December 2012. doi: 10.1088/0004-637X/761/1/34.

[222] D. Crampton, W. A. Fisher, and A. P. Cowley. The orbit of GK Persei. *ApJ*, 300: 788–793, January 1986. doi: 10.1086/163856.

[223] L. Morales-Rueda, M. D. Still, P. Roche, J. H. Wood, and J. J. Lockley. The stellar mass ratio of GK Persei. *MNRAS*, 329:597–604, January 2002. doi: 10.1046/j.1365-8711.2002.05013.x.

[224] B. Warner. Observations of Dwarf Novae. In P. Eggleton, S. Mitton, and J. Whelan, editors, *Structure and Evolution of Close Binary Systems*, volume 73 of *IAU Symposium*, page 85, 1976.

[225] M. G. Watson, A. R. King, and J. Osborne. The old nova GK Per - Discovery of the X-ray pulse period. *MNRAS*, 212:917–930, February 1985.

[226] V. Suleimanov, V. Doroshenko, L. Ducci, G. V. Zhukov, and K. Werner. GK Persei and EX Hydrae: Intermediate polars with small magnetospheres. *A&A*, 591:A35, June 2016. doi: 10.1051/0004-6361/201628301.

[227] P. A. Evans, A. P. Beardmore, J. P. Osborne, and G. A. Wynn. The unusual 2006 dwarf nova outburst of GK Persei. *MNRAS*, 399:1167–1174, November 2009. doi: 10.1111/j.1365-2966.2009.15376.x.

[228] A. R. King, M. J. Ricketts, and R. S. Warwick. The detection of an X-ray outburst from the old nova GK Per. *MNRAS*, 187:77P–81P, June 1979.

[229] A. Bianchini and F. Sabadin. The old-nova GK Per (1901). III - Accretion disc models. *A&A*, 125:112–116, August 1983.

[230] A. J. Norton, M. G. Watson, and A. R. King. GK Per - X-ray observations in quiescence. *MNRAS*, 231:783–793, April 1988. doi: 10.1093/mnras/231.3.783.

[231] C. Hellier, S. Harmer, and A. P. Beardmore. On the magnetic accretor GK Persei in outburst. *MNRAS*, 349:710–714, April 2004. doi: 10.1111/j.1365-2966.2004.07539.x.

[232] D. Nogami, T. Kato, and H. Baba. Time-Resolved Photometry of GK Persei during the 1996 Outburst. *PASJ*, 54:987–997, December 2002. doi: 10.1093/pasj/54.6.987.

[233] B. Warner. Rapid Oscillations in Cataclysmic Variables. *PASP*, 116:115–132, February 2004. doi: 10.1086/381742.

[234] B. Warner and P. A. Woudt. Dwarf nova oscillations and quasi-periodic oscillations in cataclysmic variables - II. A low-inertia magnetic accretor model. *MNRAS*, 335:84–98, September 2002. doi: 10.1046/j.1365-8711.2002.05596.x.

[235] S. Vrielmann, J.-U. Ness, and J. H. M. M. Schmitt. On the nature of the X-ray source in GK Persei. *A&A*, 439:287–300, August 2005. doi: 10.1051/0004-6361:20053017.

[236] C. Hellier, K. Mukai, and A. P. Beardmore. An outburst of the magnetic cataclysmic variable XY ARIETIS observed with RXTE. *MNRAS*, 292:397, December 1997.

[237] J. Brunschweiger, J. Greiner, M. Ajello, and J. Osborne. Intermediate polars in the Swift/BAT survey: spectra and white dwarf masses. *A&A*, 496:121–127, March 2009. doi: 10.1051/0004-6361/200811285.

[238] V. Suleimanov, M. Revnivtsev, and H. Ritter. RXTE broadband X-ray spectra of intermediate polars and white dwarf mass estimates. *A&A*, 435:191–199, May 2005. doi: 10.1051/0004-6361:20041283.

[239] V. Šimon. The intermediate polar GK Persei: An unstable relation of the X-ray and the optical intensities in a series of outbursts. *A&A*, 575:A65, March 2015. doi: 10.1051/0004-6361/201424910.

[240] D. N. Burrows, J. E. Hill, J. A. Nousek, J. A. Kennea, A. Wells, J. P. Osborne, A. F. Abbey, A. Beardmore, K. Mukerjee, A. D. T. Short, G. Chincarini, S. Campana, O. Citterio, A. Moretti, C. Pagani, G. Tagliaferri, P. Giommi, M. Capalbi, F. Tamburelli, L. Angelini, G. Cusumano, H. W. Bräuninger, W. Burkert, and G. D. Hartner. The Swift X-Ray Telescope. *Space Sci. Rev.*, 120:165–195, October 2005. doi: 10.1007/s11214-005-5097-2.

[241] J. E. Hill, L. Angelini, D. C. Morris, D. N. Burrows, A. F. Abbey, S. Campana, G. Cusumano, J. A. Kennea, R. Klar, C. Mangels, A. Moretti, M. Perri, J. Racusin, G. Tagliaferri, F. Tamburelli, P. Wood, J. A. Nousek, and A. Wells. The unique observing capabilities of the Swift x-ray telescope. In O. H. W. Siegmund, editor, *UV, X-Ray, and Gamma-Ray Space Instrumentation for Astronomy XIV*, volume 5898 of *Proc. SPIE*, pages 313–328, January 2005. doi: 10.1117/12.618026.

[242] C. R. Canizares, J. E. Davis, D. Dewey, K. A. Flanagan, E. B. Galton, D. P. Huenemoerder, K. Ishibashi, T. H. Markert, H. L. Marshall, M. McGuirk, M. L. Schattenburg, N. S. Schulz, H. I. Smith, and M. Wise. The Chandra High-Energy Transmission Grating: Design, Fabrication, Ground Calibration, and 5 Years in Flight. *PASP*, 117:1144–1171, October 2005. doi: 10.1086/432898.

[243] P. A. Evans, A. P. Beardmore, K. L. Page, J. P. Osborne, P. T. O'Brien, R. Willingale, R. L. C. Starling, D. N. Burrows, O. Godet, L. Vetere, J. Racusin, M. R. Goad, K. Wiersema, L. Angelini, M. Capalbi, G. Chincarini, N. Gehrels, J. A. Kennea, R. Margutti, D. C. Morris, C. J. Mountford, C. Pagani, M. Perri, P. Romano, and N. Tanvir. Methods and results of an automatic analysis of a complete sample of Swift-XRT observations of GRBs. *MNRAS*, 397:1177–1201, August 2009. doi: 10.1111/j.1365-2966.2009.14913.x.

[244] P. A. Evans, A. P. Beardmore, K. L. Page, L. G. Tyler, J. P. Osborne, M. R. Goad, P. T. O'Brien, L. Vetere, J. Racusin, D. Morris, D. N. Burrows, M. Capalbi,

M. Perri, N. Gehrels, and P. Romano. An online repository of Swift/XRT light curves of γ-ray bursts. *A&A*, 469:379–385, July 2007. doi: 10.1051/0004-6361:20077530.

[245] J. Eastman, R. Siverd, and B. S. Gaudi. Achieving Better Than 1 Minute Accuracy in the Heliocentric and Barycentric Julian Dates. *PASP*, 122:935–946, August 2010. doi: 10.1086/655938.

[246] H. A. Krimm, S. T. Holland, R. H. D. Corbet, A. B. Pearlman, P. Romano, J. A. Kennea, J. S. Bloom, S. D. Barthelmy, W. H. Baumgartner, J. R. Cummings, N. Gehrels, A. Y. Lien, C. B. Markwardt, D. M. Palmer, T. Sakamoto, M. Stamatikos, and T. N. Ukwatta. The Swift/BAT Hard X-Ray Transient Monitor. *ApJS*, 209:14, November 2013. doi: 10.1088/0067-0049/209/1/14.

[247] A. J. Norton and M. G. Watson. Spin modulated X-ray emission from intermediate polars. *MNRAS*, 237:853–874, April 1989. doi: 10.1093/mnras/237.4.853.

[248] K. Mukai, V. Rana, F. Bernardini, and D. de Martino. Unambiguous Detection of Reflection in Magnetic Cataclysmic Variables: Joint NuSTAR-XMM-Newton Observations of Three Intermediate Polars. *ApJ*, 807:L30, July 2015. doi: 10.1088/2041-8205/807/2/L30.

[249] M. Eracleous, J. Patterson, and J. Halpern. A search for periodicities in the X-ray emission from cataclysmic variables. *ApJ*, 370:330–340, March 1991. doi: 10.1086/169819.

[250] J. Patterson. Rapid oscillations in cataclysmic variables. VII - GK Persei. *PASP*, 103:1149–1157, November 1991. doi: 10.1086/132935.

[251] C. W. Mauche. The Spin-Up Rate of the White Dwarf in GK Per. In S. Vrielmann and M. Cropper, editors, *IAU Colloq. 190: Magnetic Cataclysmic Variables*, volume 315 of *Astronomical Society of the Pacific Conference Series*, page 120, December 2004.

[252] T. Kato, A. Imada, M. Uemura, D. Nogami, H. Maehara, R. Ishioka, H. Baba, K. Matsumoto, H. Iwamatsu, K. Kubota, K. Sugiyasu, Y. Soejima, Y. Moritani, T. Ohshima, H. Ohashi, J. Tanaka, M. Sasada, A. Arai, K. Nakajima, S. Kiyota, K. Tanabe, K. Imamura, N. Kunitomi, K. Kunihiro, H. Taguchi, M. Koizumi, N. Yamada, Y. Nishi, M. Kida, S. Tanaka, R. Ueoka, H. Yasui, K. Maruoka, A. Henden, A. Oksanen, M. Moilanen, P. Tikkanen, M. Aho, B. Monard, H. Itoh, P. A. Dubovsky, I. Kudzej, R. Dancikova, T. Vanmunster, J. Pietz, G. Bolt, D. Boyd, P. Nelson, T. Krajci, L. M. Cook, K. Torii, D. R. Starkey, J. Shears, L.-T. Jensen, G. Masi, T. Hynek, Nová, R. K, Kociá, R. N, Krá, L. L, Kučá, H. Ková,

M. Kolasa, P. Šťastný, B. Staels, I. Miller, Y. Sano, P. de Ponthière, A. Miyashita, T. Crawford, S. Brady, R. Santallo, T. Richards, B. Martin, D. Buczynski, M. Richmond, J. Kern, S. Davis, D. Crabtree, K. Beaulieu, T. Davis, M. Aggleton, E. Morelle, E. P. Pavlenko, M. Andreev, A. Baklanov, M. D. Koppelman, G. Billings, L. Urbancok, Y. Ögmen, B. Heathcote, T. L. Gomez, I. Voloshina, A. Retter, K. Mularczyk, K. Zoczewski, A. Olech, P. Kedzierski, R. D. Pickard, C. Stockdale, J. Virtanen, K. Morikawa, F.-J. Hambsch, G. Garradd, C. Gualdoni, K. Geary, T. Omodaka, N. Sakai, R. Michel, A. A. Cárdenas, K. D. Gazeas, P. G. Niarchos, A. V. Yushchenko, F. Mallia, M. Fiaschi, G. A. Good, S. Walker, N. James, K.-I. Douzu, W. M. Julian, II, N. D. Butterworth, S. Y. Shugarov, I. Volkov, D. Chochol, N. Katysheva, A. E. Rosenbush, M. Khramtsova, P. Kehusmaa, M. Reszelski, J. Bedient, W. Liller, G. Pojmanski, M. Simonsen, R. Stubbings, P. Schmeer, E. Muyllaert, T. Kinnunen, G. Poyner, J. Ripero, and W. Kriebel. Survey of Period Variations of Superhumps in SU UMa-Type Dwarf Novae. *PASJ*, 61:S395–S616, December 2009. doi: 10.1093/pasj/61.sp1.S395.

[253] C.-C. Wu, A. V. Holm, R. J. Panek, J. C. Raymond, L. W. Hartmann, and J. H. Swank. Ultraviolet spectrophotometry and optical and infrared photometry of the old nova GK Persei. *ApJ*, 339:443–454, April 1989. doi: 10.1086/167309.

[254] C. Done and P. Magdziarz. Complex absorption and reflection of a multitemperature cyclotron-bremsstrahlung X-ray cooling shock in BY Cam. *MNRAS*, 298: 737–746, August 1998. doi: 10.1046/j.1365-8711.1998.01636.x.

[255] C. Hellier and K. Mukai. On the iron Kα complex in magnetic cataclysmic variables. *MNRAS*, 352:1037–1040, August 2004. doi: 10.1111/j.1365-2966.2004.07995.x.

[256] A. H. Gabriel and C. Jordan. Interpretation of solar helium-like ion line intensities. *MNRAS*, 145:241, 1969. doi: 10.1093/mnras/145.2.241.

[257] D. Porquet and J. Dubau. X-ray photoionized plasma diagnostics with helium-like ions. Application to warm absorber-emitter in active galactic nuclei. *A&AS*, 143: 495–514, May 2000. doi: 10.1051/aas:2000192.

[258] A. Bianchini, R. Canterna, S. Desidera, and C. Garcia. Evidence for Magnetic Accretion during the 2002 Optical Outburst of the Old Nova GK Persei (1901). *PASP*, 115:474–478, April 2003. doi: 10.1086/374347.

[259] G. J. M. Luna, J. C. Raymond, N. S. Brickhouse, C. W. Mauche, and V. Suleimanov. Testing the cooling flow model in the intermediate polar EX Hydrae. *A&A*, 578:A15, June 2015. doi: 10.1051/0004-6361/201525755.

[260] M. Ishida, T. Sakao, K. Makishima, T. Ohashi, M. G. Watson, A. J. Norton, M. Kawada, and K. Koyama. GINGA observations of the old nova GK Persei in quiescence and outburst. *MNRAS*, 254:647–654, February 1992. doi: 10.1093/mnras/254.4.647.

[261] T. Yuasa, T. Hayashi, and M. Ishida. Suzaku X-ray observation of the GK Persei dwarf nova outburst in 2015. *MNRAS*, 459:779–788, June 2016. doi: 10.1093/mnras/stw734.

[262] J. Frank, A. King, and D. J. Raine. *Accretion Power in Astrophysics: Third Edition*. January 2002.